INVESTIGATION OF FIELD QUANTITIES IN A 500 KV DC SWITCHYARD

By

15

Changyi Charlie Lu

A Thesis
Submitted to the Faculty of Graduate Studies
in Partial Fulfillment of the Requirements
for the Degree of

Master of Science

Department of Electrical and Computer Engineering
University of Manitoba
Winnipeg, Manitoba, Canada

ISBN 0-612-13317-6

Name Changyi C. Lu

Dissertation Abstracts International is arranged by broad, general subject categories. Please select the one subject which most nearly describes the content of your dissertation. Enter the corresponding four-digit code in the spaces provided.

Electronics and Electrical — SUBJECT TERM

0544 — SUBJECT CODE

U·M·I

Subject Categories

THE HUMANITIES AND SOCIAL SCIENCES

COMMUNICATIONS AND THE ARTS
Architecture 0729
Art History 0377
Cinema 0900
Dance 0378
Fine Arts 0357
Information Science 0723
Journalism 0391
Library Science 0399
Mass Communications 0708
Music 0413
Speech Communication 0459
Theater 0465

EDUCATION
General 0515
Administration 0514
Adult and Continuing 0516
Agricultural 0517
Art 0273
Bilingual and Multicultural 0282
Business 0688
Community College 0275
Curriculum and Instruction 0727
Early Childhood 0518
Elementary 0524
Finance 0277
Guidance and Counseling 0519
Health 0680
Higher 0745
History of 0520
Home Economics 0278
Industrial 0521
Language and Literature 0279
Mathematics 0280
Music 0522
Philosophy of 0998
Physical 0523
Psychology 0525
Reading 0535
Religious 0527
Sciences 0714
Secondary 0533
Social Sciences 0534
Sociology of 0340
Special 0529
Teacher Training 0530
Technology 0710
Tests and Measurements 0288
Vocational 0747

LANGUAGE, LITERATURE AND LINGUISTICS
Language
- General 0679
- Ancient 0289
- Linguistics 0290
- Modern 0291

Literature
- General 0401
- Classical 0294
- Comparative 0295
- Medieval 0297
- Modern 0298
- African 0316
- American 0591
- Asian 0305
- Canadian (English) 0352
- Canadian (French) 0355
- English 0593
- Germanic 0311
- Latin American 0312
- Middle Eastern 0315
- Romance 0313
- Slavic and East European 0314

PHILOSOPHY, RELIGION AND THEOLOGY
Philosophy 0422
Religion
- General 0318
- Biblical Studies 0321
- Clergy 0319
- History of 0320
- Philosophy of 0322

Theology 0469

SOCIAL SCIENCES
American Studies 0323
Anthropology
- Archaeology 0324
- Cultural 0326
- Physical 0327

Business Administration
- General 0310
- Accounting 0272
- Banking 0770
- Management 0454
- Marketing 0338

Canadian Studies 0385
Economics
- General 0501
- Agricultural 0503
- Commerce-Business 0505
- Finance 0508
- History 0509
- Labor 0510
- Theory 0511

Folklore 0358
Geography 0366
Gerontology 0351
History
- General 0578
- Ancient 0579
- Medieval 0581
- Modern 0582
- Black 0328
- African 0331
- Asia, Australia and Oceania 0332
- Canadian 0334
- European 0335
- Latin American 0336
- Middle Eastern 0333
- United States 0337

History of Science 0585
Law 0398
Political Science
- General 0615
- International Law and Relations 0616
- Public Administration 0617

Recreation 0814
Social Work 0452
Sociology
- General 0626
- Criminology and Penology 0627
- Demography 0938
- Ethnic and Racial Studies 0631
- Individual and Family Studies 0628
- Industrial and Labor Relations 0629
- Public and Social Welfare 0630
- Social Structure and Development 0700
- Theory and Methods 0344

Transportation 0709
Urban and Regional Planning 0999
Women's Studies 0453

THE SCIENCES AND ENGINEERING

BIOLOGICAL SCIENCES
Agriculture
- General 0473
- Agronomy 0285
- Animal Culture and Nutrition 0475
- Animal Pathology 0476
- Food Science and Technology 0359
- Forestry and Wildlife 0478
- Plant Culture 0479
- Plant Pathology 0480
- Plant Physiology 0817
- Range Management 0777
- Wood Technology 0746

Biology
- General 0306
- Anatomy 0287
- Biostatistics 0308
- Botany 0309
- Cell 0379
- Ecology 0329
- Entomology 0353
- Genetics 0369
- Limnology 0793
- Microbiology 0410
- Molecular 0307
- Neuroscience 0317
- Oceanography 0416
- Physiology 0433
- Radiation 0821
- Veterinary Science 0778
- Zoology 0472

Biophysics
- General 0786
- Medical 0760

EARTH SCIENCES
Biogeochemistry 0425
Geochemistry 0996
Geodesy 0370
Geology 0372
Geophysics 0373
Hydrology 0388
Mineralogy 0411
Paleobotany 0345
Paleoecology 0426
Paleontology 0418
Paleozoology 0985
Palynology 0427
Physical Geography 0368
Physical Oceanography 0415

HEALTH AND ENVIRONMENTAL SCIENCES
Environmental Sciences 0768
Health Sciences
- General 0566
- Audiology 0300
- Chemotherapy 0992
- Dentistry 0567
- Education 0350
- Hospital Management 0769
- Human Development 0758
- Immunology 0982
- Medicine and Surgery 0564
- Mental Health 0347
- Nursing 0569
- Nutrition 0570
- Obstetrics and Gynecology 0380
- Occupational Health and Therapy 0354
- Ophthalmology 0381
- Pathology 0571
- Pharmacology 0419
- Pharmacy 0572
- Physical Therapy 0382
- Public Health 0573
- Radiology 0574
- Recreation 0575
- Speech Pathology 0460
- Toxicology 0383

Home Economics 0386

PHYSICAL SCIENCES
Pure Sciences
Chemistry
- General 0485
- Agricultural 0749
- Analytical 0486
- Biochemistry 0487
- Inorganic 0488
- Nuclear 0738
- Organic 0490
- Pharmaceutical 0491
- Physical 0494
- Polymer 0495
- Radiation 0754

Mathematics 0405
Physics
- General 0605
- Acoustics 0986
- Astronomy and Astrophysics 0606
- Atmospheric Science 0608
- Atomic 0748
- Electronics and Electricity 0607
- Elementary Particles and High Energy 0798
- Fluid and Plasma 0759
- Molecular 0609
- Nuclear 0610
- Optics 0752
- Radiation 0756
- Solid State 0611

Statistics 0463

Applied Sciences
Applied Mechanics 0346
Computer Science 0984

Engineering
- General 0537
- Aerospace 0538
- Agricultural 0539
- Automotive 0540
- Biomedical 0541
- Chemical 0542
- Civil 0543
- Electronics and Electrical 0544
- Heat and Thermodynamics 0348
- Hydraulic 0545
- Industrial 0546
- Marine 0547
- Materials Science 0794
- Mechanical 0548
- Metallurgy 0743
- Mining 0551
- Nuclear 0552
- Packaging 0549
- Petroleum 0765
- Sanitary and Municipal 0554
- System Science 0790

Geotechnology 0428
Operations Research 0796
Plastics Technology 0795
Textile Technology 0994

PSYCHOLOGY
General 0621
Behavioral 0384
Clinical 0622
Developmental 0620
Experimental 0623
Industrial 0624
Personality 0625
Physiological 0989
Psychobiology 0349
Psychometrics 0632
Social 0451

Nom ____________________

Dissertation Abstracts International est organisé en catégories de sujets. Veuillez s.v.p. choisir le sujet qui décrit le mieux votre thèse et inscrivez le code numérique approprié dans l'espace réservé ci-dessous.

U·M·I

SUJET ____________________ CODE DE SUJET ☐☐☐☐

Catégories par sujets

HUMANITÉS ET SCIENCES SOCIALES

COMMUNICATIONS ET LES ARTS
Architecture 0729
Beaux-arts 0357
Bibliothéconomie 0399
Cinéma 0900
Communication verbale 0459
Communications 0708
Danse 0378
Histoire de l'art 0377
Journalisme 0391
Musique 0413
Sciences de l'information 0723
Théâtre 0465

ÉDUCATION
Généralités 515
Administration 0514
Art 0273
Collèges communautaires 0275
Commerce 0688
Économie domestique 0278
Éducation permanente 0516
Éducation préscolaire 0518
Éducation sanitaire 0680
Enseignement agricole 0517
Enseignement bilingue et multiculturel 0282
Enseignement industriel 0521
Enseignement primaire. 0524
Enseignement professionnel 0747
Enseignement religieux 0527
Enseignement secondaire 0533
Enseignement spécial 0529
Enseignement supérieur 0745
Évaluation 0288
Finances 0277
Formation des enseignants 0530
Histoire de l'éducation 0520
Langues et littérature 0279
Lecture 0535
Mathématiques 0280
Musique 0522
Orientation et consultation 0519
Philosophie de l'éducation 0998
Physique 0523
Programmes d'études et enseignement 0727
Psychologie 0525
Sciences 0714
Sciences sociales 0534
Sociologie de l'éducation 0340
Technologie 0710

LANGUE, LITTÉRATURE ET LINGUISTIQUE
Langues
- Généralités 0679
- Anciennes 0289
- Linguistique 0290
- Modernes 0291

Littérature
- Généralités 0401
- Anciennes 0294
- Comparée 0295
- Mediévale 0297
- Moderne 0298
- Africaine 0316
- Américaine 0591
- Anglaise 0593
- Asiatique 0305
- Canadienne (Anglaise) 0352
- Canadienne (Française) 0355
- Germanique 0311
- Latino-américaine 0312
- Moyen-orientale 0315
- Romane 0313
- Slave et est-européenne 0314

PHILOSOPHIE, RELIGION ET THÉOLOGIE
Philosophie 0422
Religion
- Généralités 0318
- Clergé 0319
- Études bibliques 0321
- Histoire des religions 0320
- Philosophie de la religion 0322

Théologie 0469

SCIENCES SOCIALES
Anthropologie
- Archéologie 0324
- Culturelle 0326
- Physique 0327

Droit 0398
Économie
- Généralités 0501
- Commerce-Affaires 0505
- Économie agricole 0503
- Économie du travail 0510
- Finances 0508
- Histoire 0509
- Théorie 0511

Études américaines 0323
Études canadiennes 0385
Études féministes 0453
Folklore 0358
Géographie 0366
Gérontologie 0351
Gestion des affaires
- Généralités 0310
- Administration 0454
- Banques 0770
- Comptabilité 0272
- Marketing 0338

Histoire
- Histoire générale 0578
- Ancienne 0579
- Médiévale 0581
- Moderne 0582
- Histoire des noirs 0328
- Africaine 0331
- Canadienne 0334
- États-Unis 0337
- Européenne 0335
- Moyen-orientale 0333
- Latino-américaine 0336
- Asie, Australie et Océanie 0332

Histoire des sciences 0585
Loisirs 0814
Planification urbaine et régionale 0999
Science politique
- Généralités 0615
- Administration publique 0617
- Droit et relations internationales 0616

Sociologie
- Généralités 0626
- Aide et bien-àtre social 0630
- Criminologie et établissements pénitentiaires 0627
- Démographie 0938
- Études de l' individu et de la famille 0628
- Études des relations interethniques et des relations raciales 0631
- Structure et développement social 0700
- Théorie et méthodes. 0344
- Travail et relations industrielles 0629

Transports 0709
Travail social 0452

SCIENCES ET INGÉNIERIE

SCIENCES BIOLOGIQUES
Agriculture
- Généralités 0473
- Agronomie. 0285
- Alimentation et technologie alimentaire 0359
- Culture 0479
- Élevage et alimentation 0475
- Exploitation des péturages 0777
- Pathologie animale 0476
- Pathologie végétale 0480
- Physiologie végétale 0817
- Sylviculture et faune 0478
- Technologie du bois 0746

Biologie
- Généralités 0306
- Anatomie 0287
- Biologie (Statistiques) 0308
- Biologie moléculaire 0307
- Botanique 0309
- Cellule 0379
- Écologie 0329
- Entomologie 0353
- Génétique 0369
- Limnologie 0793
- Microbiologie 0410
- Neurologie 0317
- Océanographie 0416
- Physiologie 0433
- Radiation 0821
- Science vétérinaire 0778
- Zoologie 0472

Biophysique
- Généralités 0786
- Medicale 0760

SCIENCES DE LA TERRE
Biogéochimie 0425
Géochimie 0996
Géodésie 0370
Géographie physique 0368
Géologie 0372
Géophysique 0373
Hydrologie 0388
Minéralogie 0411
Océanographie physique 0415
Paléobotanique 0345
Paléoécologie 0426
Paléontologie 0418
Paléozoologie 0985
Palynologie 0427

SCIENCES DE LA SANTÉ ET DE L'ENVIRONNEMENT
Économie domestique 0386
Sciences de l'environnement 0768
Sciences de la santé
- Généralités 0566
- Administration des hipitaux 0769
- Alimentation et nutrition 0570
- Audiologie 0300
- Chimiothérapie 0992
- Dentisterie 0567
- Développement humain 0758
- Enseignement 0350
- Immunologie 0982
- Loisirs 0575
- Médecine du travail et thérapie 0354
- Médecine et chirurgie 0564
- Obstétrique et gynécologie 0380
- Ophtalmologie 0381
- Orthophonie 0460
- Pathologie 0571
- Pharmacie 0572
- Pharmacologie 0419
- Physiothérapie 0382
- Radiologie 0574
- Santé mentale 0347
- Santé publique 0573
- Soins infirmiers 0569
- Toxicologie 0383

SCIENCES PHYSIQUES
Sciences Pures
Chimie
- Genéralités 0485
- Biochimie 487
- Chimie agricole 0749
- Chimie analytique 0486
- Chimie minérale 0488
- Chimie nucléaire 0738
- Chimie organique 0490
- Chimie pharmaceutique 0491
- Physique 0494
- PolymÇres 0495
- Radiation 0754

Mathématiques 0405
Physique
- Généralités 0605
- Acoustique 0986
- Astronomie et astrophysique 0606
- Electronique et électricité 0607
- Fluides et plasma 0759
- Météorologie 0608
- Optique 0752
- Particules (Physique nucléaire) 0798
- Physique atomique 0748
- Physique de l'état solide 0611
- Physique moléculaire 0609
- Physique nucléoire 0610
- Radiation 0756

Statistiques 0463

Sciences Appliqués Et Technologie
Informatique 0984
Ingénierie
- Généralités 0537
- Agricole 0539
- Automobile 0540
- Biomédicale 0541
- Chaleur et ther modynamique 0348
- Conditionnement (Emballage) 0549
- Génie aérospatial 0538
- Génie chimique 0542
- Génie civil 0543
- Génie électronique et électrique 0544
- Génie industriel 0546
- Génie mécanique 0548
- Génie nucléaire 0552
- Ingénierie des systômes 0790
- Mécanique navale 0547
- Métallurgie 0743
- Science des matériaux 0794
- Technique du pétrole 0765
- Technique minière 0551
- Techniques sanitaires et municipales 0554
- Technologie hydraulique 0545

Mécanique appliquée 0346
Géotechnologie 0428
Matières plastiques (Technologie) 0795
Recherche opérationnelle 0796
Textiles et tissus (Technologie) 0794

PSYCHOLOGIE
Généralités 0621
Personnalité 0625
Psychobiologie 0349
Psychologie clinique 0622
Psychologie du comportement 0384
Psychologie du développement 0620
Psychologie expérimentale 0623
Psychologie industrielle 0624
Psychologie physiologique 0989
Psychologie sociale 0451
Psychométrie 0632

INVESTIGATION OF FIELD QUANTITIES IN A 500 KV DC SWITCHYARD

BY

CHANGYI CHARLIE LU

A Thesis submitted to the Faculty of Graduate Studies of the University of Manitoba in partial fulfillment of the requirements for the degree of

MASTER OF SCIENCE

Table of Contents

ABSTRACT

In recent years environmental concern on electromagnetic fields has triggered a large amount of research work in this area. However there is very few concerning research in HVdc switchyard. It is of interest to study the electric field quantities in a dc switchyard.

Measurements of electric field intensity and ion current density were carried out over a five–month period in the 500 kV dc switchyard of Dorsey Converter Station of Manitoba Hydro. Initially a portable miniature field meter was used to measure the electric field at various locations in the switchyard at approximately 1m above ground level. Locations which yielded high values of electric field were chosen for data acquisition. A total of 37 ground level locations were chosen for measurement. At each location data was recorded once every five minutes over a three–day consecutive period. The electric field was also measured at 1m and 1.5m above ground and adjacent to a switch–line. Simultaneously complete weather information was compiled. The collected data was analyzed using a database approach.

Since the measured quantities are not only affected by wind and space charge but also influenced by surrounding bus conductors and system voltage, it is not unusual to observe both positive and negative readings at a location and at some locations these readings are comparable. The maximum value of the electric field at certain locations in the dc switchyard is much higher than that in 735 kV ac substations but comparable to corresponding values measured under the dc line.

It is shown that the dependence of the field quantities on wind is best examined by comparing the maximum and average values corresponding to different wind categories. Also assessment of the field quantities in the dc switchyard is best carried out by examination of average and maximum values corresponding to all wind speeds.

The Charge Simulation Method was used to calculate ground–level and above–ground electric fields in the vicinity of a switch–line. Five models are considered. It is concluded that good agreement between calculated and measured data can not be expected by using electrostatic simulation model because of excessive corona activity existing in a dc switchyard.

ACKNOWLEDGEMENTS

The author would like to express his special gratitude to his advisor Dr. M.R. Raghuveer for his valuable guidance, suggestion and patience during the course of this postgraduate study.

The author also wishes to thank Mr. Oliver C. Norris–Elye, Project Leader of Manitoba HVDC Research Centre for his valuable advice.

Funding provided by the Manitoba Hydro Research Committee and instrumentation made available by the Manitoba HVDC Research Centre are gratefully acknowledged.

Partial funding from NSERC Canada is also acknowledged.

Last but not least, the author sincerely thanks Mr. Norman J. Tarko for his excellent cooperation and assistance in experiments, for his innovative technical ideas, for his efforts in helping me accomplish this task, and for his kindness and being considerate to a foreign student.

List of Figures

List of Tables

SYMBOLS, DEFINITIONS, UNITS AND VALUES OF CONSTANTS

Symbol	Definition	Value	Unit
d	distance		m
$\mathbf{E}$	electric field strength vector		V/m
E	electric field strength magnitude		V/m
E_x	x component of electric field strength		V/m
E_y	y component of electric field strength		V/m
E_z	z component of electric field strength		V/m
$\mathbf{J}$	ion current density vector		A/m^2
u	electric potential		V
P	electric potential coefficient		V/C
P	electric potential coefficient		V/C
W	wind speed		Km/h
$\mathbf{a}_x$	unit vector in x direction		V
$\mathbf{a}_y$	unit vector in y direction		
$\mathbf{a}_z$	unit vector in z direction		

CHAPTER 1

Introduction

1.1 Environmental Concern about Electromagnetic Fields

Electric energy is generated at remote sites and then transmitted over long distances through high voltage ac or dc transmission lines to load centers. Transmission voltage levels vary and the maximum dc transmission line voltage in use to day is ± 500 kV. During the early years of high voltage transmission, little attention was paid to the possible environmental or health effects of the accompanying electric and magnetic fields and very few papers were published on this issue [1–3].

Public concern about power frequency fields first emerged in the late 1960's as utility companies turned increasingly to extra high voltage (EHV) transmission lines to efficiently handle the large increase in demand for electric energy. Public attention to EHV transmission lines focused first on the aesthetic impact of the large steel towers, on the aesthetic and ecological impacts of the right–of–way (R.O.W), and on the various nuisance effects created by the strong electric fields. These nuisance effects include audible noise (AN), TV/radio interference (TVI, RI), and induced shocks that can occur when a person standing beneath an EHV line touches a large ungrounded metal object such as a truck or a farm vehicle. By the early 1970s, the American National Standards Institute (ANSI) had issued voluntary standards to address the nuisance effects.

The first evidence that power frequency electric fields might have a direct effect on human health appeared in 1972 when Soviet investigators reported that workers in Soviet EHV switchyards suffered from a number of "nonspecific ailments" [4]. The Soviet investigators concluded that prolonged periods of work in 500 kV substations without protective measures result in a "shattering of the dynamic state of the central nervous system, the heart and blood vessel system, and in a changed blood structure". Also young men complained of reduced sexual potency. As a result of the studies, the duration of unprotected exposure to field strengths above 5 kV/m was restricted in the USSR. Furthermore, substations were provided with an intricate system of shields to reduce the field strength in working areas.

The conclusions of the Soviet researchers alarmed transmission engineers in the western world and triggered research work in this new area in spite of the contradictory conclusions obtained in earlier work in Ohio and Maryland in USA in 1960s [1]. Further research on the environmental impact of fields covered a wide range of areas which included:

1. electrical measurements at different locations in power system, i.e. beneath transmission lines, in substations and in residential areas [5–26]
2. research on biological effects of the electric and magnetic fields including the biophysical mechanism of interaction of electric and magnetic fields [27,28].
3. human epidemiological studies regarding childhood cancer, adult cancer, occupational cancer and other possible bioeffects [29,30].

Until the 1970s most of the research and survey work was focused on the effects of electric fields produced by power transmission lines. Later, in the 1980s continuing research, especially involving studies of human epidemiology study, revealed that the magnetic fields should also be regarded as a potential health risk. Thereafter, much research was directed to the effects of magnetic fields. Since distribution power lines carrying high current are a major source of electromagnetic fields in urban settings, they quickly became the target of environmental groups.

In spite of contradictory interpretation of research results, electric and magnetic fields were deemed to be a threat to public health by environmental agencies and environmental community activists. Since 1985, more than one hundred lawsuits have been launched in the United States. Reference 31 contains cases covering the period 1985 – 1994 involving court confrontations between the communities/environmental organizations and utilities/government organizations over the adverse environmental effect of the electric and magnetic fields. This information was downloaded via Internet at freenet.carleton.ca in Ottawa, Canada and is free and open to public access.

Three typical cases are cited below involving conflicts between community/school and local utility companies [31].

Case One: Santa Monica, California, USA, 1992

The Kenter Canyon Elementary School in Brentwood, a wealthy suburb of Santa Monica, California is located beside a 230 kV and two 138 kV transmission lines. When magnetic field levels of nearly 1.2 uT were measured in the school–yard in the spring of 1992, school authorities and parents pressured the utility to do something about the problem. Since then the utility has re–phased the lines, reducing the magnetic fields by fifty per cent, and has announced that it is planning to take measures to further reduce the magnetic field levels.

Case two: British Columbia, Canada, 1989

BC Hydro has offered to pay a fair market price to landowners concerned about increased electromagnetic fields (EMFs) from a new 230 kV power line on Vancouver Island, although they claim there is no reason to believe the line poses a health risk. 90% of those eligible have indicated an interest in the purchase offer.

Since then the British Columbia Utilities Commission has ordered BC Hydro to stop all work on the line until a public inquiry could be held into the safety of the line and ordered it to extend its offer to buy the homes along the right–of way until September 15, 1989.

Case three: Rhode Island, USA, 1990

On October 9, 1990 the town council of East Greenwich, RI, banned all new power lines above 60 kV for three years. The ordinance came about in response to widespread citizen concern about the EMFs from proposed new 345 kV and 115 kV lines which the Narragansett Electric Company plans to run through parts of East Greenwich. This is the first moratorium on power line construction in the U.S.

Rhode Islanders for Safe Power (RISP) pushed for the three–year moratorium because of the need for further research on the health effects of EMFs and because it "was the least noxious formula and most likely to be sustained by the PUC." RISP's Ed Seiler told Microwave News.

The nearby towns of Coventry and Foster have followed East Greenwich's lead by passing moratoriums of their own, and a state–wide ban on high voltage power lines was proposed during the 1991 legislative session.

1.2 Overview of Previous Research in Electric Power System

1.2.1 General Views and Methods

As pointed out in the previous section, electromagnetic fields have become a major environmental concern. Power utilities are increasingly required to design transmission lines to reduce environmental effects to acceptable levels to meet rigid regulations.

Knowledge of the strength of the electric and magnetic fields under power transmission lines and in substations is useful in optimizing future transmission line and substation design and to provide accurate information for medical research and for safety criteria determination. Some research results related to on–site field measurements have been published [8,14,16–21,26]. This information has been used to draw up regulations which are often in variance.

For example, Russian investigators have specified maximum exposure times (Table 1.1) to electric fields for linemen working in substations; these times should not exceed over a 24 hour period [4].

Electric field (kV/m)	Permitted residence time
5	unlimited
10	180 minutes
15	90 minutes
20	10 minutes
25	5 minutes

Table 1.1 Maximum exposure times set by USSR.

These values of residency time assume that the maximum field to which a subject is exposed is less than 5 kV/m for the rest of the day.

Other researchers considered the induced currents inside a human body and proposed different threshold values of the electric field strength: Barber [5] proposed a ground level threshold of 10 kV/m ac to limit the short circuit current when a person touches a parked vehicle below an ac transmission line. Similarly, Balderston [6] proposed a maximum field strength of 14 kV/m while Barnes [7] suggested 15 kV/m, both referring solely to the physical perception at such field strength levels.

A survey made by IREQ, the Research Institute of Hydro–Quebec has shown [9] that a large divergence exists in published experimental results: while some authors reported negligible effects due to a certain field strength, others reported pronounced effects under similar conditions.

Despite controversial interpretation of field measurement results, it is commonly agreed [16] that further research to provide more detailed information regarding electric and magnetic fields is very important and should be continued. The accumulated information will be used to compare and improve transmission line and substation design and to specify conditions applicable to biological experiments. Such research will eventually lead to formulation of realistic safety regulations.

Calculation and on–site measurement of electric and magnetic fields are among those frequently used methods for field analysis below transmission lines and in substations. The calculation method is often used in the preliminary planning stage and in research and development work. Measurement, in addition to provide measured data, can also be used to verify the validity of the construction of simulation models by comparison of calculated and measured values on existing structures. Calculation methods are usually unable to model precisely the complex configuration in a substation; in such cases measurements are preferred [9,16].

1.2.2 Transmission Line Fields

Considerable research work concerning the electric and magnetic fields of ac power transmission lines has been carried out over the past decades. Measurements of electric and magnetic fields were usually taken at ground level, i.e. from 0 – 2 meters above ground to obtain lateral and longitudinal characteristics of field strengths obtained. Figure 1.1 shows a typical electric field distribution in the cross–sectional plane of a HVac transmission line.

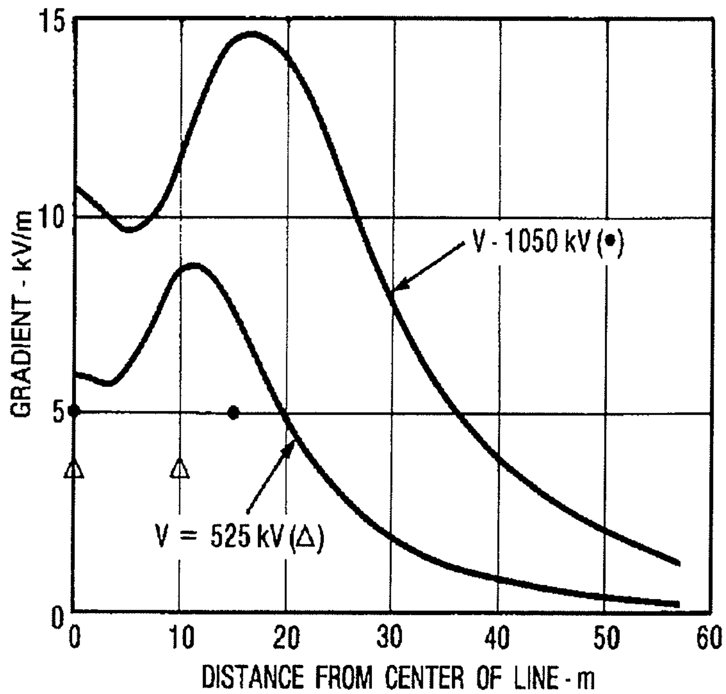

Fig.1.1 Typical electric field profile in a cross–sectional plane of an HVac transmission line [13]

Besides the operating voltage levels and physical configurations of HVac lines, other factors which may affect the measurement have been taken into consideration, i.e. screening effect of grounded objects such as vegetation, trees and buildings whose conductivity is high enough to distort the electric field around them. In general, the screening effect results in an enhancement of the electric field above the object and a reduction of the electric field around it out to a distance of the order of its height.

Since most of the measurements were carried out under selected fair weather conditions, there is a lack of meteorological information, or more importantly, its influence on the measurements.

Calculation models have also been developed under different assumptions. The most often used electrostatic models are quite straightforward and use a two dimensional approach which is shown to be sufficiently accurate [32]. It has been reported that good agreement with measured data can be obtained when the ground plane is reasonably flat.

1.2.3 Substation Fields:

Over the past twenty years, many series of electric field measurements in high voltage and extra–high voltage stations have been conducted and reported. Since the ground level electric field is attributable to every electrical component, calculation of the maximum field strength and field distribution is a formidable task. In order to describe quantitatively the electric field environment, the field strength must be obtained. In general, three approaches have been used:

1. Calculation approach: The calculation of electric fields is possible for relatively simple configurations. Several calculation models have been recommended. However, theoretical calculations of station fields are very difficult due to the three dimensional nature of substation configurations. The calculation usually yields some useful information of local field strengths and field distribution, but results cannot be generalized.

Almost all numerical calculation models are based on the Charge Simulation Method, which is especially suitable for analyzing an unbounded problem. In the application of this method, necessary simplifications are introduced due to the physical complexity of substations.

2. Scale model approach [33]: In this approach, the entire station is modeled according to a linear scale factor. Miniature probes are used to measure the electric field. This

method proves quite effective, though the construction of a scaled–down model is a painstaking exercise. Besides, the versatility in simulation is limited.

3. Field measurement approach: For substations of complex geometrical structures, it is very difficult to analyze the field characteristics by using analytical or scaled–down models. Therefore field measurement is often the only recourse. Furthermore, initial determination of electric fields, whether by calculation or by scaled–down modeling, must be verified by direct field measurements.

The electric field strength is measured by field strength meters. Apparently a large number of tests must be conducted before general observations can be made. Although this method is time–consuming, knowledge of electrical quantities can be accumulated and test results are reliable.

From the existing data in literature pertaining to HVac substations with operating voltage levels from 138 to 765 kV, some common observations can be made [9,12,16,18,21]:

1. The maximum electric field strengths are close to or higher than those under overhead lines of the same operating voltage level due mainly to the congregation of station conductors and equipment.

2. Higher values of ground level fields are measured in the vicinity of electrical apparatus such as circuit breakers whose clearance of the bus connection is usually the lowest.

3. The maximum field strengths are confined to a very small area. Also electric field strengths can be reduced by a proper phasing arrangement.

1.3 Objectives of this Thesis

Concerning dc substations, the few papers that have been published have centered around electromagnetic field measurements conducted near ac/dc converter valves and beneath HVdc transmission lines [10,25,26]. There is no data concerning field quantities in a dc switchyard. Although a HVdc switchyard is not normally accessible to the public, the electric field distribution is of concern to a utility and to its switchyard maintenance staff. In an HVdc switchyard, the fields are expected to be higher than those under HVdc transmission lines. Furthermore, no benefits can be derived from phase cancellation as in ac fields. Also the field strengths within a dc switchyard are highly dependent not only upon the operating voltages and station configuration, but also on prevailing weather conditions. This latter aspect has not been dealt with in existing literature.

In this thesis, the author presents the results of field measurements in the HVdc switchyard of the Dorsey Converter Station of Manitoba Hydro as well as results of computer simulation of the electrostatic field distribution in the same switchyard. There were two types of measurements involved: ground level measurements and measurements above ground. Ground level measurements of electric field and ion current density were carried out at a total of 37 locations in the switchyard. Above–ground measurements of the electric field were carried out at locations near switch–lines at heights of 1.0m and 1.5m. The measurement locations were chosen based on the results of initial measurements. The recorded field quantities together with weather and system parameters were processed and analyzed by using a database approach.

The calculated results were compared with measured data and conclusions were made upon data analysis and comparison.

CHAPTER 2

Instrumentation Used in Field Measurements

2.1 Description of Measuring System

Two electrical field quantities were measured. They are the electric field strength (E: kV/m) and ion current density (J: nA/m^2). Ground level electric field strength and ion current density were measured by using the IREQ field mill and Wilson plate respectively. An additional miniature field probe was used for measuring electric field components above ground level.

2.1.1 The IREQ Field Mill:

An IREQ field mill was used for measuring the dc field strength at ground level. This equipment consists essentially of two parts [34]:

1. 16 probes in two groups of eight
2. central conditioning unit

The probes:

The function of the probes is to measure the ground–level dc electric field strength within the range from 0.2 to 100 kV/m and its polarity. Each probe is comprised of a mechanical and an electronic part. A rotating mechanical electrode serves to convert the dc electric field signal into a 210–Hz ac field signal, which is then amplified, filtered and converted into a dc signal proportional to the strength of the measured electric field. This dc voltage is subsequently encoded in digital form and transmitted to the central conditioning unit via a standard 300–baud communication interface (modem). Fig. 2.1 shows a picture of this field mill with the associated analyzer. The housing of this field mill measures 171mm in diameter and 178mm in height.

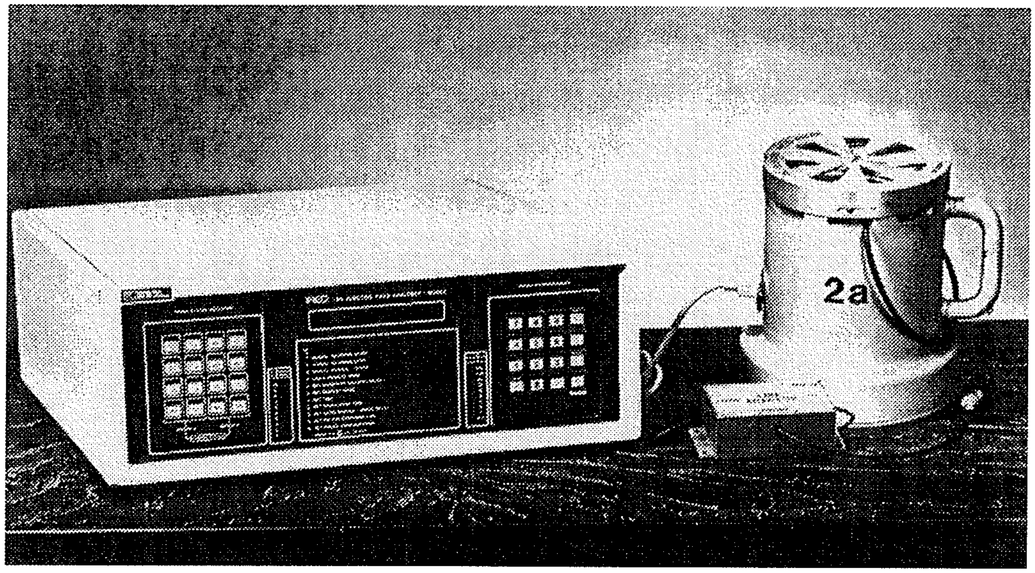

Fig.2.1 The IREQ field mill with the analyzer

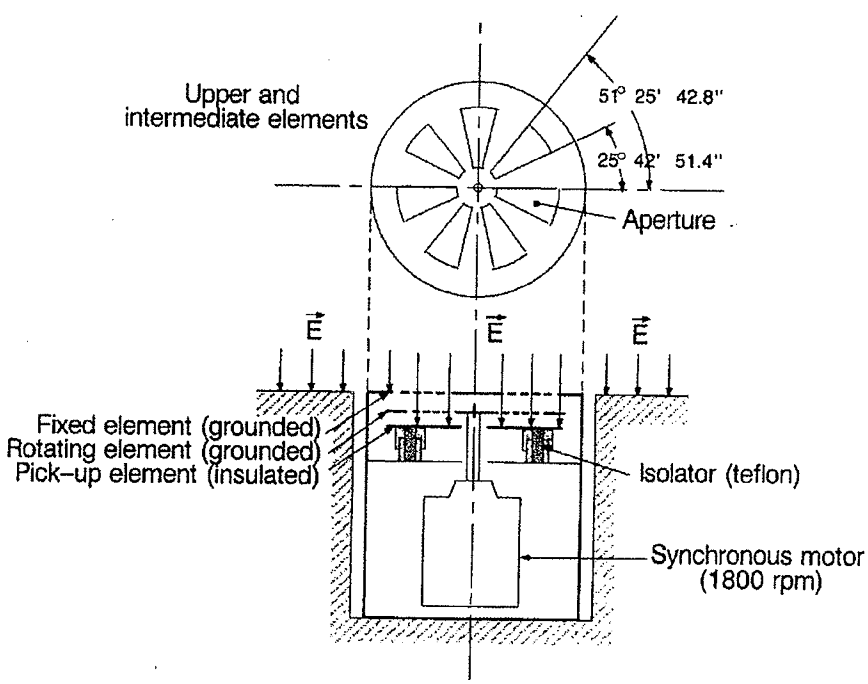

Fig.2.2 Mechanical details of the probe

More clearly shown in Figure 2.2, the probe consists of three superimposed disk–shaped elements, i.e grounded fixed element, grounded rotating element and insulated pick–up element. The upper and middle elements each contain seven apertures located radially and evenly around the axis of rotation. The rotating middle element is driven by a synchronous motor at 1800 rpm. The lower element is a solid disk fixed to four Teflon supports so that it is well insulated electrically from the housing.

The electric flux passing through the seven apertures in the fixed upper element is either fully or partially detected by the lower element, depending on the relative position of the apertures in the rotating middle element. Thus a current varying according to the speed of the rotating element multiplied by seven is generated in the sensing electrode.

The signal obtained is quasi–sinusoidal and has a frequency of

$$\frac{1800 \times 7}{60} = 210 \ Hz$$

The electronic part of the probe consists of an analog–input circuit, an encoder/decoder and a probe heating and status monitoring circuit.

The function of the analog input circuit is to amplify, filter, convert and match the current signal generated from the mechanical part of the probe as illustrated in Figure 2.2.

After receiving the dc signal from the analog input circuit, the encoder/decoder converts it into a binary code and transmits it via the modem. The encoder/decoder also serves to decode binary instructions from the central unit for controlling the probe scan, data transmission and probe self–check times.

Other units include a temperature controller for the analog–input circuit as well as a status detector for the probe's synchronous motor and a high and low temperature detector for the box housing the analogue circuits.

The central conditioning unit:

The function of the central conditioning unit is to switch on each probe in turn, decode its signal, process this signal and display the absolute value at its various outputs. It controls all 16 probes, allowing the data to be scanned on all 16 probes in 2 seconds. For this purpose, the probes are divided into two groups of eight, each group connected to the central unit by its own communication link. Therefore two separate modems are used in the central unit, both powered by two microprocessor–controlled units.

2.1.2 The Wilson Plate

A Wilson plate was used to measure the ground–level intensity and polarity of an ion current produced by the movement of ions due to the presence of high voltage dc structures in surrounding areas. It has a dynamic range from 100 pA to 100 nA/m^2.

This Wilson plate, or ion current analyzer, has a similar structure as the IREQ field mill. It comprises of three parts [35]: the probes, a central conditioning unit and associated communication links. The major difference between the IREQ field mill and the Wilson plate lies in the mechanical part of the probes. The mechanical part of the Wilson plate consists of a square aluminum plate, 1m by 1m, insulated from its support by four Teflon spacers as shown in Figs. 2.3 and 2.4. A sealed aluminum cylinder houses the electronic circuits that process the current signals generated by the ions sensed by the square plate.

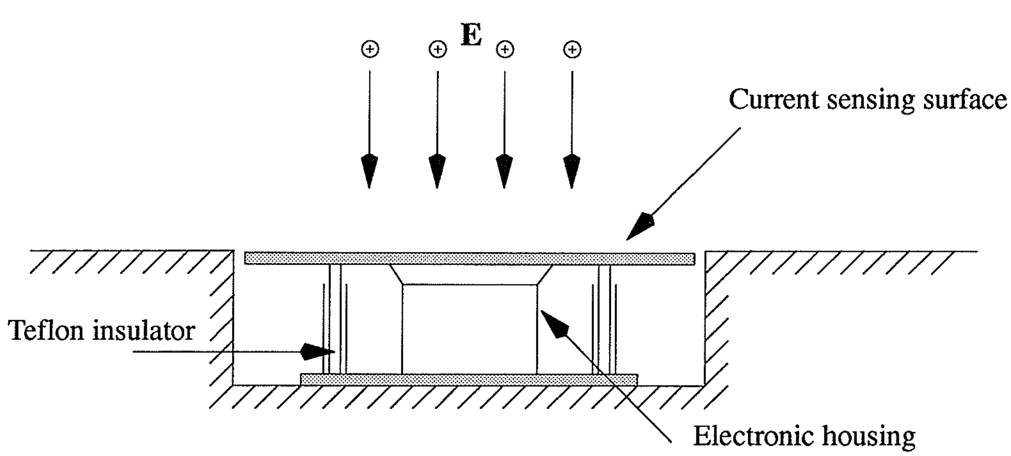

Fig.2.3 Sketch of the Wilson plate

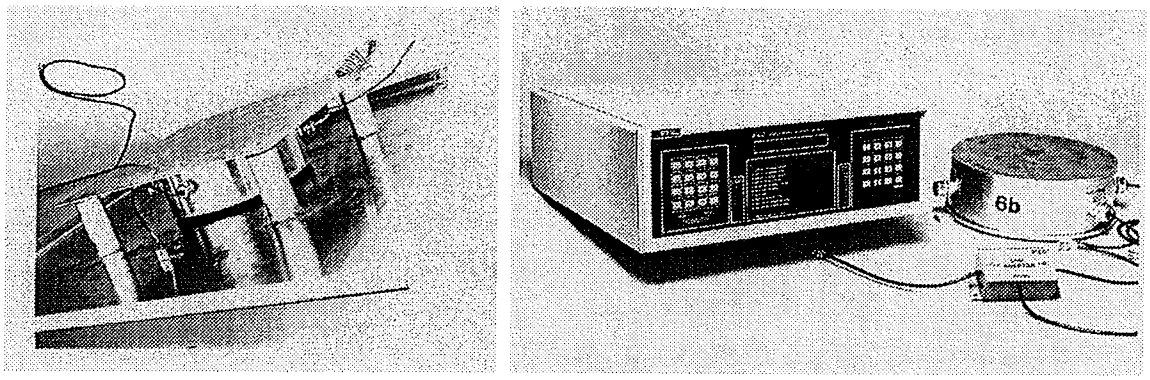

Fig.2.4 The Wilson plate
Left: the Wilson plate (up side down)
Right: the housing of the Wilson plate and the analyzer

All the electronic parts of the Wilson plate including the central conditioning unit and the communication links are similar to if not exact as those in the IREQ field mill.

2.1.3 The Miniature Field Meter

A portable space–potential electric dc field meter was used to measure both the horizontal and vertical components of dc electric fields above ground. It has an operating range from about 30 V/m up to about 500 kV/m in space, with or without presence of ions in the field being measured [36].

This miniature field meter consists of a rotating probe and a receiver, connected by a support pole containing three optical fibers and one air hose. Fig. 2.5 shows the probe and its complete system. A rotating probe, at the end of a fiberglass pole senses the field and communicates recordings of its direction and magnitude to a remote readout device. Fiber optical cable is used to minimize field perturbation due to the presence of the miniature field probe.

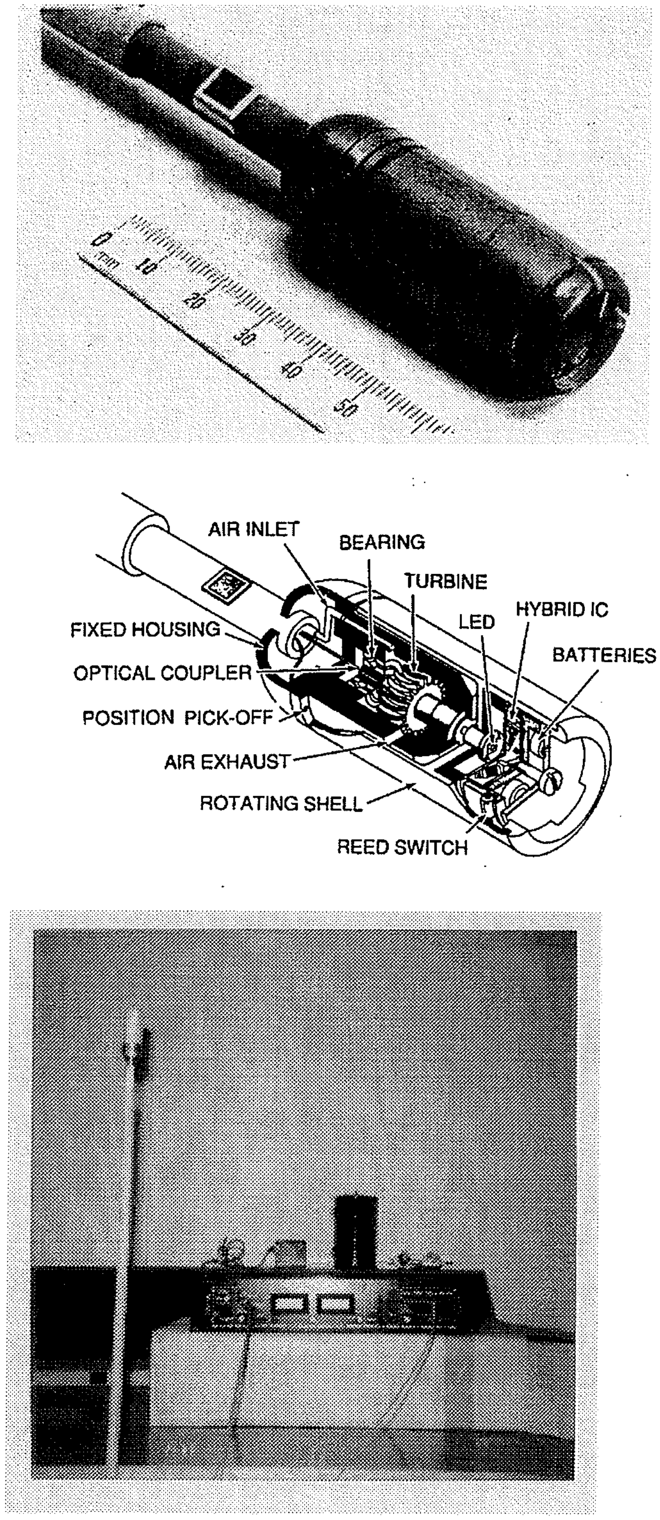

(a)

(b)

(c)

Fig.2.5 Illustration of the miniature field probe
(a) : Miniature probe
(b) : Cut–view of the sensor probe
(c) : Complete system including probe, cable, analyzer etc.

2.2 Instrument Checks and Calibration

Standard calibration procedures are available only for measurements of ac electric fields [37]. For instruments used in dc field measurement, users have recourse to manufacturer's instructions and common knowledge in certain specific areas.

2.2.1 Check of the IREQ Field Mill

The initial laboratory calibration of the field mill was carried out under controlled conditions which included the generation of an electric field with and without ion current by the manufacturer. Prior to site measurements of the electric field, a laboratory check of the field meter was performed in a uniform field provided by a calibration cage comprising of a 1m x 1m x 1m cube, as illustrated in Figure 2.6. The vertical sides of the cage were lined with 20 horizontal wires and were interconnected by twenty one 2 MΩ resistors. The top and bottom of the cube consisted of aluminum plates. The bottom plate has a hole in the center through which the top of the field mill resides flush. A dc voltage was applied between the two aluminum plates to form a uniform field.

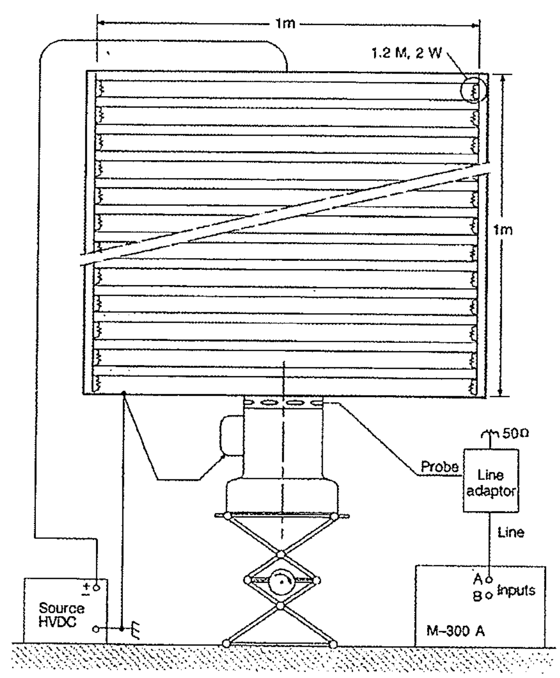

Fig.2.6 Calibration circuit for IREQ field mill

According to its manual, this dc field mill requires very little maintenance as far as the central conditioning unit is concerned. Nevertheless, due to exposure of the probe to various working conditions, periodic checks are recommended. The frequency and extent of such checks are best determined by means of site checks which provide an opportunity to remove the inevitable pollution which may cause measuring errors.

In practice, prior to relocating the field mill to a new test location, all exposed parts were cleaned and calibrated using a portable plate device which fit parallelly over the head of the field mill (Figure 2.7). The separation between the plate and the ground plane was fixed at 0.023 meter. A known voltage (±5V) was imposed on the portable plate to set up an electric field for the IREQ field mill and the reading could be used to assess the accuracy of the field mill by comparing with the calculated value, which was the voltage divided by the plate separation.

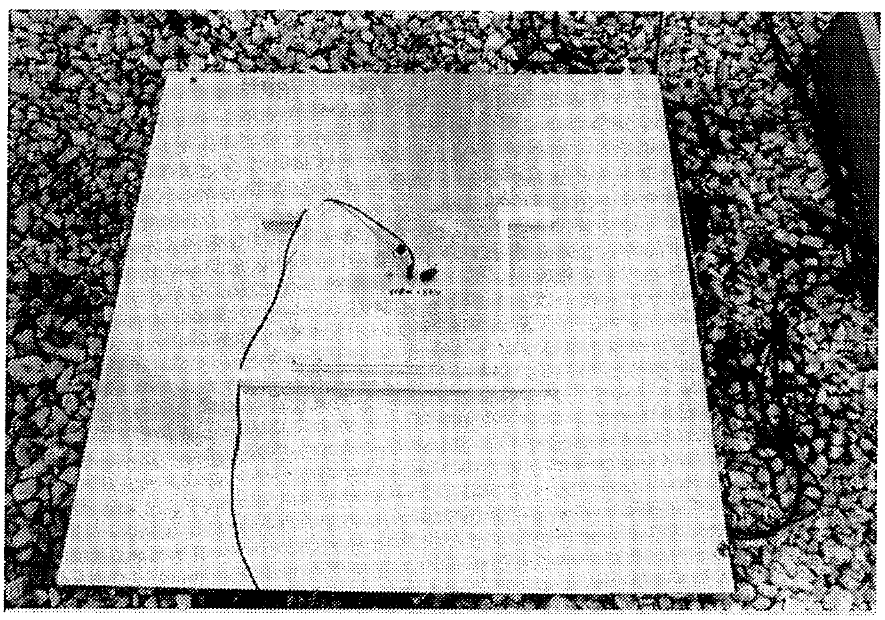

Fig.2.7 On–site check of IREQ field mill

2.2.2 Check of the Wilson Plate

The Wilson plate was checked using the calibration circuit shown in Figure 2.8.

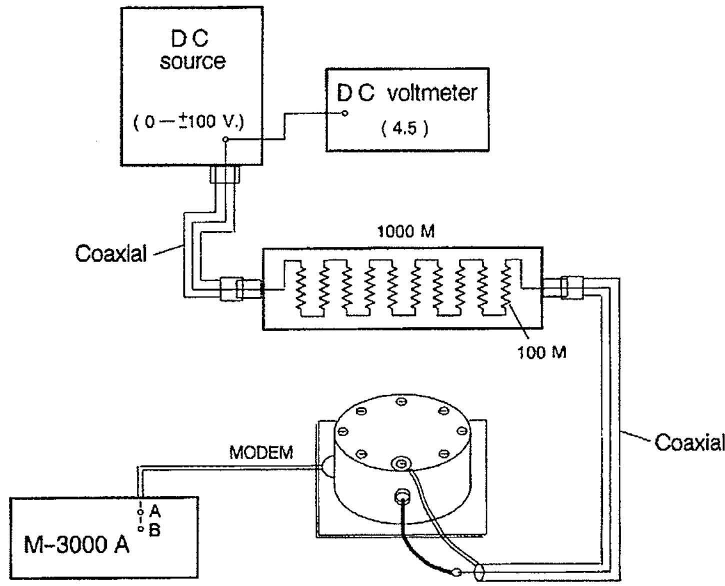

Fig.2.8 Calibration circuit for Wilson plate

In order to effectively check the Wilson plate, a high impedance current source was required. The high impedance current source was a combination of a dc source and high resistors as illustrated in Figure 2.8.

2.2.3 Check of the Miniature Field Meter

Because the miniature field meter operates with an isolated probe, a separate calibration with and without space charge is not necessary; a simple electrostatic field suffices.

Calibration was performed in the same field cage as used for the calibration of the IREQ field mill. Held by a tripod, the probe was centered in the calibration cage; with a known field applied, the calibration was readily checked. Both the magnitude and direction of readings were obtained.

2.3 Data Acquisition System

Three self-contained data acquiring instruments, or data loggers, were used for recording all signals. Each contained mainly a Rustrak Ranger II data logger. These data loggers together with previously mentioned measuring instruments formed three separate data acquisition systems.

The first data acquisition system included a data logger, the IREQ field mill and the Wilson plate which enabled compilation of data concerning electrical effects. This data logger, as part of the on site measurement system, was housed in a protective container on the site (Figure 2.9). The raw data recorded from the IREQ field mill and the Wilson plate were periodically down–loaded to floppy discs via a micro–computer.

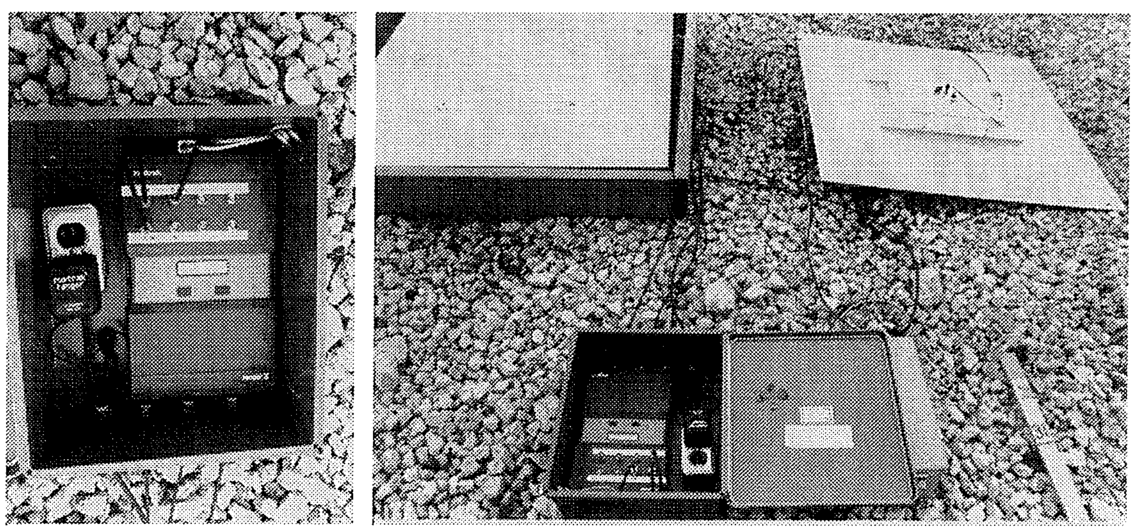

Fig.2.9 Data acquisition instruments
Left: a data logger Right: On–site data acquisition system

The second data acquisition system included another data logger for measurement of pole voltages derived from outdoor voltage dividers. The third one consisted of a data logger and a computerized monitoring system for collecting meteorological parameters, such as wind speed and direction, temperature, relative humidity and pressure. The absence or presence of rainfall was also recorded. The later two data acquisition systems were part of the Dorsey station instrumentation system and their recordings could be down–loaded and copied on to floppy discs.

Because data from all three systems were to be merged and compiled into a spreadsheet, a preset data retrieving frequency was required to keep a synchronous recording. This frequency was set at once every five minutes.

2.4 Database Approach for Data Analysis

To deal with large amount of measured data obtained from various measuring instruments and to analyze the possible relationship among them, it was indispensable to adopt database applications, or in this case simply the spreadsheet applications. Database software, the Microsoft Excel (v3.0), was used to process the collected data. As described in the previous section, raw data was stored in floppy discs. The data on the floppy discs was restored and combined to form a spread sheet in the database environment. Once in spreadsheet, raw data had to be processed and converted into "real" data by multiplying certain scale factors depending on polarities of the data and the configuration of the measurement system. Then different types of measured data under each title were formed into database. Data analysis was carried out by performing statistical calculations upon selecting criteria.

CHAPTER 3

Site Measurement Procedures

3.1 Switchyard Examination

Initially the switchyard was examined in order to choose proper locations where site measurements could be carried out.

The Dorsey ac/dc converter station consists of mainly four parts: a dc 500 kV switchyard, a valve and thryster building, an ac 500 kV switchyard and an ac 230 kV switchyard. Figure 3.1 shows a bird's–eye view of the 500 kV dc switchyard. This photograph was taken from the roof of the valve and thryster building.

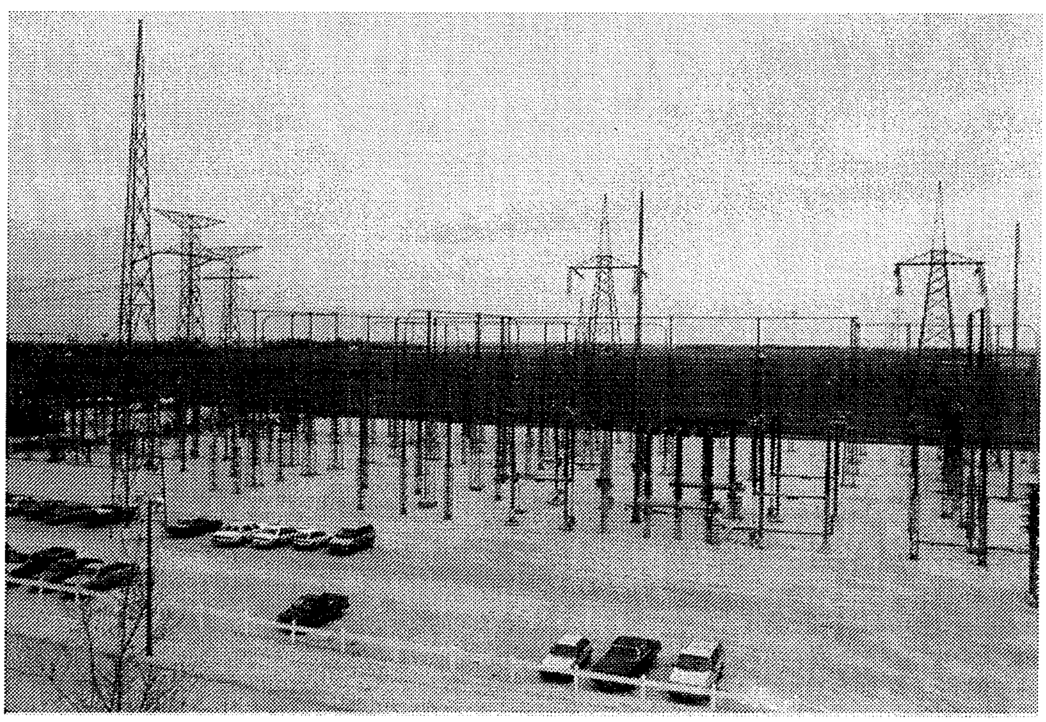

Fig.3.1 Bird's–eye view of the 500kV dc switchyard.

Figure 3.2 shows the detailed configuration of the dc switchyard whose major components are high speed line switches (HSLS), disconnectors, dc transductors, bus conductors, bus supporters and towers.

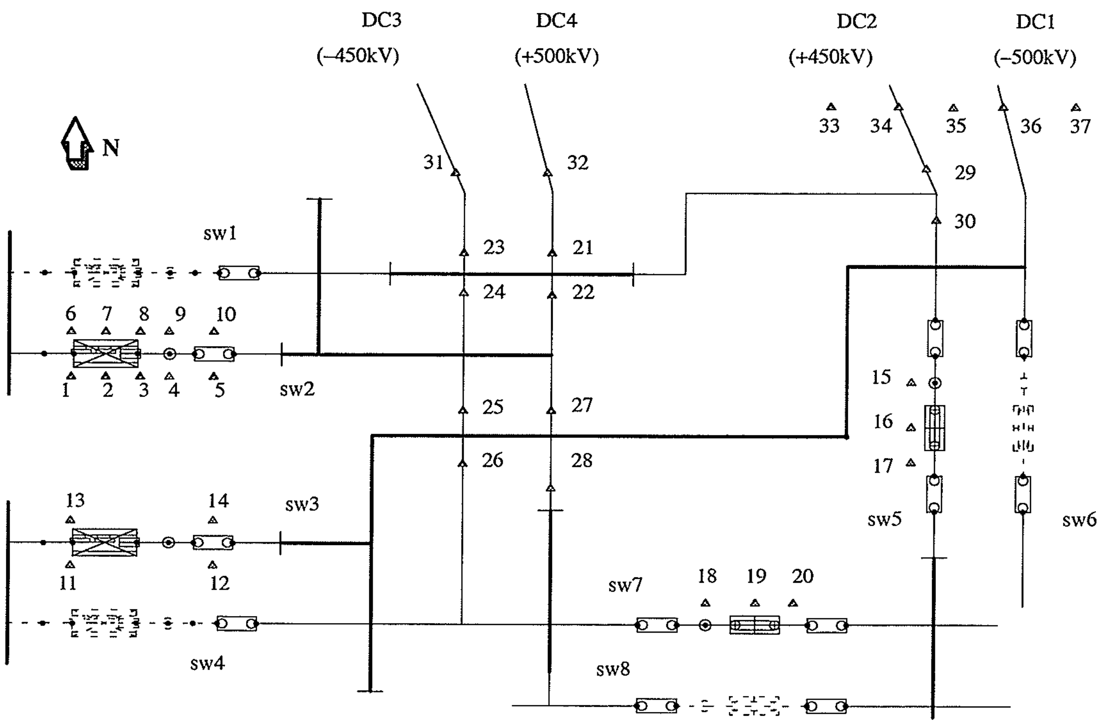

Fig.3.2 Partial layout of the dc switchyard (Scale: 10 m)

sw: switch–line : disconnect switch : high speed line switch without metal support structure

⊙ : transductor ▴ : ground level measurement location : high speed line switch with metal support structure

There are eight switch–lines in this switchyard, two at the east edge, two at the south edge and four at the west edge. Half of these switches were not energized, i.e. dead or not in use. These de–energized switch–lines are represented by broken lines in Fig. 3.2. The high speed line switches in switch–lines sw1 to sw4 have additional metal support structures (see Fig. 3.3); other switches in the remaining four switch–lines, i.e. sw5 to sw8, are not similarly equipped (see Fig. 3.4). Figures 3.3 and 3.5 show close–up pictures of the high speed line switches.

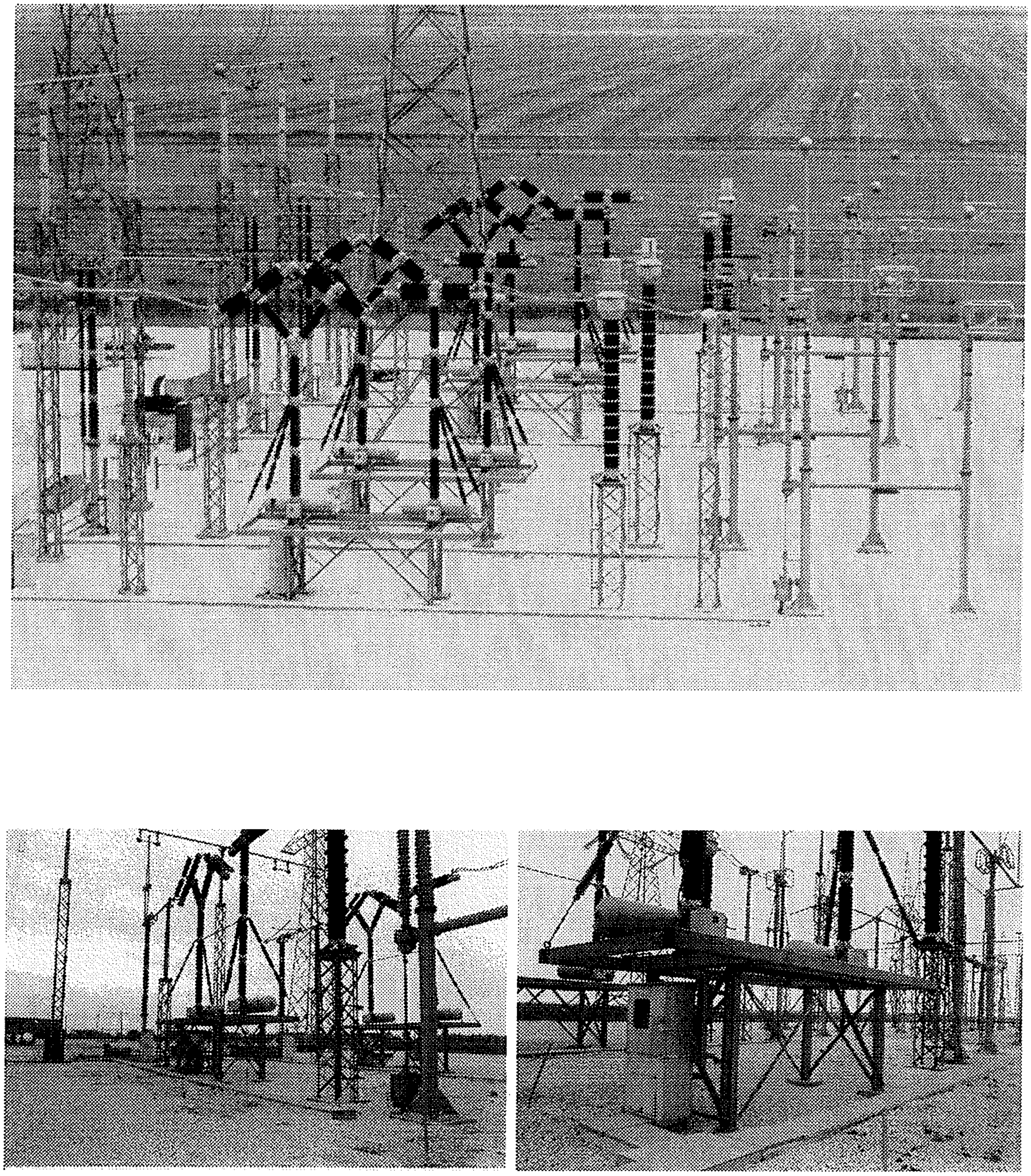

Fig.3.3 Switch–lines with high speed line switches equipped with metal support structures (sw1 – sw4) at west edge of the switchyard

Upper: Switch–lines sw1 – sw4

Bottom: Close–up pictures of metal supports of HSLS

Figure 3.5 shows close–up pictures of the high speed line switches with and without metal supports.

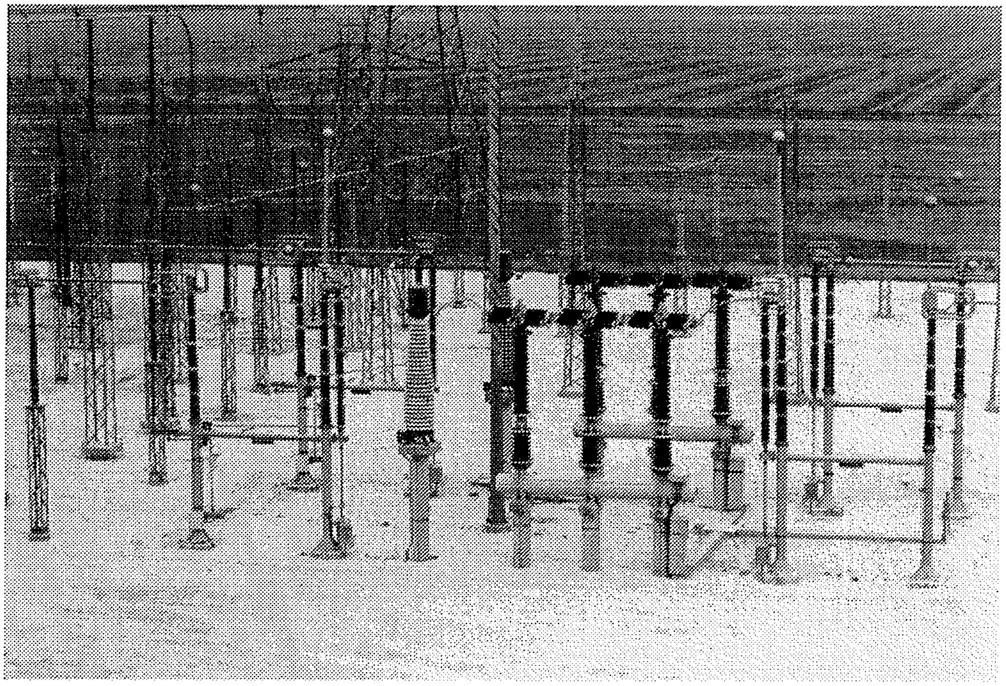

Fig.3.4 Switch–lines with high speed line switches not equipped with metal support structures (sw7 & sw8) at south edge of the switchyard

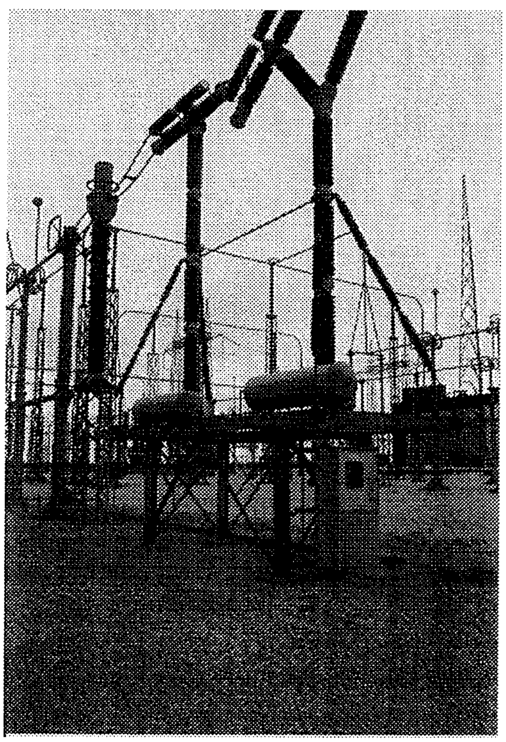

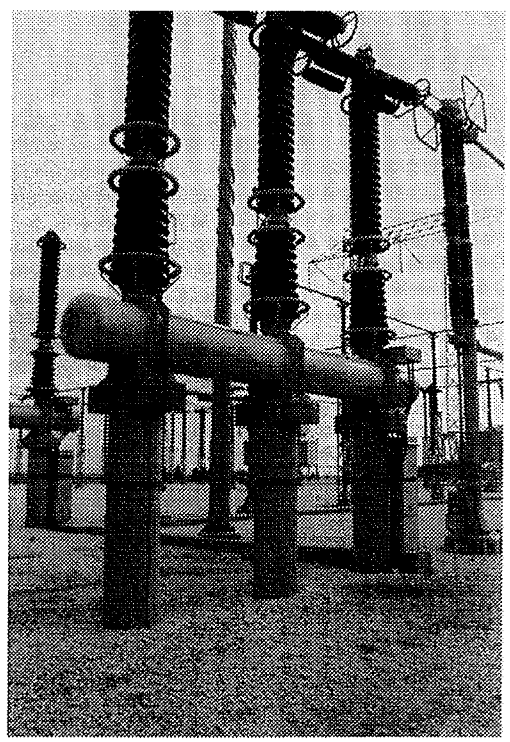

Fig.3.5 Close–up pictures of high speed line switches with and without metal supports

Left: high speed line switch with metal support structure

Right: high speed line switch without metal support structure

Figure 3.2 also shows that incoming lines, which enter the switchyard from the north, are connected to the switchyard through switch–lines sw2, sw3, sw5, and sw7. Bus conductors, inter–connecting the incoming transmission lines, have two elevations, the higher ones at about 19 meters and the lower ones at about 10 meters, represented by heavy and thin solid lines in Fig. 3.2 respectively. The inter–connection of the transmission line and the substation bus conductors is shown in Fig. 3.6.

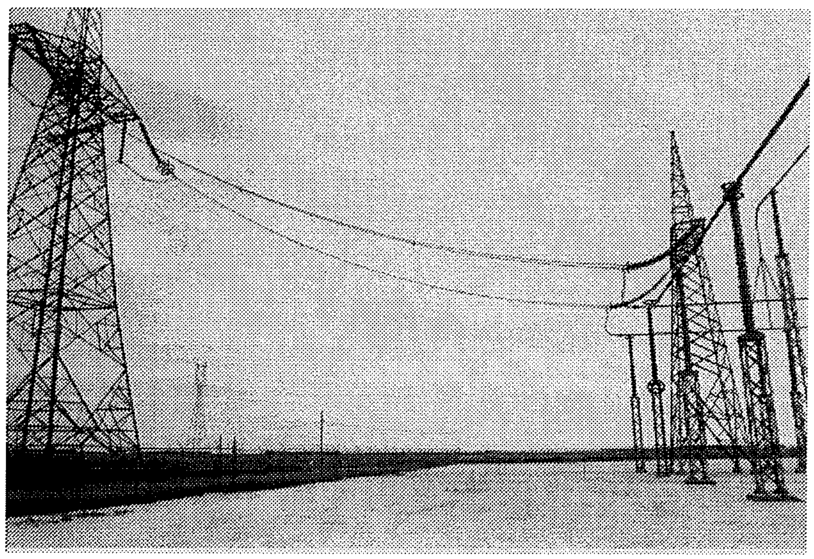

Fig.3.6 Incoming lines from HVdc TL tower (left) to switchyard buses (right)

Influence from ac sources in this converter station is negligible because the ac sources are separated from this dc switchyard by a tall building housing the valves, controlling system and offices of the converter station.

3.2 Determination of measurement locations

It is impractical and unnecessary to divide the whole switchyard area into a fine mesh of grids and then measure at each node to obtain the field information in the switchyard. Theoretical analysis and previous publications support the fact that high field intensities are recorded only in a small percentage of the total area in a switchyard. These areas are usually in the vicinity of switches and current transformers where lower conductor elevations are observed.

In order to acquire a general knowledge of the electric field distribution within the switchyard, the miniature field meter was initially used to measure the electric field strength at various locations in the switchyard at one meter above ground level. These trial measurements yielded higher electric field values in the vicinity of the high voltage dc switch–lines. This was in agreement with analogous analysis and previous observations as mentioned above.

In addition, consultation with Manitoba Hydro personnel at Dorsey station proved that these areas are the most frequently accessed by maintenance staff. Therefore, full measurements were carried out at these selected areas.

Besides locations near switch–lines, other interesting locations in the switchyard were also chosen for measurement: for example, those beneath incoming lines and under bus conductors as indicated in Fig. 3.2.

3.3 Measurement procedures

Once a measurement location was selected, a hole was dug to house the IREQ field mill. The depth of the hole was such that it could accommodate the cylindrical housing of the IREQ field mill with its upper surface flush with the ground. A 1m by 1m aluminum square plate was also used to provide a flat surrounding although the ground in the switchyard was rather flat and devoid of vegetation.

The Wilson plate was always located within half a meter adjacent to the IREQ field mill. It is supposed to be as close as possible to the IREQ field mill so that both the electric field and ion current density readings can be regarded as belonging to the same location.

Figure 3.7 shows some of the measurement settings in the dc switchyard.

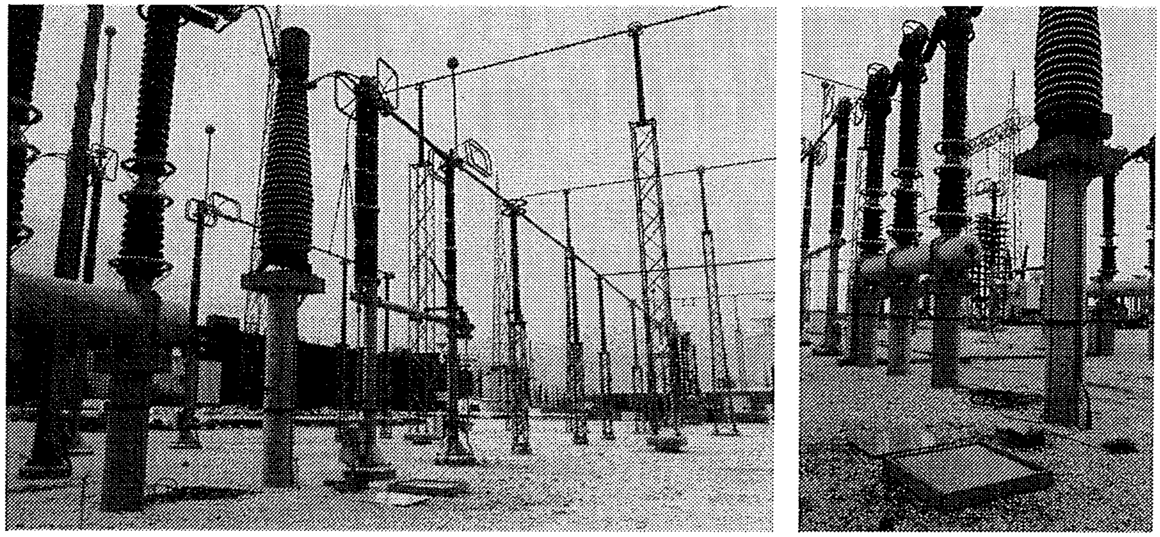

Fig.3.7 On–site measurement settings

Other instruments, e.g. analyzers and data retrieving system, were housed in two small protective boxes (less than 0.2 meter high, see Fig.2.16) which were always at least one meter away from the measurement locations.

Measurements were taken for three consecutive days at each location. Accordingly, these data were down–loaded every three days and the memory of the on–site data acquiring system was then cleared for the next recording.

System data and weather parameters were available at Dorsey converter station. Signals from high voltage transductors or dividers were transmitted through underground cables to control rooms where system voltage data was stored in a computer automatically. Weather information including wind speed, wind direction, temperature, humidity, etc. were collected from different sensors and recorded in a similar manner. All data could be copied to floppy discs via micro–computer and later incorporated with measured data to form a database.

Signals from the IREQ field mill and the Wilson plate including raw magnitudes and polarities were converted from analog to digital form by an A/D modular and then stored in the high capacity memory of a data logger whose information could also be down loaded to floppy discs via a micro–computer.

Upon completion of data acquisition, the data files including raw data were initially calculated, combined and transferred to form a database spread sheet. The database was manipulated to retrieve valuable and pertinent information according to chosen criteria. Table 3.1 shows a part of a database file in which not only measured data but also system and weather information are presented.

Date	Time	FM kV/m	WP nA/m^2	Time	Temp ^{0}C	Wdir *	Wspd km/h	RH %	Bar mB	Rain mm	W/D (1/0)	Time	DC3 p1 neg	DC4 p4 pos	DC2 p2 pos	DC1 p3 neg
5/11/93	17:00	−15.2	−0.1	1701	27.4	282	23.1	34	995	0	0	17:00	282	429	471	460
5/11/93	17:05	−14.6	2.7	1706	27.1	281	23.0	34	994	0	0	17:05	281	428	470	459
5/11/93	17:10	−16.2	6.6	1711	27.1	281	21.7	34	994	0	0	17:10	282	428	471	459
5/11/93	17:15	−14.7	5.1	1716	27.0	281	22.1	34	994	0	0	17:15	282	428	471	460
5/11/93	17:20	−14.8	0.0	1721	26.8	281	21.3	34	995	0	0	17:20	282	429	470	459
5/11/93	17:25	−15.2	−9.6	1726	26.5	281	20.2	34	995	0	0	17:25	282	429	471	460
5/11/93	17:30	−15.0	−18.2	1731	26.4	280	20.9	34	995	0	0	17:30	283	430	471	460
5/11/93	17:35	−18.7	−59.8	1736	26.5	280	18.4	34	995	0	0	17:35	283	430	471	460
5/11/93	17:40	−17.5	−44.4	1741	26.5	281	18.8	34	994	0	0	17:40	283	430	471	460
5/11/93	17:45	−15.3	5.9	1746	26.4	282	18.3	34	994	0	0	17:45	283	429	471	460
5/11/93	17:50	−20.3	−63.9	1751	26.2	282	19.3	35	994	0	0	17:50	282	429	470	459
5/11/93	17:55	−16.9	−34.0	1756	26.1	282	20.2	35	994	0	0	17:55	283	430	471	460
5/11/93	18:00	−15.8	−9.7	1801	26.0	282	20.8	35	994	0	0	18:00	284	432	472	460
5/11/93	18:05	−16.2	−35.6	1766	25.9	281	20.5	35	994	0	0	18:05	283	431	471	460
5/11/93	18:10	−14.9	−6.4	1771	25.9	281	19.3	35	994	0	0	18:10	283	431	472	460
5/11/93	18:15	−15.2	−0.9	1776	25.8	281	19.3	36	994	0	0	18:15	282	430	472	460

Table 3.1 Sample sheet of a database file.
* Wind direction is in degree. The zero degree represents the north wind.

The ground level measurement was started in May 1993 and more than five months of data have been collected.

CHAPTER 4

Measurement Results and Discussions

Two types of measurements were carried out in the switchyard. The first one was the measurement of the electric field intensity E (kV/m) and the ion current density J (nA/m^2) at ground level at selected locations in the switchyard. The IREQ field mill and the Wilson plates were used in this task. The second one was the measurement of the electric field intensity at locations above ground parallel to a switch–line but not directly beneath it. This was accomplished by using the miniature field meter; in this case both the horizontal and vertical field components were recorded.

4.1 Results of Ground Level Measurements in the Whole Switchyard

Table 4.1 lists the field quantities measured at the 37 locations identified in Figure 3.2. Both the average and maximum values are presented. The average values represent the three day average of measured data at each location. At many locations both positive and negative maximum electric field values were recorded whose magnitudes are even comparable to each other at certain locations, for example at locations 24, 26 and 31.

Since these measurements spanned a period of about five months, neither the system nor the environmental conditions were constant. Therefore data in Table 4.1 only give a rough view of the field quantities. For example, the operating voltage changed during the measurements conducted at certain locations which resulted in some readings not fully representing the field characteristics at the supposed operating voltage level. Nevertheless, Table 4.1 offers the "real world" information of field quantities existing in this switchyard.

Measurement Locations		Electric Field (kV/m)		Ion Current (nA/m^2)	
		Emax	Eav	Jmax	Jav
1	HSLS	33.5/–2.9	10.6	99.5	8.0
2	HSLS	22.3/–2.0	11.9	99.0	18.7
3	HSLS	25.2/–0.5	14.3	99.7	15.5
4	HSLS	28.1	16.6	99.0	27.1
5	HSLS	30.4/–0.8	9.9	116.6/–2.6	6.5
6	HSLS	24.2/–0.7	10.2	78.2	7.1
7	HSLS	22.6	15.8	71.9	5.0
8	HSLS	26.7/–1.7	16.2	85.0	5.2
9	HSLS	34.4	22.9	95.4	12.6
10	HSLS	30.6	16.5	99.1	16.6
11	HSLS	–20.3/1.2	–10.6	–71.7/4.3	–6.6
12	HSLS	–23.8/1.9	–9.3	–97.2	–6.1
13	HSLS	–22.6/0.6	–5.4	–95.6/4.3	–1.7
14	HSLS	–29.4/4.4	–10.3	–99.0	–7.9
15	HSLS	20.0	9.6	75.1	14.6
16	HSLS	19.8/–2.3	8.0	46.0	7.0
17	HSLS	19.5/–3.7	5.4	72.1	18.5
18	HSLS	–9.9/4.6	–4.4	–74.2	–4.9
19	HSLS	–13.6/6.4	–5.7	–54.4/14.9	–3.2
20	HSLS	–14.9/1.0	–6.6	–61.3/10.9	–5.3
21	Bus	19.2	10.9	71.0/–14.1	13.0
22	Bus	27.2	19.9	98.5	31.4
23	Bus	–13.5/6.8	–2.0	–58.4/14.4	–1.5
24	Bus	–32.9/24.5	–0.04	34.8	4.9
25	Bus	–8.9/4.3	–3.0	–22.2/11.3	–1.8
26	Bus	–16.0/13.4	–3.8	85.9	8.3
27	Bus	37.0/–8.8	18.4	100.0	24.5
28	Bus	32.8	18.0	99.1	26.4
29	Incoming	23.1/–11.0	14.1	59.4	16.8
30	Bus	18.3	8.9	60.0/–19.4	8.2
31	Incoming	–12.3/12.0	2.3	26.8	5.9
32	Incoming	30.4	25.8	99.6	50.5
33	Incoming	21.5/–1.2	9.4	7.3	2.3
34	Incoming	23.0/–14.0	0.3	7.4/–1.2	2.0
35	Incoming	–27.0/8.0	–3.5	–4.8/3.9	–2.4
36	Incoming	–32.8/16.4	–19.7	–7.3/1.1	–3.7
37	Incoming	–26.7	–11.8	–6.1/0.3	–1.7

Table 4.1 Measured values of electric field and ion current density in the switchyard at ground level locations

4.1.1 Discussions

Table 4.1 shows that the maximum value of the electric field at certain locations exceeds 30 kV/m which is much higher than that in EHVac switchyards. From [9] the maximum field in a 735 kV ac substation is about 14 kV/m rms and varies between 4 and 14 kV/m rms. In a 500 kV substation a maximum field of approximately 11 kV/m rms has been reported in [21]. Also it is seen that the average values of the measured electric fields at some locations are found to be higher than those in HVac substations of same or even higher operating voltage levels. However the maximum measured values of field quantities in the dc switch–yard are also comparable to corresponding values measured under the dc line [10,38].

The maximum values of the measured electric fields are much higher than the corresponding average values. The difference is even more prominent in terms of the ion current density. Some extremely low average values of the electric field can be attributed to a large number of readings of opposite polarity caused by the influence of the system voltage changes and the varying space charge distribution in together.

This behavior is due to the fact that the measured quantities at a certain location are influenced by system voltage changes, neighboring bus conductors and the effects of wind and space charge. For example at location 31, which is beneath the incoming line DC3 (–500 kV), one may expect to register only negative values of field quantities. However, during the measurement period, the line voltage of DC3 remained only at about –280 kV level. This measurement location was surrounded by neighboring positively energized conductors (see Fig.3.2). Negative E–field values were recorded only during the periods of de–energization of the neighboring positive incoming line DC4 or operation of this line at a lower voltage. This is shown in Fig. 4.1 which also shows that the ion current remains positive even when the electric field becomes negative. Therefore it is not unusual to observe that positive and negative maximum values of the electric field are very close and a positive mean value of the electric field was recorded.

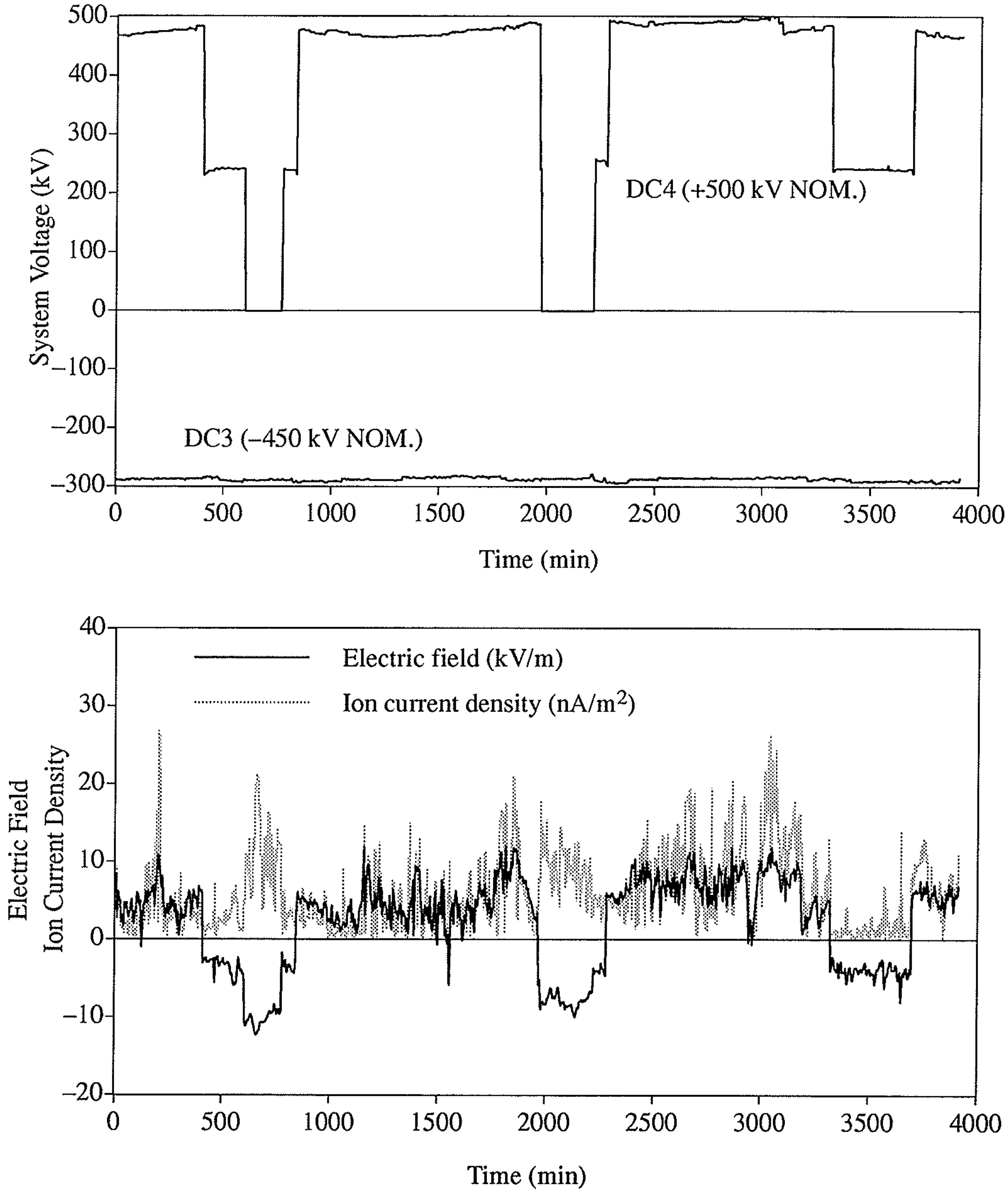

Fig. 4.1 Dependence of electric field and ion current on system voltage at location 31

On the other hand, at location No.12 (Fig. 3.2), the influence of buses of opposite polarity, i.e. switch–line sw2 at +500 kV, is much smaller. Of the 768 valid readings of the electric field strength at this location, only 6 or 0.8% were found to be positive. The values of the positive readings were rather small with the highest one being only 1.9 kV/m. Therefore the measured maximum and average values have the same sign and the average value is not abnormally low as at location No.31.

Apparently locations which are surrounded by densed live structures of both polarities such as locations No.23–26, usually have more opposite readings due to the influence of the neighboring structures, or more specifically the space charges and wind effects (to be discussed later). This contributes to a lowered average value. It is an unique phenomena in HVdc switchyard.

The difference in corona activity is also shown in Table 4.1 which shows that the ion current density below incoming lines is much lower than that measured elsewhere in the switchyard. This may be attributed to the higher corona activity from bus conductors in the switchyard which in turn affects the electric field readings and causes higher maximum values of electric fields in a dc switchyard.

To eliminate the influence of system voltage changes and to analyze the influence of the weather, database technology was used to extract useful information and the results and relevant discussions are presented in a later section of this chapter.

4.2 Results of Ground Level Measurements adjacent to a Switch–line

It is reported [18,23] that in HVac substations, higher electric fields are observed near circuit breakers. From the results of initial measurements obtained by using the miniature field meter, higher electric field intensities were measured near the HVdc switch–lines, though not exactly near the high speed line switches. Detailed measurements were therefore planned along a chosen switch–line sw2 in Figure 3.2. The measurements were expected to provide a near complete picture of the electric field distribution along a typical high voltage switch–line in a dc switchyard.

Switch–line sw2 was chosen not only because high electric fields were recorded in its vicinity during the initial measurements, but also because its operating voltage level was found to be most stable.

As shown in Figure 3.2, ten ground level locations were selected along switch–line sw2 with five on each side of it. They were all chosen close to apparatus such as the high speed line switch, voltage dividers and disconnector. On each side, the locations were along a line parallel to the switch–line with a separation of 3 meters from the axis of the switch–line.

Measured data from the ten ground level locations were sorted and analyzed by using database technology together with system and weather parameters. Three criteria used in the database to extract data were set as follows:

1. Operating voltage level including that of the neighboring switch–line (sw3), i.e. $V_{sw2} > 450kV$ and $V_{sw3} < -450kV$. This ensured that only data at full operating voltage levels were extracted.

2. Wind speed classification, $0 \leq Wind\ speed \leq 2$ (still), $2 \leq Wind\ speed \leq 15$ (low), $Wind\ speed \geq 15$ (strong) and overall wind speeds. Unit: km/hour.

These speed criteria were essentially chosen based on author's on–site perception and with reference to the Beauford Wind Scale in meteorology [39,40].

In the present analysis, a wind speed less than 2 km/hour is regarded as still, while a wind speed between 2 and 15 km/hour and larger than 15 km/hour is regarded as low and strong respectively. Since wind speeds less than 2 km/hour are rare, only low wind, strong wind and overall wind data are presented for comparison purposes.

3. No rain.

The absence or presence of rainfall was detected by two sets of sensors which monitor both the rain/no rain and wet/dry.

The processed results are shown in Tables 4.2 and 4.3 which contain information about electric field intensity and ion current density at locations near switch–line sw2. It can be seen that due to the system voltage change, a few low percentages of valid data which meet the three criteria are observed, e.g. being 12.8% at location 5.

Loc	Wind speed (km/h) ≤ 2			$2 \leq$ Wind speed (km/h) ≤ 15			Wind speed (km/h) $\geq$ 15			All wind speeds		
	$E_{max}/W/W_{(t-1)}$	E_{av}/W_{av}/Num/%	$E_{min}/W/W_{(t-1)}$	$E_{max}/W/W_{(t-1)}$	E_{av}/W_{av}/Num/%	$E_{min}/W/W_{(t-1)}$	$E_{max}/W/W_{(t-1)}$	E_{av}/W_{av}/Num/%	$E_{min}/W/W_{(t-1)}$	$E_{max}/E_{av}/E_{min}$	$W_{max}/W_{av}/W_{min}$	Num/N/%
1	29.6/1.1/6.0	16.2/1.0/165/12	5.3/1.1/0.9	30.1/7.0/6.6	16.4/8.9/248/18	11.7/14.2/13.1	28.5/25.3/22.4	13.4/24.1/440/31.9	4.2/22.9/21.5	30.1/14.8/4.2	43.3/15.2/0.8	853/1379/61.9
2	N/A	N/A	N/A	20.9/4.4/6.1	12.1/10.2/338/40.0	8.1/14.6/24.8	22.2/21.8/22.3	12.4/21.6/333/39.5	5.3/18.8/14.7	22.2/12.2/–0.6	30.9/15.9/4.4	671/844/79.5
3	N/A	N/A	N/A	25.0/8.3/9.5	16.0/9.8/247/31.0	5.2/10.6/11.2	25.2/16.4/15.7	17.1/21.9/231/29.0	4.6/21.6/22.2	25.2/16.5/4.6	30.8/15.6/2.5	478/796/60.1
4	15.4/1.9/2.5	15.4/1.9/1/0.1	15.4/1.9/2.5	27.1/10.8/11.7	17.4/9.7/544/65.8	11.9/11.1/11.2	28.1/18.0/15.2	15.2/20.9/214/25.9	6.5/22.9/22.4	28.1/16.8/6.5	29.6/12.9/1.9	759/827/91.8
5	29.7/0.8/0.8	20.5/0.9/39/5.2	13.9/0.8/0.8	30.4/11.6/10.7	19.7/8.9/57/7.6	7.1/13.0/13.7	N/A	N/A	N/A	30.4/20.0/7.1	14.4/5.6/0.8	96/751/12.8
6	N/A	N/A	N/A	24.2/8.7/9.0	14.9/9.4/163/48.4	11.1/8.4/9.9	17.9/19.9/18.3	13.0/18.1/34/10.1	11.7/17.7/22.8	24.2/14.6/11.1	23.8/10.9/2.3	197/337/58.5
7	N/A	N/A	N/A	22.6/10.1/11.1	17.8/10.3/473/46.6	12.7/13.2/14.0	21.8/15.1/15.3	14.3/22.8/319/53.4	10.6/32.7/33.7	22.6/14.0/10.6	40.0/17.0/5.2	592/592/100
8	N/A	N/A	N/A	26.7/4.0/3.9	16.0/9.5/467/59.6	12.3/8.7/5.4	22.9/18.5/16.7	16.4/18.9/268/34.2	12.1/23.2/26.7	26.7/16.1/6.1	30.2/12.9/2.8	735/784/93.8
9	28.2/0.8/0.8	19.5/0.9/246/37.7	8.6/0.8/0.8	30.6/6.7/17.3	21.4/8.4/148/22.7	15.0/8.2/3.1	28.9/19.5/4.2	16.9/19.5/41/6.3	14.4/21.4/21.2	30.6/19.9/8.6	26.3/5.2/0.8	435/653/66.6
10	N/A	N/A	N/A	34.4/10.5/11.0	21.0/10.3/610/81.4	15.2/8.5/9.0	32.4/18.0/13.5	22.7/16.9/61/8.1	15.9/18.2/18.5	34.4/21.0/15.2	22.7/10.9/3.9	671/749/89.6

Table 4.2 Tabulation of measured electric field data along switch–line sw2 meeting chosen criteria

Loc	Wind speed (km/hr) ≤ 2			$2 \leq$ Wind speed (km/hr) ≤ 15			Wind speed (km/hr) ≥ 15			All wind speeds		
	$J_{max}/W/W_{(t-1)}$	$J_{av}/W_{av}/Num/\%$	$J_{min}/W/W_{(t-1)}$	$J_{max}/W/W_{(t-1)}$	$J_{av}/W_{av}/Num/\%$	$J_{min}/W/W_{(t-1)}$	$J_{max}/W/W_{(t-1)}$	$J_{av}/W_{av}/Num/\%$	$J_{min}/W/W_{(t-1)}$	$J_{max}/J_{av}/J_{min}$	$W_{max}/W_{av}/W_{min}$	Num/N/%
1	97.5/0.8/0.8	16.8/1.0/165/12	0.0/0.8/0.8	99.5/6.8/6.5	10.2/8.9/248/18	0.0/4.0/2.0	92.4/21.9/18.3	9.3/24.1/440/31.9	0.0/23.9/22.6	99.5/11.0/0.0	43.3/15.2/0.8	853/1379/61.9
2	N/A	N/A	N/A	82.1/9.5/9.2	14.9/10.2/338/40.0	0.0/9.3/10.1	99.0/22.5/26.4	17.9/21.6/333/39.5	0.0/18.8/18.7	99.0/16.4/0.0	30.9/15.9/4.4	671/844/79.5
3	N/A	N/A	N/A	98.6/6.2/7.6	20.3/9.8/247/31.0	0.0/11.1/11.2	99.3/20.4/22.8	19.1/21.9/231/29.0	0.0/20.6/22.5	99.3/19.7/0.0	30.8/15.6/2.5	478/796/60.1
4	18.7/1.9/2.5	18.7/1.9/1/0.1	15.4/1.9/2.5	98.4/7.3/7.7	34.9/9.7/544/65.8	0.1/14.0/11.3	99.0/19.4/18.0	24.3/20.9/214/25.9	0.0/19.8/18.5	99.0/29.1/0.0	29.6/12.9/1.9	759/827/91.8
5	116.4/1.0/3.2	36.3/0.9/39/5.2	−1.6/0.8/0.8	116.6/8.7/9.0	30.5/8.9/57/7.6	−1.2/6.5/5.5	N/A	N/A	N/A	116.3/32.8/−1.6	14.4/5.6/0.8	96/751/12.8
6	N/A	N/A	N/A	78.2/11.6/11.4	10.9/9.4/163/48.4	0.0/11.1/8.4	72.5/18.3/16.1	9.4/18.1/34/10.1	0.0/17.7/22.8	78.2/10.6/0.0	23.8/10.9/2.3	197/337/58.5
7	N/A	N/A	N/A	72.0/10.1/11.1	5.7/10.3/473/46.6	4.1/13.2/14.0	69.2/15.1/15.3	4.6/22.8/319/53.4	3.4/31.5/30.3	72.0/5.1/3.4	40.0/17.0/5.2	592/592/100
8	N/A	N/A	N/A	85.1/4.0/3.9	5.1/9.5/467/59.6	3.9/8.7/5.4	73.0/18.5/16.7	5.2/18.9/268/34.2	3.9/20.5/21.4	85.1/5.1/2.0	30.2/12.9/2.8	735/784/93.8
9	99.1/0.8/0.8	19.7/0.9/246/37.7	0.1/0.8/0.8	98.7/5.1/6.6	31.9/8.4/148/22.7	0.0/12.3/0.8	89.4/19.3/21.5	15.9/19.5/41/6.3	0.1/21.5/22.2	99.1/22.6/0.0	26.3/5.2/0.8	435/653/66.6
10	N/A	N/A	N/A	95.4/7.3/8.5	12.6/10.3/610/81.4	0.5/6.6/8.8	83.8/15.1/12.1	9.0/16.9/61/8.1	2.3/15.3/14.9	95.4/12.3/0.5	22.7/10.9/3.9	671/749/89.6

Table 4.3 Tabulation of ion current density data meeting chosen criteria along switch–line sw2

The magnitudes of the electric field in the all wind speeds category in Table 4.2 are extracted from database upon chosen criteria and are therefore higher than those in Table 4.1. These processed data were then used to obtain Figures 4.2 to 4.5. These figures present the ground level values of the electric field E and ion current density J along switch–line sw2. In these figures, the scale of the X–axis of the switch–line elevation drawings (i.e. Figs. 4.2 to 4.5a) is the same as those used in the graphs in Figs. 4.2 to 4.5 b and c. Thus it becomes possible to relate a measured field quantity directly to its measurement location in the drawings of elevation layout of the switch–line.

Legend for Table 4.2 and 4.3

Loc: Location number (see Fig.3.2 or Table 4.1).

E_{max}: Maximum value of E field recorded at specified location and for specified wind speed criteria. Measurement period: 3 days; frequency of readings: once every five minutes. Unit: kV/m.

E_{min}: Same as above but minimum value of E–field.

E_{av}: Same as above but average value of E–field.

W_{max}: Maximum value of wind speed recorded at specified location subject to specified wind speed criteria; measurement period & frequency as specified earlier.

W_{min}: Same as above but minimum value of wind speed.

W_{av}: Same as above but average value of wind speed.

Num: Number of recorded data at specified location which not only meets specified wind speed criteria but also other criteria regarding system voltage and weather conditions.

N: Total number of recorded data at a specific location.

%: $\frac{Num}{N} \times 100$, Percentage of valid data which meet the chosen criteria.

W: Wind speed recorded at the time of occurrence of Emax or Emin.

$W_{(t-1)}$: Wind speed recorded one time interval (i.e. 5 minutes) prior to occurrence of Emax or Emin.

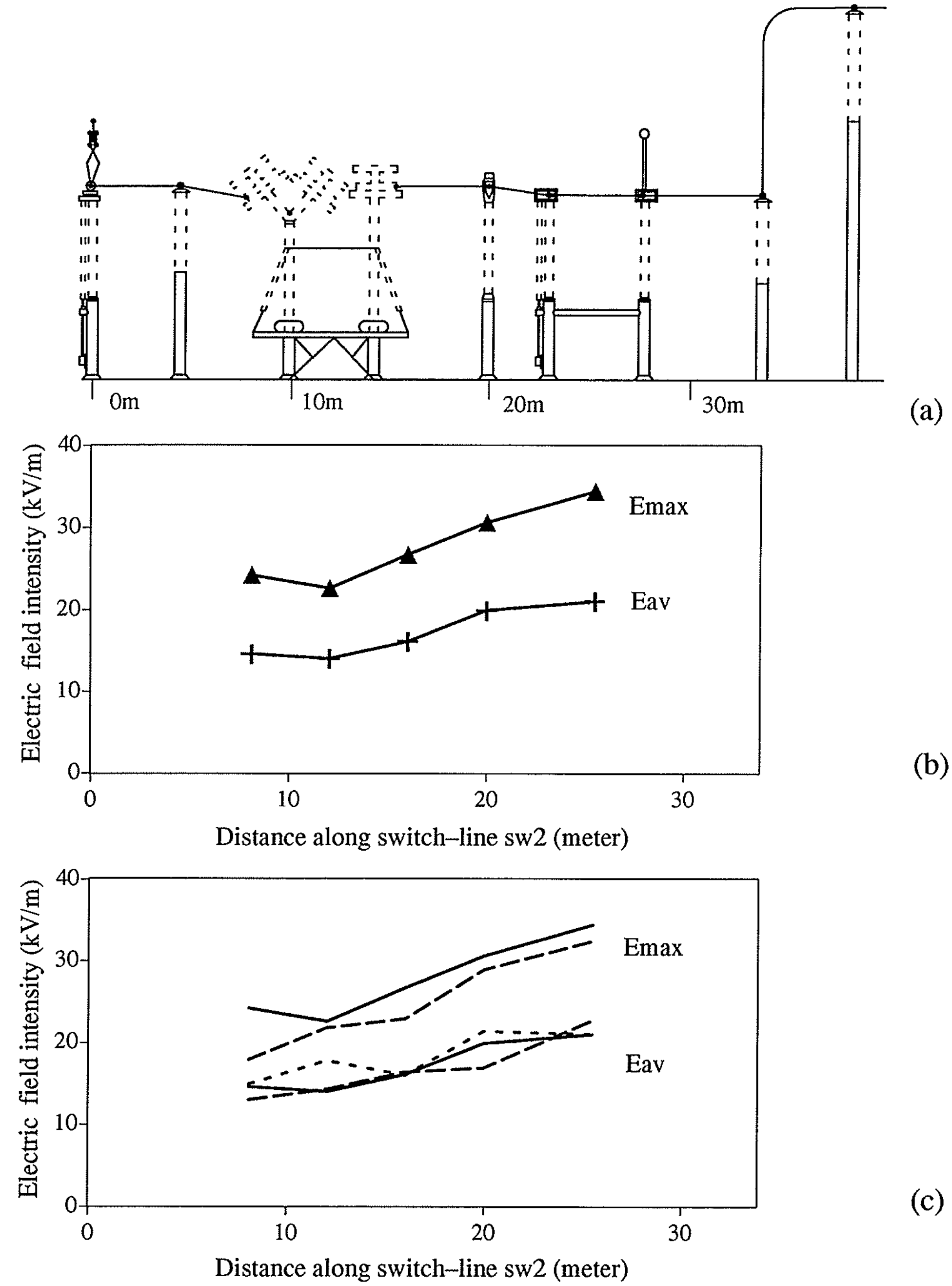

Fig. 4.2 Measured field intensity at ground level north of sw2, +500 kV

(a) Elevation layout of switch–line sw2

(b) Eav and Emax under all wind speeds

(c) Eav and Emax under low and strong wind speeds

——— Overall wind speeds

– – – Strong wind

- - - - Low wind

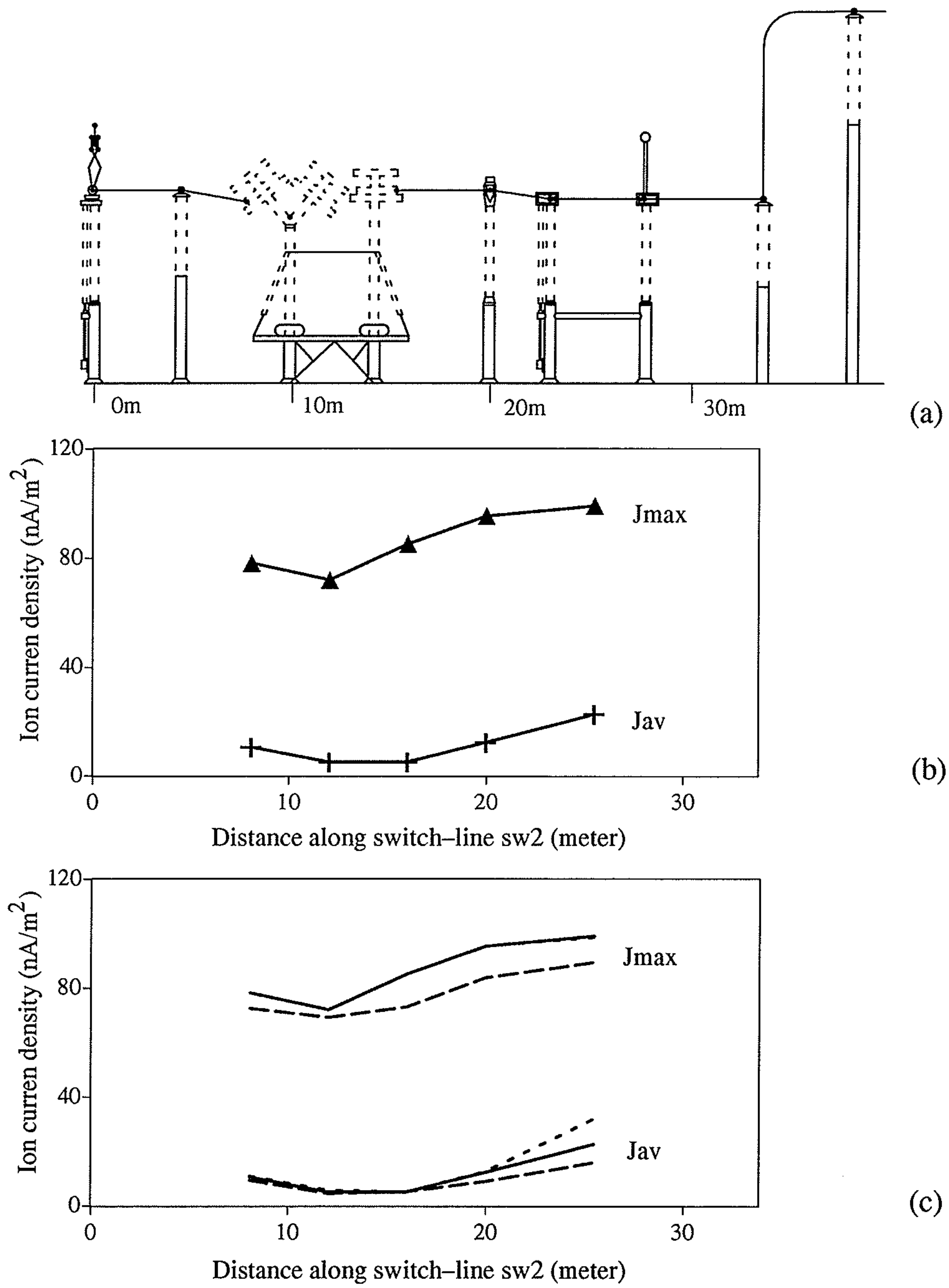

Fig. 4.3 Measured ion current density at ground level north of sw2, +500 kV

(a) Elevation layout of switch–line sw2
(b) Jav and Jmax under all wind speeds
(c) Jav and Jmax under low and strong wind speeds

——— Overall wind speeds
— — — Strong wind
- - - - Low wind

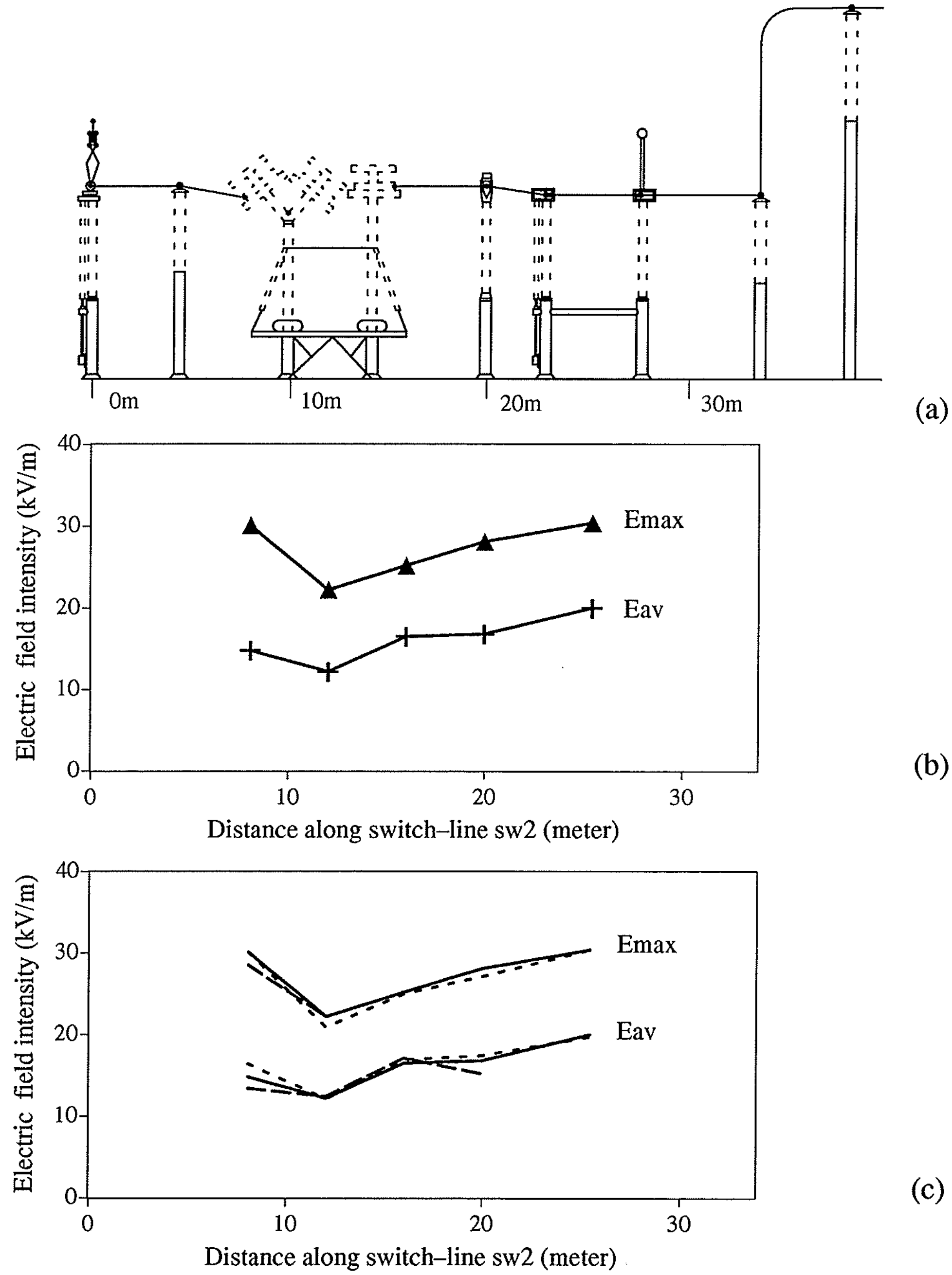

Fig. 4.4 Measured field intensity at ground level south of sw2, +500 kV

(a) Elevation layout of switch–line sw2

(b) Eav and Emax under all wind speeds

(c) Eav and Emax under low and strong wind speeds

—— Overall wind speeds

— — Strong wind

- - - - Low wind

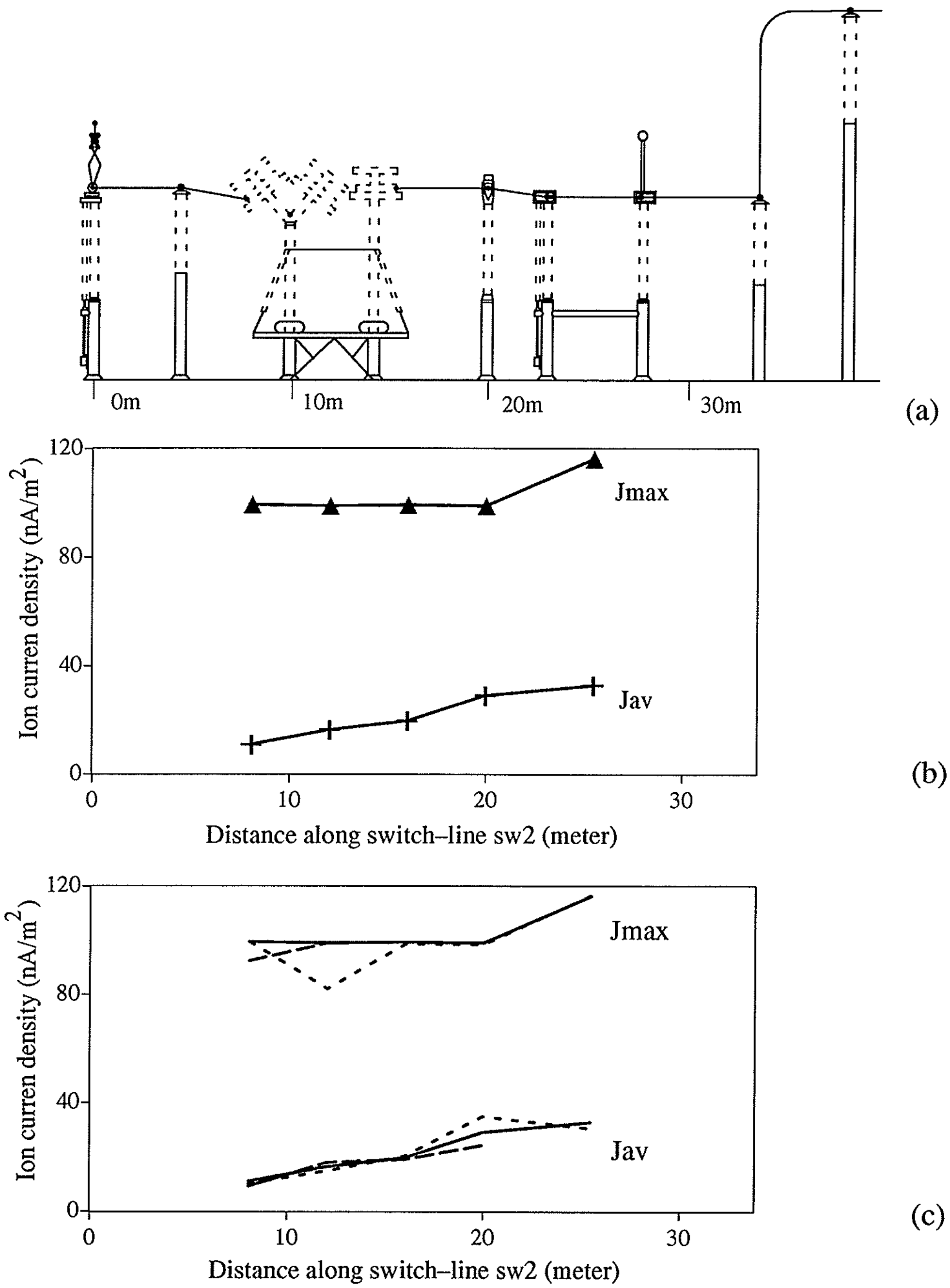

Fig. 4.5 Measured ion current density at ground level south of sw2, +500 kV

(a) Elevation layout of switch–line sw2
(b) Jav and Jmax under all wind speeds
(c) Jav and Jmax under low and strong wind speeds

——— Overall wind speeds
— — — Strong wind
- - - - Low wind

From the collected data, readings obtained at locations 1 to 10 were grouped under three categories based upon wind speed, W (km/h). These are $0 \le W < 2$ (still wind),

$2 \leq W < 15$ (low wind) and $W \geq 15$ (strong wind). During the five–month measurement period the wind speed seldom exceeded 30 km/h. Also it was found that very few data remained which corresponded to still wind conditions. Therefore the data reported in Figures 4.2 – 4.5 does not include those under still wind conditions.

4.2.1 Discussions

Some observations can be drawn from recorded ground level measurements at locations near switch–line sw2 as shown in Figs. 4.2 – 4.5:

(1). The electric field strengths and ion current densities are higher at the east end of the switch–line than at the west end and show a "U–shape" variation; the electric field is lower near the high speed line switch and reaches a higher value at the east end.

The conductors of the high speed line switch in sw2 is almost at the same elevation as the bus conductor. The only contribution to the reduction of electric field strength at locations 2 and 7 (near the middle of the length of the switch, see Fig. 3.2) in this case is the metal support structures at the bottom of the high speed line switch (see Figs. 3.3 and 3.5). The grounded vertical and horizontal supports up to 2.0m high shield the electric field around and below these supports and thus lower the electric field strength at locations nearby.

(2). The electric field strengths on the north side of sw2 are slightly higher than those on the south side, but the ion current densities on the north side are smaller than those on the south side.

(3). The average values of the electric field along this +500 kV dc switch–line are between 12 and 22 kV/m. The maximum electric field value has reached 35 kV/m. These values are higher than those in corresponding 500 kV and 735 kV ac substations [9,11,13,14,16,17,21,23], but are comparable to those under the Nelson River 500 kV dc line [10,38].

The above observations can be explained by taking into account the effect of space charge and wind (wind direction and wind speed) as well as switchyard configuration.

First, the space charges caused by coronating conductors migrate to ground or to opposite polarity conductors and then alter the electric field environment in the neighboring areas.

Generally the space charges have the same polarity as the conductor itself. The presence of space charges of like polarity under a conductor has an effect of increasing the electric field at ground level, while that of opposite polarity decreases the electric field strength. Therefore the electric field distribution at ground level depends on the density and distribution of the space charges. The density of space charges depends on the corona intensity at the conductor surface which in turn depends on prevailing atmospheric conditions.

Second, the distribution of space charges is influenced greatly by the wind. Under no wind condition, the ground level electric field is enhanced by the migration of space charges moving along flux lines and is higher than if corona is absent.

The presence of wind affects the movement of space charges. Depending on the speed and direction of the wind, the space charge distribution can be changed significantly to such a degree that it is possible (see Table 4.1) that positive field quantities can be observed under negative conductors and vice versa.

Statistical meteorological data gathered in the Dorsey substation shows that the winds are mostly from north and northwest direction. This explains first why the ion current density at the south side of sw2 is much higher than that at the north side; second, it also explains why the electric field strength at the east end of sw2 is higher than that at west end.

Third, unlike wind direction, wind speed has a less significant effect on field measurements. The average values of the electric field strength and ion current density are slightly higher under low wind than under strong wind (see Figs. 4.2 – 4.5). It is because strong wind tends to blow off more space charges and reduces the electric field strength.

Examination of the data in Figures 4.2 – 4.5 shows that the electric field and ion current density under either wind speed category do not show a significant dependence on wind speed. This can be explained that in a dc switchyard space charges are produced by coronating conductors which are situated at a lower elevation than transmission lines, wind effects are then less noticeable. Assessment of the field levels in the switchyard is therefore best carried out by examination of overall average and maximum values.

Another contributing factor to the above results is switchyard configuration. The neighboring switch–line sw1 was open during the measurements and therefore no space charges were produced by it. However, conductors at the east end of the de–energized sw1 were connected to +500 kV buses. These are at a lower elevation and stretch out over a larger area (see Fig. 3.2). This results in higher electrostatic field strengths at the east end of sw2. This is in agreement with the observation that the electric field at the northeast side of sw2 is slightly higher than that on the southeast side. Moreover, under north or northwest wind, locations at the east end of sw2 experience a higher space charge density of the same polarity (in this case, positive) and thus in turn produce higher electric field readings. This has been observed in Figs. 4.2 and 4.4.

The above explanations are in agreement with and supported by the measurement results of ion current density. Comparison between Figs. 4.3 and 4.5 shows both the maximum and mean values of ion current density on the south side locations are much higher than north side locations.

In the central area of the switchyard where there are mainly bus structures of both polarities crossing each other at different elevations, the distribution of the space charges generated from these structures is extremely unstable and even a qualitative analysis is difficult. Therefore the recorded data under these live structures could not be analyzed using the database approach. The only solution is an overall data processing as presented in Table 4.1. However at locations beneath incoming lines database approach is still possible due to the relatively simple configuration in that area (Fig.3.2), the results from the database analysis are present in the next section.

The use of the database approach also reveals the correlation between the electric field and ion current density. Figure 4.6 shows how E and J correlate with each other under external influence instantaneously (Fig. 4.6a) or statistically (Fig. 4.6b).

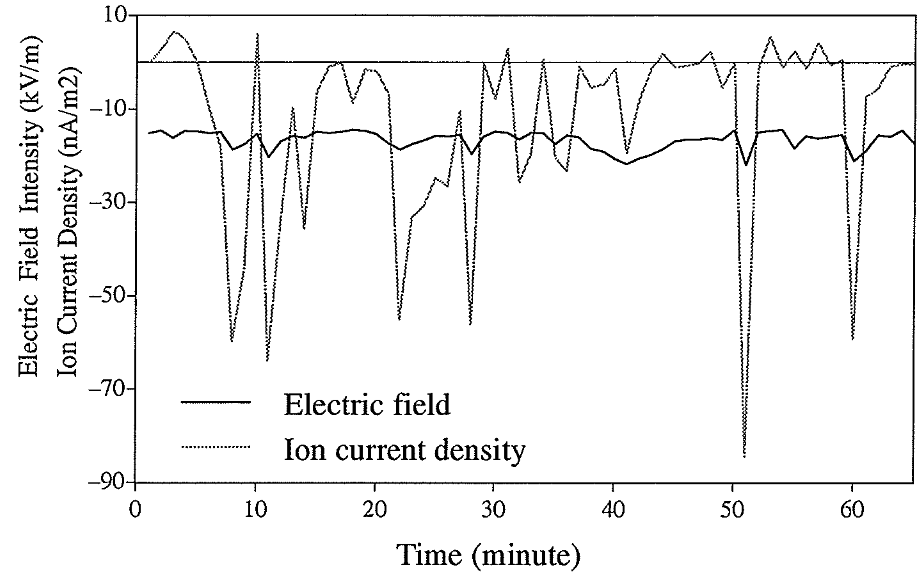

(a)

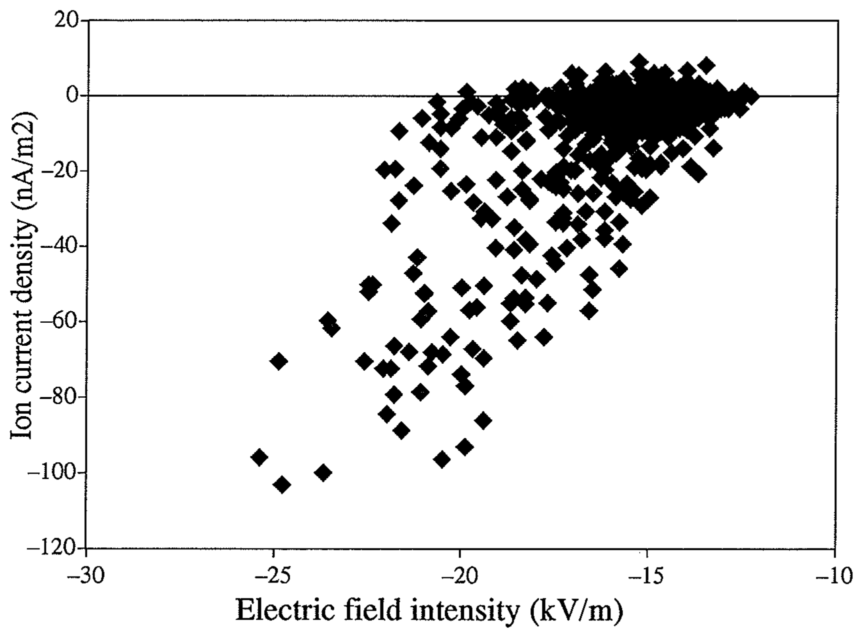

(b)

Fig. 4.6 Correspondence between E and J

(a) Instantaneous correlation between E and J

(b) Accumulative correlation between E and J

4.3 Results from above Ground Measurements adjacent to a Switch–line

Measurements were also carried out at up to 15 locations on each side of sw2 by using miniature field meter at 1.0m and 1.5m above ground. Both horizontal and vertical components of the electric field were measured. Since these measurements were conducted by using the miniature field meter which was much easier to manipulate, more locations were considered. The average wind speed on the date of measurement was about less than 10 km/hour (low wind) and the temperature was 21 degree Celsius. The measurement results are presented in Figs. 4.7 and 4.8.

For comparison purposes, another switch–line sw5 energized at +450 kV was chosen along which measurements were carried out at 1.0m and 1.5m above ground level. In this switch–line all structures were similar to those in sw2 except the high speed line switch, which was not equipped with grounded metal supports. The results are presented in Fig. 4.9.

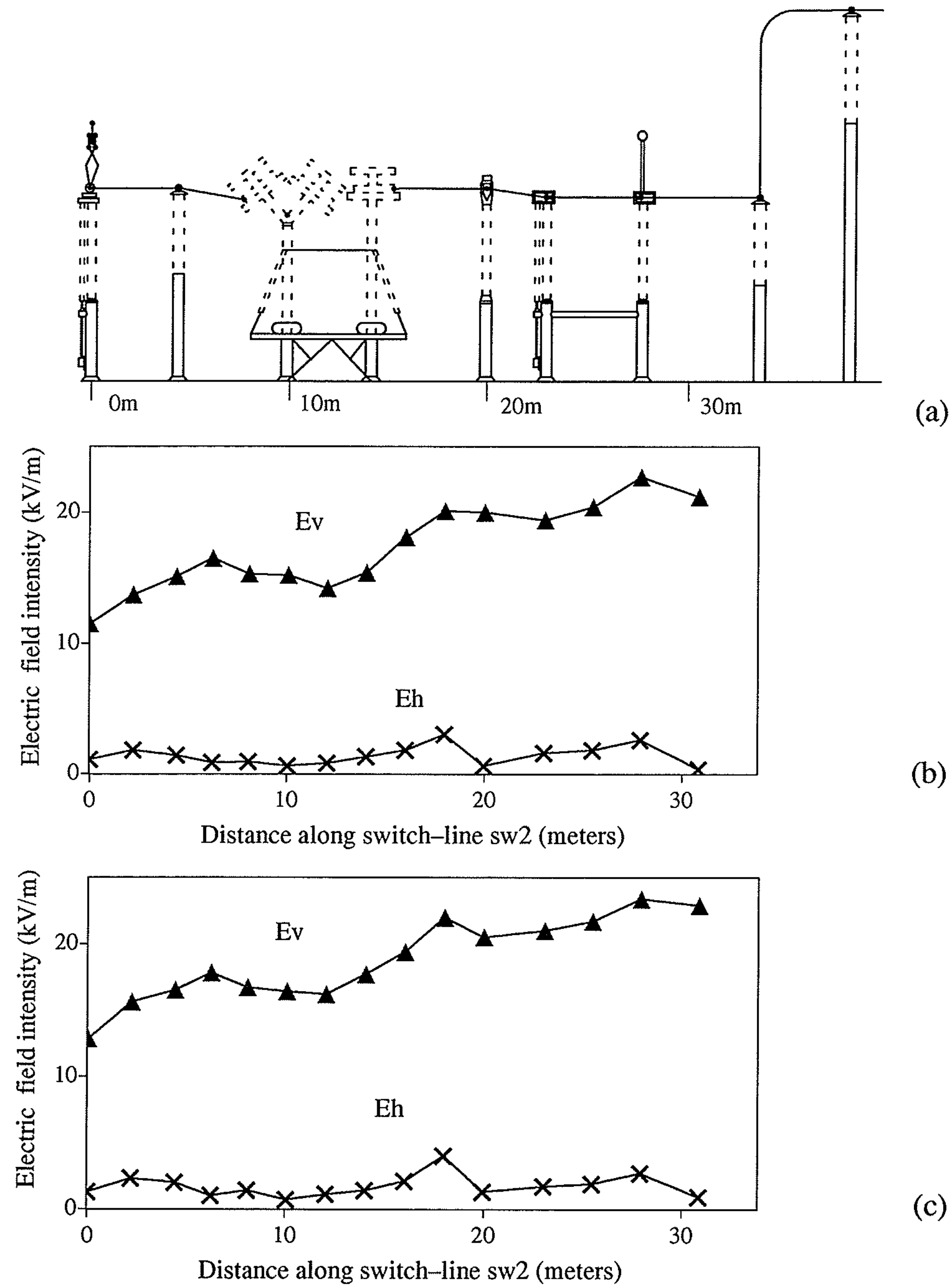

Fig. 4.7 Measured field intensity at above–ground level north of sw2, +500 kV

(a) Elevation layout of switch–line sw2
(b) Ev and Eh at 1.0m high
(c) Ev and Eh at 1.5m high

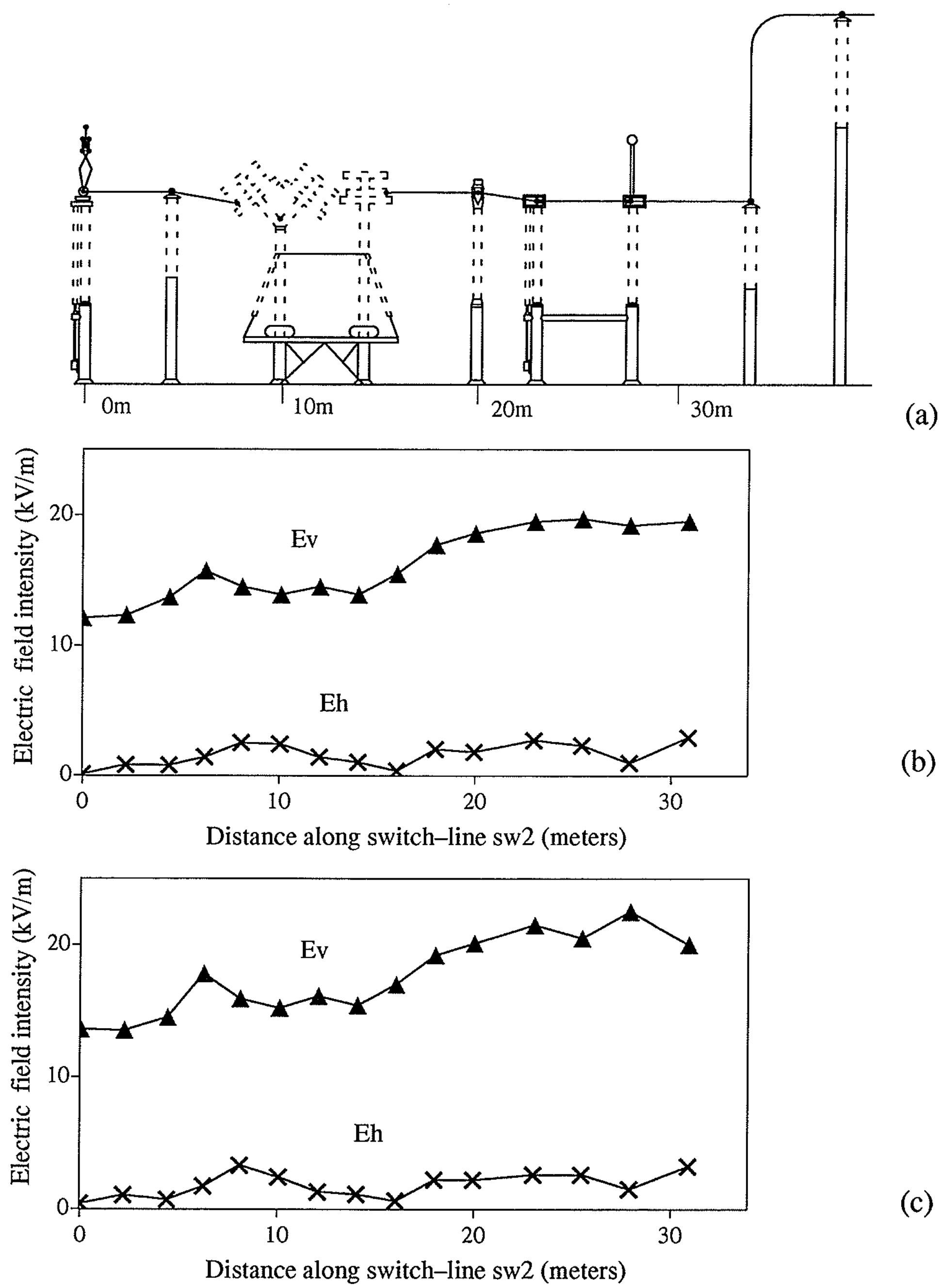

Fig. 4.8 Measured field intensity at above–ground level south of sw2, +500 kV

(a) Elevation layout of switch–line sw2
(b) Ev and Eh at 1.0m high
(c) Ev and Eh at 1.5m high

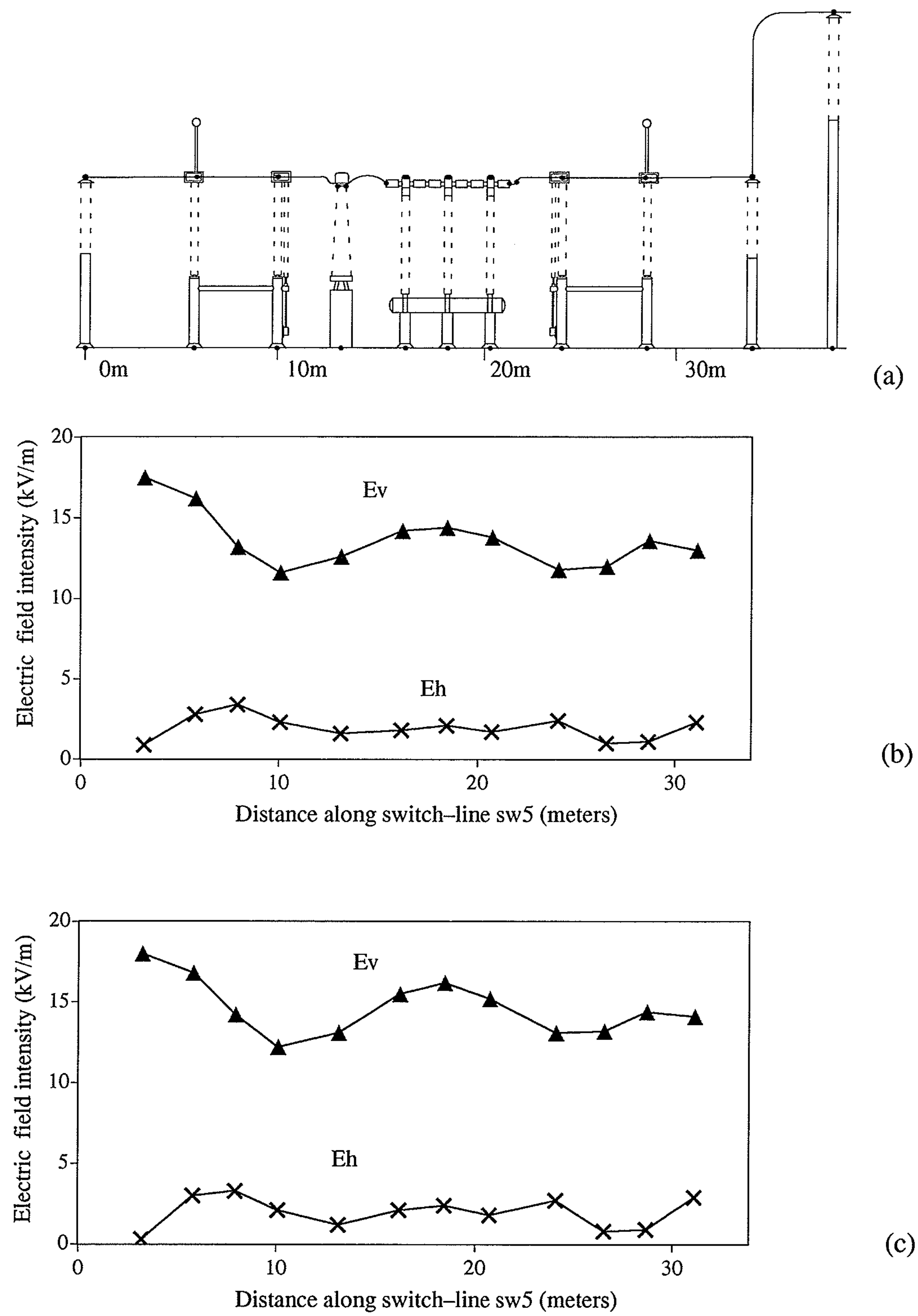

Fig. 4.9 Measured field intensity at above–ground level west of sw5, +450 kV

(a) Elevation layout of switch–line sw5
(b) Ev and Eh at 1.0m high
(c) Ev and Eh at 1.5m high

4.3.1 Discussions

Above–ground measurements included the measurements of the electric field at two different heights of 1.0m and 1.5m at selected locations on both sides of sw2 by using the miniature field meter. At each height, both horizontal and vertical components of electric field were measured. Data are presented in Figs. 4.7 and 4.8.

As analyzed in the previous section, electric field readings are affected by space charge distribution which varies with the instantaneous wind speed and direction. Gusts were observed but the transient data was avoided. The measured data taken at each location is an approximate average at the moment of the author's reading from the instrument panel. The reading was taken during a half–minute interval at each location. Other parameters such as temperature, operating voltage level remained constant.

The results show that the vertical components of the electric field are much higher than the horizontal components. This is in agreement with theoretical analysis.

Since no measurement of ion current density were involved, data analysis can only reveal the relationship between the measured electric field strengths and the measurement locations. Obviously similar variation of the electric field along the length of the switch–line is observed, i.e. lower electric field strengths exist at near high speed line switch and higher electric field strengths exist at east end. The explanation in the previous section is applicable.

It is noted that the electric field strengths at quite a few locations are around 20 kV/m. Compared with the average values of electric field strengths at ground level, the effect of measurement height is not prominent. This also means that the electric field distribution from ground level up to 1.5 meter was almost constant. Therefore, the only means to reduce the electric field is to change the switch–line structure, i.e. add grounded metal supports.

Similar measurements were also carried out along one side of another switch–line, sw5, which was energized at +450 kV. This switch–line is similarly equipped except for the high speed line switch which does not have additional metal supports (see Figs. 3.4 and 3.5).

The measurement results shown in Fig. 4.9 reveal a higher electric field profile near the high speed line switch, in contrast to that observed near sw2. This is in agreement with observations in HVac substations where higher fields were measured at near circuit breakers. This also proves that the use of additional grounded supports (in sw2) is an effective way to reduce the electric field strength at sensitive locations.

4.4 Results of Measurements under Incoming Lines

Electric field quantities beneath the incoming transmission lines at ground level and along an east–west line are listed in Tables 4.4 and 4.5. Both maximum and average values are shown as obtained from data collected over a three day period. Once again these data were extracted from the database under chosen criteria.

The data in Tables 4.4 and 4.5 are also used to illustrate the distribution profile of the electric field and ion current density beneath the incoming line in Fig.4.10.

4.4.1 Discussions

The incoming lines, unlike at midspan elsewhere along the transmission lines, are neither parallel to each other nor to ground. However the overall profile of the distribution of electric field and ion current density is still in reasonable agreement with theoretical considerations, i.e. high electric field magnitudes are observed directly beneath the corresponding lines; low electric field magnitudes occur in–between with an accompanying polarity reversal.

Similar observation can be drawn from Tables 4.4 and 4.5 that neither the electric field nor ion current shows a significant dependence upon wind speed, especially in terms of average values. It also supports the conclusion obtained in previous section that field levels in a dc switchyard can best be determined by the average and maximum values of overall wind speed.

Loc	Wind speed (km/hr) ≤ 2			$2 \leq$ Wind speed (km/hr) ≤ 15			Wind speed (km/hr) ≥ 15			All wind speeds		
	$E_{max}/W/W_{(t-1)}$	E_{av}/W_{av}/Num/%	$E_{min}/W/W_{(t-1)}$	$E_{max}/W/W_{(t-1)}$	E_{av}/W_{av}/Num/%	$E_{min}/W/W_{(t-1)}$	$E_{max}/W/W_{(t-1)}$	E_{av}/W_{av}/Num/%	$E_{min}/W/W_{(t-1)}$	$E_{max}/E_{av}/E_{min}$	$W_{max}/W_{av}/W_{min}$	Num/N/%
33	N/A	N/A	N/A	21.5/6.5/5.4	9.6/8.3/703/81.4	–1.2/5.2/4.5	15.4/16.3/15.4	8.3/20.5/161/18.6	0.3/20.4/22.8	21.5/9.4/–1.2	27.8/10.6/2.4	864/864/100
34	N/A	N/A	N/A	19.1/7.3/6.8	14.6/8.1/333/53.6	–4.6/9.7/9.8	23.4/24.0/22.6	16.2/21.2/270/43.5	4.7/19.0/18.6	23.4/15.6/–4.6	31.0/13.9/2.5	603/621/97.1
35	N/A	N/A	N/A	–27.0/10.8/8.4	–4.2/10.9/564/70.6	8.0/9.1/7.9	–23.4/15.4/14.8	–0.9/21.5/219/27.4	7.7/23.9/24.0	–27.0/–3.5/8.0	34.7/13.9/5.3	783/798/98.1
36	N/A	N/A	N/A	–32.8/9.9/9.4	–21.2/10.1/173/28.7	–8.2/7.8/7.7	–32.0/17.0/17.2	–19.6/23.4/420/69.7	–6.6/26.1/31.2	–32.8/–20.1/–6.6	37.2/19.6/4.9	593/603/98.3
37	–23.0/1.9/2.9	–12.9/1.6/13/1.6	–7.4/1.8/2.3	–25.0/3.4/3.3	–12.7/7.2/381/46.1	–5.4/6.2/5.9	–26.7/22.4/22.9	–11.0/23.6/432/52.3	–4.1/19.7/21.2	–26.7/–11.8/–4.1	35.9/15.7/0.9	826/826/100

Table 4.4 Tabulation of measured electric field data under incoming line

Loc	Wind speed (km/hr) ≤ 2			$2 \leq$ Wind speed (km/hr) ≤ 15			Wind speed (km/hr) ≥ 15			All wind speeds		
	$J_{max}/W/W_{(t-1)}$	J_{av}/W_{av}/Num/%	$J_{min}/W/W_{(t-1)}$	$J_{max}/W/W_{(t-1)}$	J_{av}/W_{av}/Num/%	$J_{min}/W/W_{(t-1)}$	$J_{max}/W/W_{(t-1)}$	J_{av}/W_{av}/Num/%	$J_{min}/W/W_{(t-1)}$	$J_{max}/J_{av}/J_{min}$	$W_{max}/W_{av}/W_{min}$	Num/N/%
33	N/A	N/A	N/A	7.2/5.8/6.5	3.1/8.3/703/81.4	0.1/5.6/5.1	4.9/16.3/15.4	2.6/20.5/161/18.6	0.1/20.4/22.8	7.2/3.0/0.1	27.8/10.6/2.4	864/864/100
34	N/A	N/A	N/A	7.8/4.2/4.2	3.8/8.1/333/53.6	0.1/8.1/8.6	7.2/24.9/25.7	3.8/21.2/270/43.5	0.3/17.2/18.0	7.8/3.8/0.1	31.0/13.9/2.5	603/621/97.1
35	N/A	N/A	N/A	–7.4/14.0/13.5	–5.2/10.9/564/70.6	2.6/7.9/7.5	–7.3/33.7/32.6	–4.0/21.5/219/27.4	2.5/24.0/19.1	–7.4/–4.8/2.6	34.7/13.9/5.3	783/798/98.1
36	N/A	N/A	N/A	–5.7/7.7/7.8	–3.4/10.1/173/28.7	0.5/11.7/11.6	–6.1/23.0/26.1	–3.9/23.4/420/69.7	1.0/19.7/23.9	–6.1/–3.7/1.0	37.2/19.6/4.9	593/603/98.3
37	–5.1/1.8/2.3	–3.3/1.6/13/1.6	–0.1/1.9/2.9	–4.8/6.2/5.9	–1.5/7.2/381/46.1	0.0/3.4/3.3	–5.3/19.7/21.2	–1.8/23.6/432/52.3	0.0/22.4/22.9	–5.3/–1.7/0.0	35.9/15.7/0.9	826/826/100

Table 4.5 Tabulation of measured ion current density data under incoming line

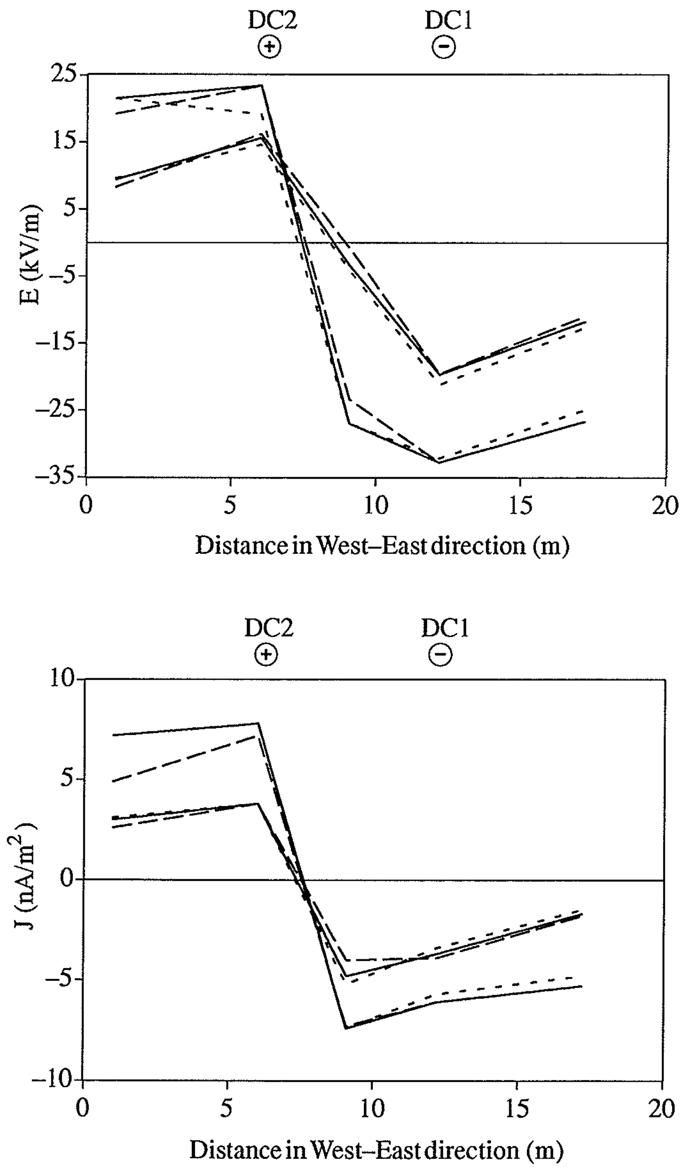

Fig. 4.10 Profile of E and J beneath incoming lines DC1(–500kV) & DC2(+450kV)

Overall wind speed

Low wind speed

Strong wind speed

CHAPTER 5

Calculation Results and Comparison with Measured Data

5.1 Charge Simulation Method (CSM)

The calculation of the electric fields requires the solution of either Laplace's equation and/or Poisson's equation with appropriate boundary conditions. This can be done either by analytical or numerical methods. Analytical solutions of these equations are practical only for relatively simple charge distributions and conductor configurations. However in the case of substations, the physical systems are so complex that analytical solutions are impossible to obtain. Therefore, numerical methods are often used to solve such problems.

Many papers have been published on the numerical solution of Laplace's and Poisson's equations. These methods include the Finite Element Method(FEM), the Finite Difference Method(FDM), the Monte Calo Method, the Boundary Element Method (BEM), the Moment Method and the Charge Simulation Method(CSM). Among them, the Charge Simulation Method has proven to be successful for many high voltage field problems because of its simplicity and its good applicability to three dimensional fields, especially unbounded fields like those prevailing in substations [41–45].

The Charge Simulation Method has been applied to calculate the electric field in substations [41,42,46]. Because of the complicated configuration, simplifications are necessary. In the past these simplifications have included omission of what is considered to be unnecessary detail and the use of oversimplified simulation charges to represent objects such as transformers etc. In the present work, the objective is to calculate the electric field in the vicinity of a switch–line and compare with measured data.

5.1.1. Theoretical Foundation of the CSM

The charge simulation method is relatively simple and straightforward in principle. The theoretical foundation can be traced back to Green's Theorem.

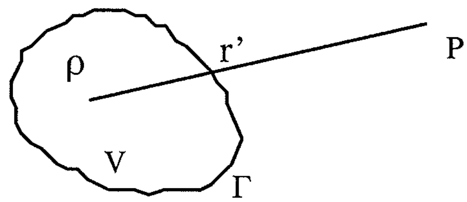

Fig.5.1 Effect of field source ρ to the point p

Figure 5.1 shows a given volume density ρ(r) distributed inside the domain V. According to the Green's theorem, to calculate the potential of any point outside V, the surface integration on Γ yields the same result as the volume integration in V, or

$$\int_V (\Psi\nabla^2\Phi - \Phi\nabla^2\Psi)\, dv = \oint_\Gamma (\Psi\frac{d\Phi}{dn} - \Phi\frac{d\Psi}{dn})\, ds \tag{1}$$

in which ψ is the fundamental solution of the 3–dimensional field, i.e.

$$\Psi = \frac{1}{4\pi r'} \tag{2}$$

r' is the distance between source point and field point P. If denote Φ as the potential inside V, then within V,

$$\nabla^2\Psi = 0 \tag{3.a}$$

$$\nabla^2\Phi = -\frac{\varrho}{\epsilon_0} \tag{3.b}$$

Substituting (2) and (3) into (1),

$$\int_V \frac{-\varrho/\epsilon}{4\pi r'} dv = \oint_\Gamma (\frac{1}{4\pi r'}\frac{\partial\Phi}{\partial n} - \frac{\Phi}{4\pi}\frac{\partial}{\partial n}(\frac{1}{r'}))ds$$

Since $\Phi_p = \int_V \frac{\varrho dv}{4\pi\epsilon\, r'}$

so $$\Phi_P = \int_V \frac{\varrho dv}{4\pi\epsilon r'} = \oint_\Gamma [\frac{\Phi}{4\pi} \frac{\partial}{\partial n}(\frac{1}{r'}) - \frac{1}{4\pi r'}] ds \tag{4}$$

It proves that the potential of any point outside the domain of source V can be expressed either by volume integration or by surface integration.

In other words, the field produced by an object with a certain charge volume density is identical to that produced by another object of equivalent surface density, or vice versa. In terms of numerical field simulation, or more specifically in the charge simulation method, solutions to the field produced by the charges on the conductor surface can be sought by means of "volume integration" inside the conductors, or beneath the surface, instead of the direct integration of charges on the real surface.

5.1.2 Basic Concepts of the CSM

Simulation charges are introduced as fictitious charges which do not really exist but are supposed to have the same field effect as the real charges residing on the conductor surface, provided certain boundary conditions are satisfied. Therefore those physically continuously distributed surface charges are replaced by discrete simulation charges which are placed outside the area in which the field is to be solved. Because of its discrete nature, the charge simulation method requires the selection and position of a large number of simulation charges to achieve satisfactory accuracy.

For the calculation of the electric fields, the distributed charges on the surface of the conductor are replaced by a set of N simulation charges (point, line or ring charges etc.) arranged inside the conductor. In order to determine the magnitude of these charges, an equal number of N points, usually called contour points, are chosen. Therefore the potential at any contour point, denoted by Vi, is given by

$$V_1 = P_{11}Q_1 + P_{12}Q_2 \quad \ldots \quad P_{1n}Q_n$$

$$V_2 = P_{21}Q_1 + P_{22}Q_2 \quad \ldots \quad P_{2n}Q_n$$

$$V_i = P_{i1}Q_1 + P_{i2}Q_2 \quad \ldots \quad P_{in}Q_n \qquad (i = 1, 2, \ldots\ldots n)$$

$$V_n = P_{n1}Q_1 + P_{n2}Q_2 \quad \ldots \quad P_{nn}Q_n \tag{5}$$

or

$$V_i = \sum_{i,j=1}^{n} P_{ij}\, Q_j \tag{6}$$

where Q_j is the discrete simulation charge and P_{ij} is the corresponding potential coefficient.

The summation of potentials at the N contour points leads to a system of N linear equations for the N charges. These equations are called charge simulation equations, or in matrix form,

$$[P]\,[Q] = [V] \tag{7}$$

For the most frequently used types of simulation charges the coefficients P_{ij} are known. The unknown charges are then found from specified boundary conditions. In the case of simple conductors, the potential of all the selected contour points are set to be a known constant, V_c, i.e.

$$\sum_{i=1}^{n} P_{ij}\, Q_j = V_c \tag{8}$$

or

$$[P][Q] = [V_c] \tag{9}$$

The magnitude of the simulation charges is obtained by solving the N linear equations. Because only a finite number of discrete contour points are used to help meet the boundary conditions, errors exist and can be examined by various ways. Usually another set of N check points are introduced so that field quantities calculated at the check points can be used to provide a visible degree of accuracy.

The most frequently used and straightforward error checking method is to examine the potential error at check points. However, since the field error is often one order higher than the potential error, a check on field quantities is often suggested. This can be done by checking the ratio of the tangential component to the normal component of the electric field, i.e. Et/En at the conductor surface. An alternative way is to check the angular deviation of the field vector from its normal direction on a conductor surface.

Once the charge simulation model has been developed, the potential and field strength at any point outside the electrodes can be calculated. Whereas the potential is determined by Eq.(6), the field strength is calculated by superposition of magnitudes of various directional components. For example, in the cartesian coordinate system, the field E_i at point P_i is given by

$$\mathbf{E_i} = \left(\sum_{j=1}^{n} \frac{\partial P_{ij}}{\partial x} Q_j\right)\mathbf{a_x} + \left(\sum_{j=1}^{n} \frac{\partial P_{ij}}{\partial y} Q_j\right)\mathbf{a_y} + \left(\sum_{j=1}^{n} \frac{\partial P_{ij}}{\partial z} Q_j\right)\mathbf{a_z}$$

$$= \left(\sum_{j=1}^{n} (F_{ij})_x Q_j\right)\mathbf{a_x} + \left(\sum_{j=1}^{n} (F_{ij})_y Q_j\right)\mathbf{a_y} + \left(\sum_{j=1}^{n} (F_{ij})_z Q_j\right)\mathbf{a_z} \tag{10}$$

where $(F_{ij})_x$, $(F_{ij})_y$, $(F_{ij})_z$ are the field intensity coefficients and $\mathbf{a_x}$, $\mathbf{a_y}$, $\mathbf{a_z}$ are unit vectors in the x, y, z directions respectively.

In many cases, the electrostatic field between a system of conductors and an infinite plane with V=0 is of interest. This plane can be taken into account by the introduction of image charges which results in a doubling of simulation charges. However, the preservation of matrix order is still possible due to the symmetrical nature of the image charges.

Traditionally, in the CSM model the accuracy of the computation depends mainly on the user's experience; therefore emphasis should be focused on

1. proper selection of the types of simulation charges,
2. the good arrangement of the charges and contour points.

When selecting the types and positions of the simulation charges, it is important to analyze qualititatively the actual field characteristics first. Usually it is recommended to choose simulation charges whose electric field characteristics resemble the actual field to be solved. For example, line charges and ring charges set along the axis are suitable for simulating fields with cylindrical symmetry. Also more simulation charges are usually needed where the local field strength is very high. This rule applies to the contour points too.

5.1.3. Sample Charges

There are various types of simulation charges available whose potential coefficients and field coefficients are known from analytical solutions. In three dimensional fields or cylindrical fields, line charges (finite line charge, semi–infinite line charge, infinite line charge), point charges and ring charges (toroidal line charge) of constant or varying charge density are often used [41,43,44,47,48]. A combination of these charges usually results in an optimized simulation. However, the more complicated the charges that are used, the more time consuming the calculation becomes. Following is an illustration of a finite line charge which was used in present work [48].

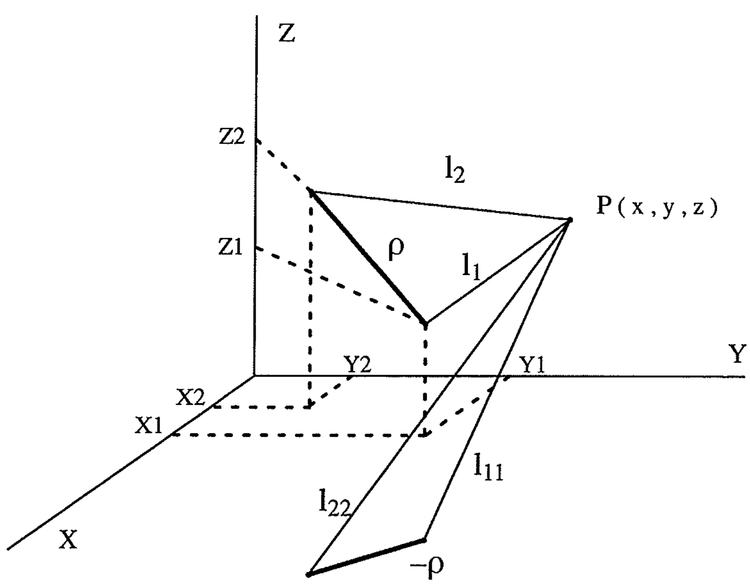

Fig.5.2 Diagram for a finite line charge in space with its image

Consider a finite line charge of density ρ and length d with its ends at (x1, y1, z1) and (x2, y2, z2). The potential coefficient Pv at the point P (x, y, z) due to this charge and its image charge –ρ with respect to the Z=0 plane is given by

$$P_v = \frac{1}{4\pi\epsilon_0}\ln\left\{\frac{(l_1+l_2+d)\ (l_{11}+l_{22}-d)}{(l_1+l_2-d)\ (l_{11}+l_{22}+d)}\right\} \tag{11}$$

where l_1, l_2, l_{11}, l_{22} and d are given by

$$l_1 = \sqrt{(x-x_1)^2+(y-y_1)^2+(z-z_1)^2}$$

$$l_2 = \sqrt{(x-x_2)^2+(y-y_2)^2+(z-z_2)^2}$$

$$l_{11} = \sqrt{(x-x_1)^2+(y-y_1)^2+(z+z_1)^2}$$

$$l_{22} = \sqrt{(x-x_1)^2+(y-y_1)^2+(z+z_2)^2}$$

$$d = \sqrt{(x_1-x_2)^2+(y_1-y_2)^2+(z_1-z_2)^2} \tag{12}$$

The x, y, and z components Fx, Fy and Fz of the field coefficient at point P are

$$F_x = \frac{1}{4\pi\epsilon_0}\left\{\left(\frac{x-x_1}{l_1}+\frac{x-x_2}{l_2}\right)\Gamma_1-\left(\frac{x-x_1}{l_{11}}+\frac{x-x_2}{l_{22}}\right)\Gamma_2\right\}$$

$$F_y = \frac{1}{4\pi\epsilon_0}\left\{\left(\frac{y-y_1}{l_1}+\frac{y-y_2}{l_2}\right)\Gamma_1-\left(\frac{y-y_1}{l_{11}}+\frac{y-y_2}{l_{22}}\right)\Gamma_2\right\}$$

$$F_z = \frac{1}{4\pi\epsilon_0}\left\{\left(\frac{z-z_1}{l_1}+\frac{z-z_2}{l_2}\right)\Gamma_1-\left(\frac{z+z_1}{l_{11}}+\frac{z+z_2}{l_{22}}\right)\Gamma_2\right\} \tag{13}$$

where Γ_1 and Γ_2 are given by

$$\Gamma_1 = \frac{1}{(l_1+l_2-d)}-\frac{1}{(l_1+l_2+d)}$$

$$\Gamma_2 = \frac{1}{(l_{11}+l_{22}-d)}-\frac{1}{(l_{11}+l_{22}+d)} \tag{14}$$

5.2 Model Setup and Refinement

When creating the charge simulation model for field calculations in a high voltage dc switchyard, the yard components can be classified as conductors and grounded supports. Usually busbars, incoming and outgoing lines, disconnectors, circuit breakers, shield rings and connections between equipments etc. can be modelled as straight and regularly curved conductors which are easily replaced by simulation charges. The cement poles and metal supports are regarded as being at zero potential and can be replaced by line charges. The ground is considered to be at zero potential so that its effect is substituted by image charges. Once the boundary conditions are satisfied, the electric field at any point can be calculated by these simulation charges and their images.

In present simulation task, charge simulation models were created to calculate the electrostatic field along the switch–line sw2 in order to produce the calculation results to compare with the measured data.

Since only locations at or near ground level are of concern and they are all far away from the conductors compared to the conductor radius, the following simplifications were introduced which have negligible effects on the accuracy of the simulation:

1. All conductor surfaces are assumed to be ideally smooth.
2. The diameters of all bus conductors were assumed to be constant throughout the length; a small number of very short curved connections were modelled as straight conductors.
3. All metal and cement supports were regarded as grounded objects. They are modelled as coaxial cylinders with constant diameters.
4. The effect of the supporting post–type insulators between conductors and grounded supports were neglected.
5. All miscellaneous structures and complex geographic details were ignored, e.g. corona rings, minor elevation change due to apparatus shape.

A total of five models were developed in order to examine the effects of model refinement on solution accuracy. Each model includes components which are not taken into account in previous models. Figure 5.3 shows a three dimensional diagram of the local area of switch–lines sw2 and sw3 including neighboring structures between sw2 and sw1.

Following is a description of each of the six simulation models comprising of finite line charges to calculate the electric field on either side of sw2 and along it (all labels are referred to Fig. 5.3):

Model 1: Only horizontal conductors (labelled AB and A'B') in sw2 and sw3 were simulated.

Model 2: Horizontal conductors (AB and A'B') + vertical bends (BC, AD, B'C' and A'D') in sw2 and sw3 were simulated

Model 3: Horizontal conductors (AB and A'B') + vertical bends (BC,AD B'C' and A'D') + horizontal stretches (CH, EF, C'H' and E'F') in sw2 and sw3 + neighboring structures (IJKL, MNO) between sw1 and sw2 were simulated

Model 4: All components in Model 3 + grounded horizontal supports (H1, H2, H1' and H2') in sw2 and sw3 were simulated

Model 5: All components in Model 4 + grounded vertical supports (VS1, VS2, ...VS9 and VS1', VS2' ...VS9') in sw2 and sw3 were simulated

The flow chart for the CSM models is shown in Fig.5.4. It is seen that this simulation method is very simple and straightforward in algorithms. This flow chart applies to all the five models listed above.

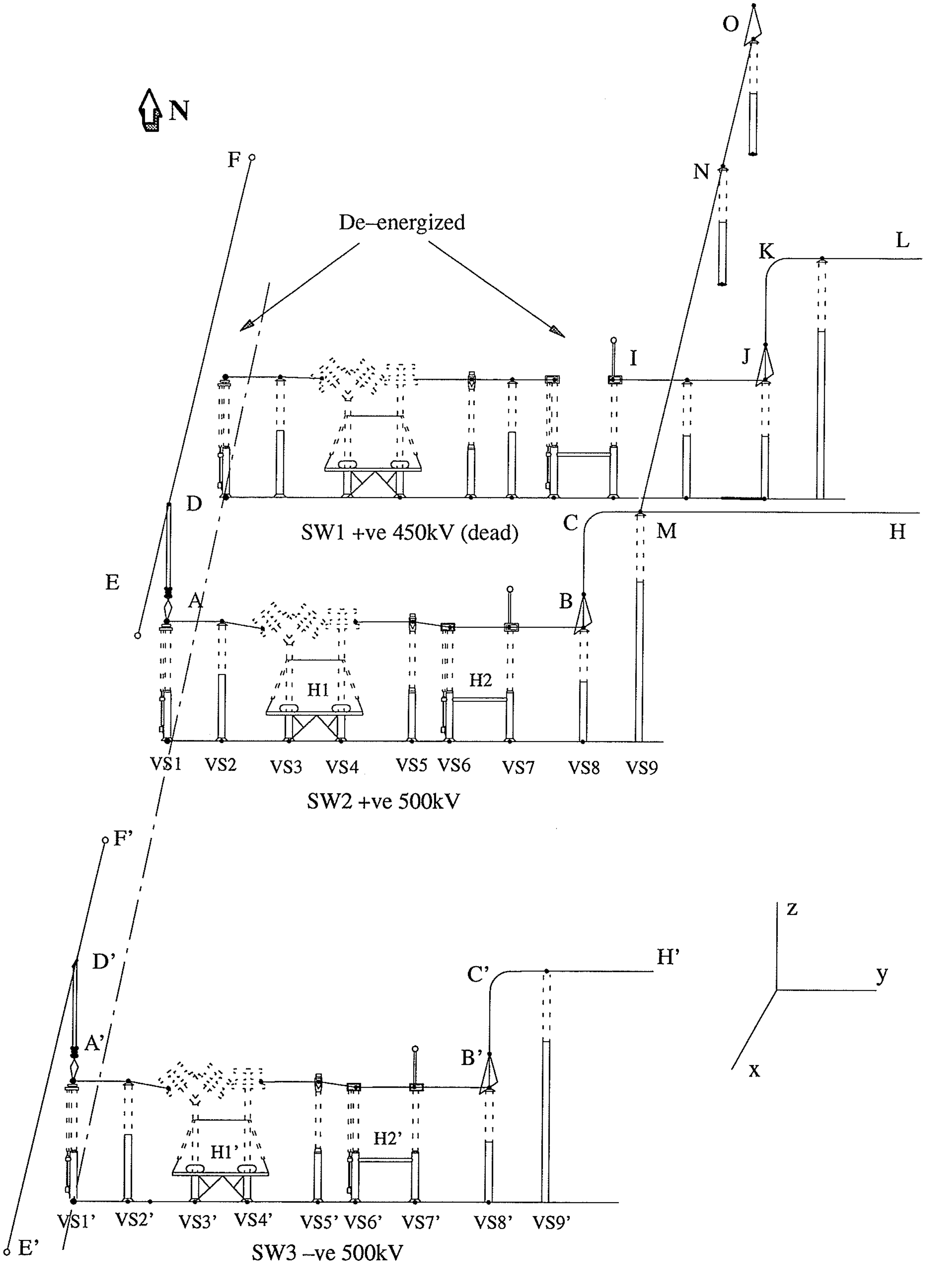

Fig.5.3 Diagram of switch–lines sw1, sw2 and sw3

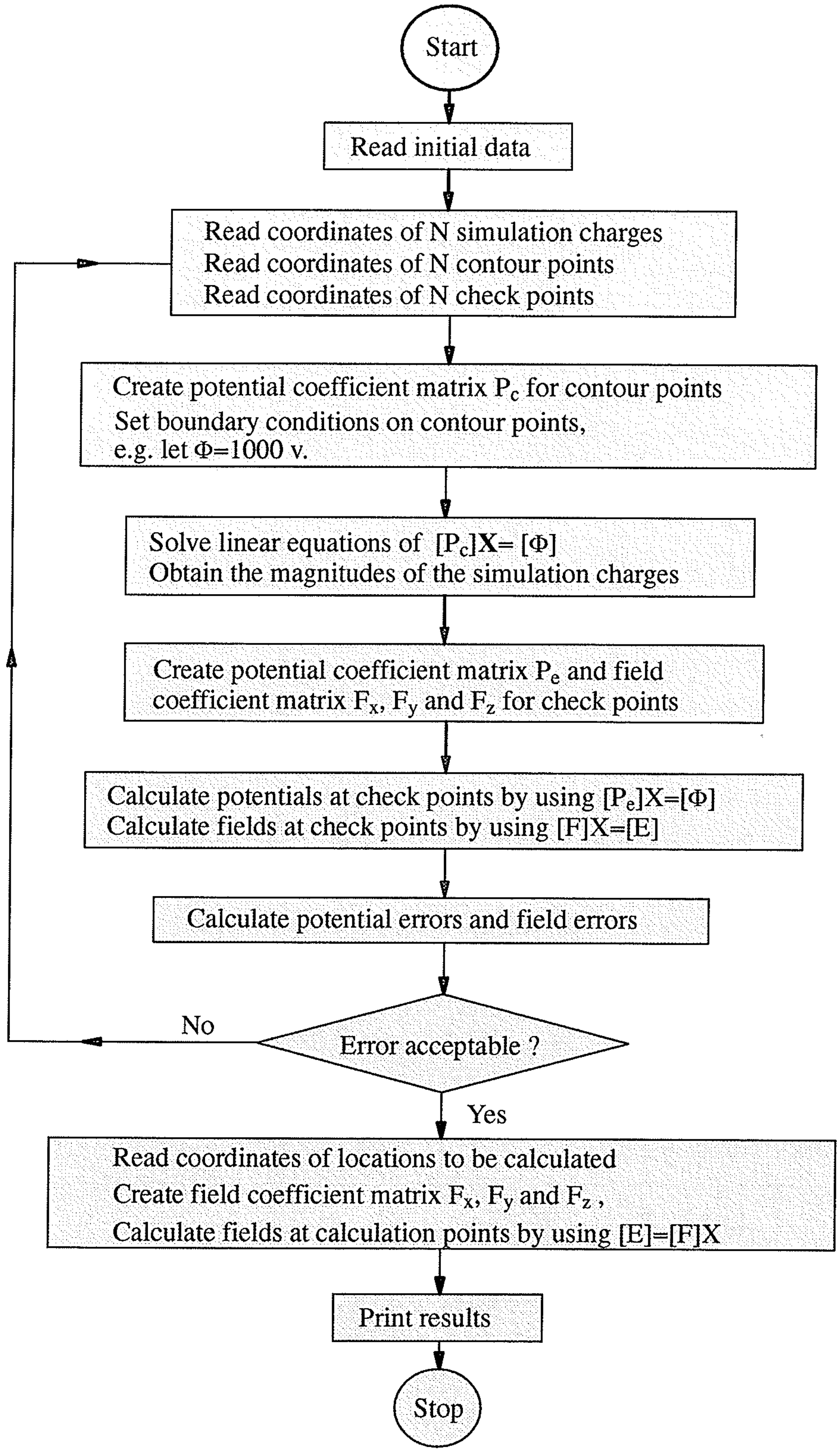

Fig.5.4 Flow chart of charge simulation model

5.3 Effect of Model Refinement

Table 5.1 shows the maximum and average potential and field errors associated with each model. It can be seen that these errors are small and therefore acceptable.

Models	Number of Simulation Charges	Potential Error (%)		Field Angle Error (°)	
		Maximum	Average	Maximum	Average
1	16	0.050	0.045	0.546	0.153
2	40	0.551	0.148	1.639	0.250
3	74	0.622	0.146	3.300	0.421
4	86	0.623	0.184	3.300	0.458
5	108	0.623	0.157	5.358	1.254

Table 5.1 Potential and field errors of models at different stages

To illustrate the evolution of the models under refinement, some preliminary calculation results are presented. The calculated electric fields at the ten locations at ground level where ground level measurements have been carried out are presented in Table 5.2. Also the variation of the calculated electric field components Ex, Ey and Ez along the length of the switch–line sw2 at 1m above ground are presented in Fig.5.5 as predicted by the five simulation models.

Locations	Model 1	Model 2	Model 3	Model 4	Model 5
1	11.96	13.48	14.84	13.05	12.06
2	12.76	13.76	14.93	12.06	11.39
3	13.02	13.81	14.90	12.96	12.06
4	12.93	13.79	14.96	13.80	11.82
5	12.08	13.53	15.11	12.76	11.24
6	12.61	14.36	16.65	14.85	13.84
7	13.47	14.67	16.74	13.85	13.17
8	13.74	14.73	16.80	14.85	13.92
9	13.64	14.71	17.11	15.94	13.93
10	12.73	14.42	18.09	15.72	14.17

Table 5.2 Calculated electric fields (kV/m) at ground level locations along switch–line sw2 using different models

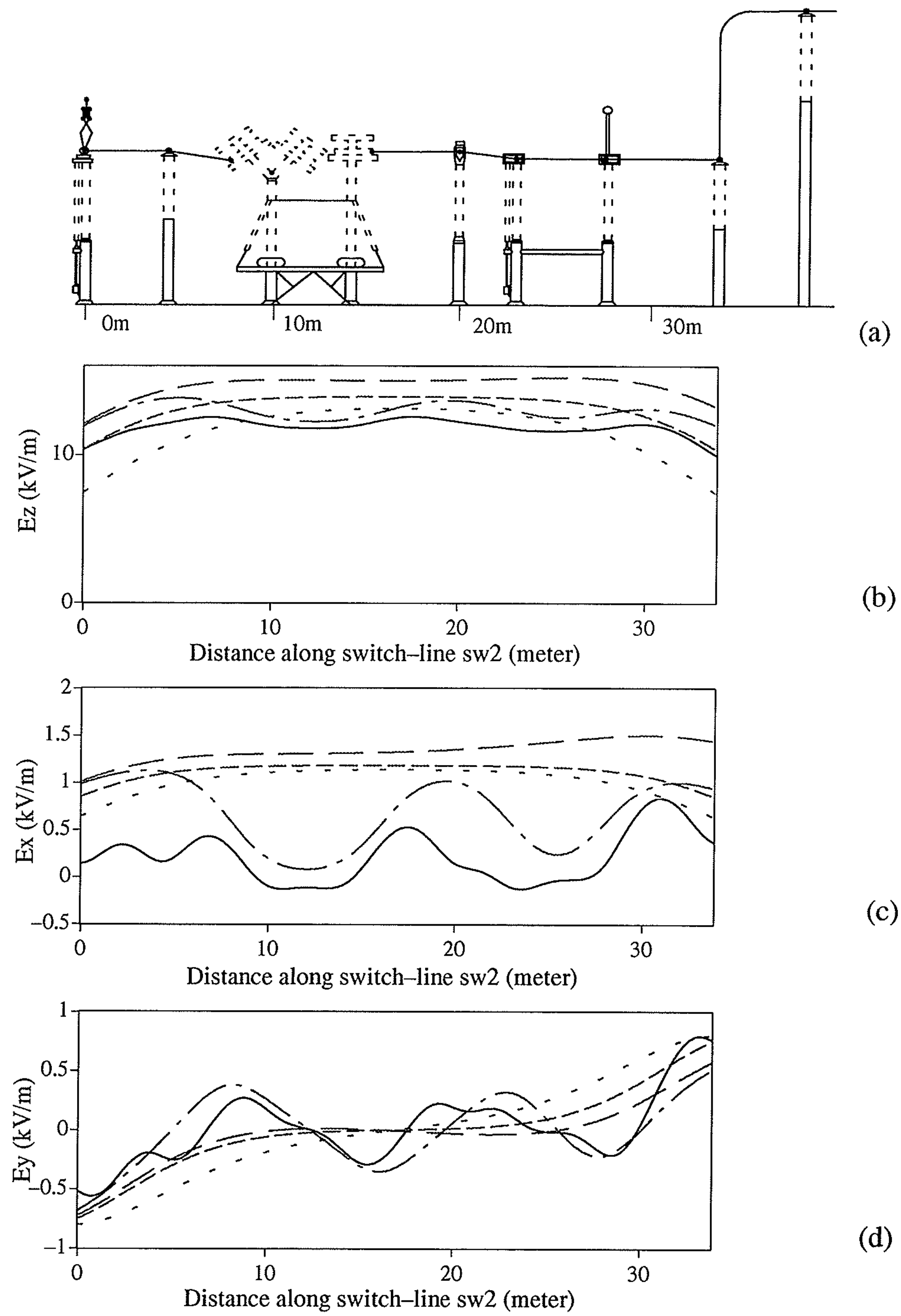

Fig.5.5 Predicted lateral variation of field components Ex, Ey and Ez on the south side of sw2 at 1.0m above ground level

(a): Elevation layout of switch–line sw2
(b): Calculated Ez
(c): Calculated Ex
(d): Calculated Ey

Model 1 Model 2 Model 3 Model 4 Model 5

It is shown that the magnitudes of vertical electric field strength first rise when more live components are included (model 1 to model 3), then drop after grounded horizontal and vertical supports are introduced (model 4 and model 5)

The evolution of the simulation model shows that model 5 represents best the field characteristics in the vicinity of the switch–line. This can be seen from the calculated horizontal field components Ex and Ey in Fig.5.5. Though their magnitudes are small, they display a demonstrative behavior of how the grounded structures in sw2 influence the direction and magnitudes of the horizontal components.

The occurrence of a significant change in the magnitude of Ex and the direction of Ey illustrates that the grounded structures of the high speed line switch can significantly alter the field characteristics beneath it. This can be seen from the relative flat and constant Ex distribution along the length of the grounded structures (e.g. high speed line switch) and a change of direction of Ey at the center point of the grounded structures. In other words, the influence of the grounded structures is so strong that the field lines near the south side of the high speed line switch are curved from the direction of southwest to northeast and from southeast to northwest. This phenomena is in agreement with analytical prediction and explanation and therefore can be used to support the validity of this simulation model.

All the other models fail to provide as much detail information on field characteristics as model 5. This is due to the fact that only model 5 has a complete inclusion of simulation charges for grounded supporters. Therefore model 5 is regarded as the refined model and is used for further calculation.

5.4 Calculated Results by Model 5

Figure 5.6 shows the calculated electric field strengths at five ground level locations on each side of switch–line sw2. Since the ground is modelled as an ideal plane, only the vertical component of the electric field exists.

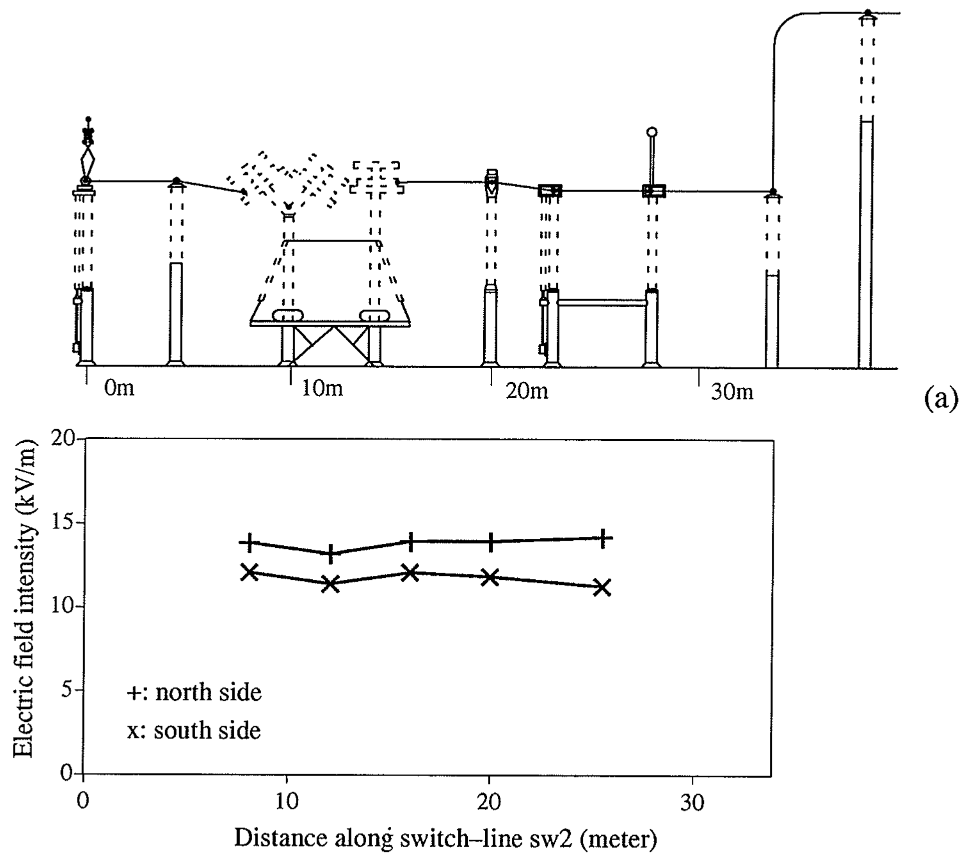

Fig.5.6 Calculated electric fields at ground level locations along sw2

Figures 5.7 – 5.13 show the detailed calculation results at locations above ground and adjacent to the switch–line sw2. Calculation was performed at a total of 112 locations on each side of the switch–line at 1m and 1.5m heights. The CSM model generated the horizontal components Ex and Ey, and the vertical components Ez. In these figures |**Eh**| (=**Ex** + **Ey**) has also been presented.

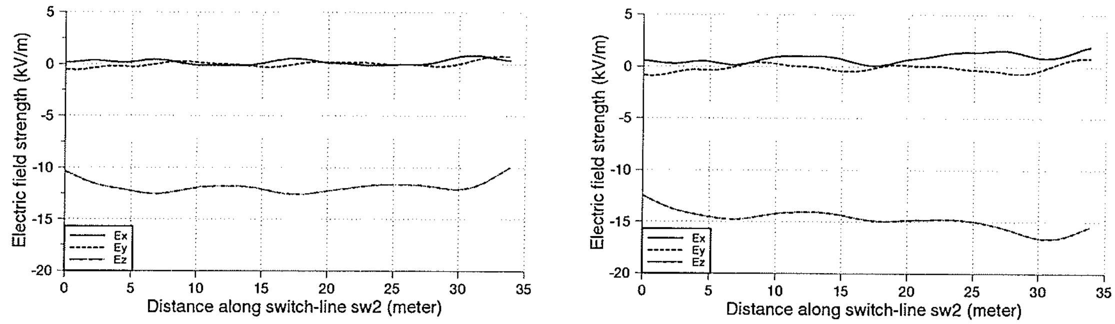

Fig.5.7 Calculated electric fields along north side of sw2 at 1.0m (left) and 1.5m (right)

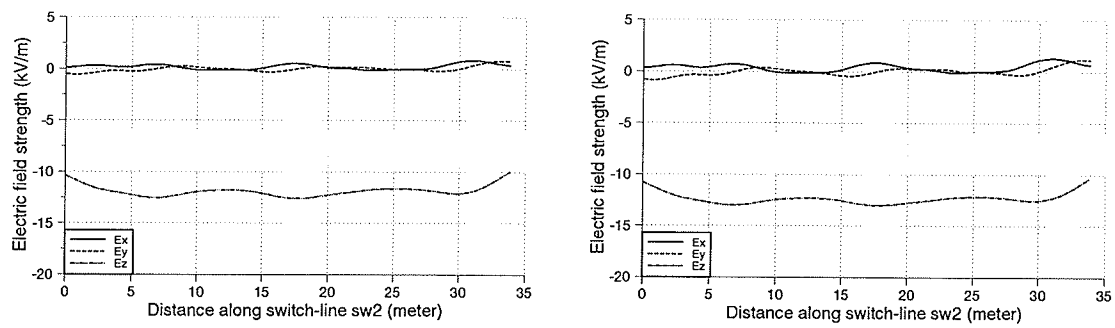

Fig.5.8 Calculated electric fields along south side of sw2 at 1.0m (left) and 1.5m (right)

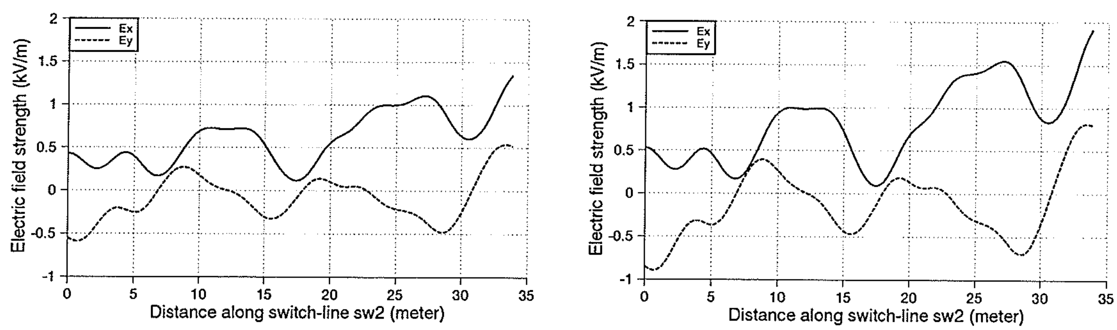

Fig.5.9 Calculated horizontal fields along north side of sw2 at 1.0m (left) and 1.5m (right)

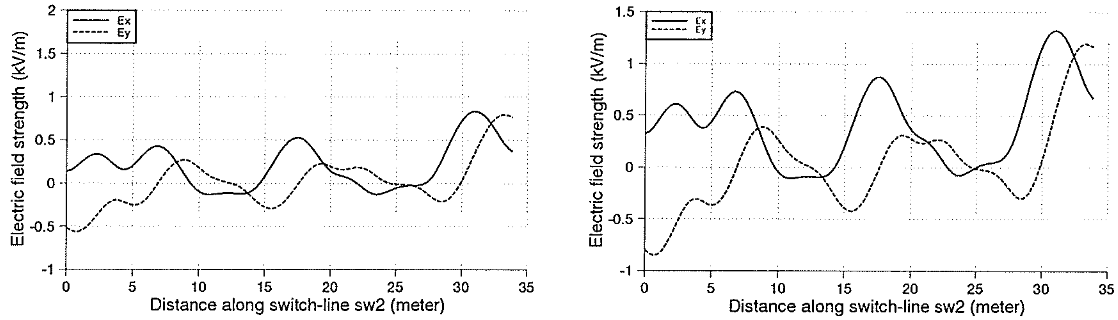

Fig.5.10 Calculated horizontal fields along south side of sw2 at 1.0m (left) and 1.5m (right)

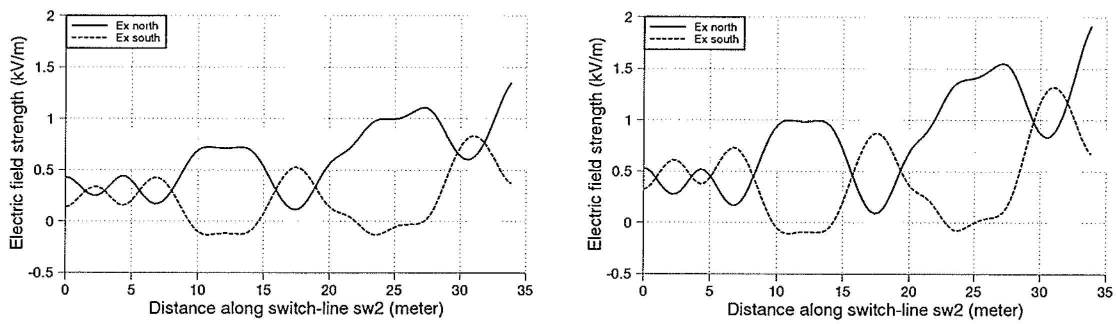

Fig.5.11 Calculated Ex components at both sides of sw2 at 1.0m (left) and 1.5m (right)

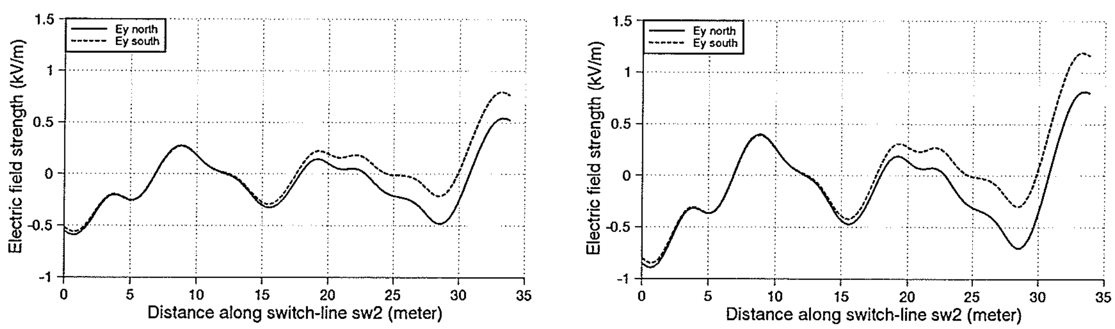

Fig.5.12 Calculated Ey components at both sides of sw2 at 1.0m (left) and 1.5m (right)

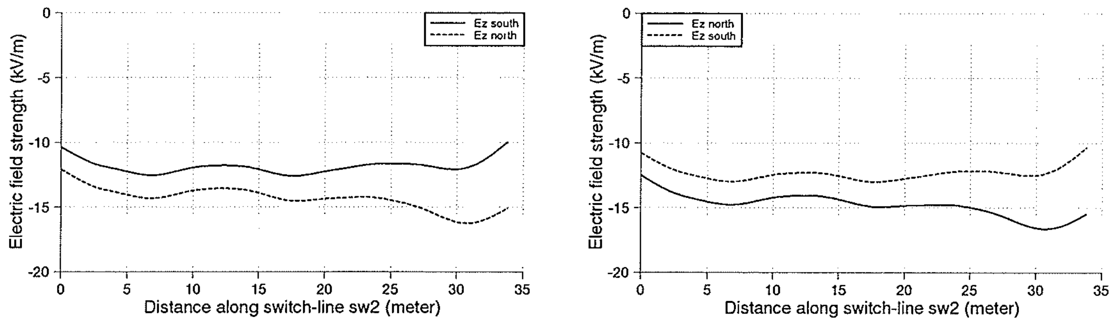

Fig.5.13 Calculated Ez components at both sides of sw2 at 1.0m (left) and 1.5m (right)

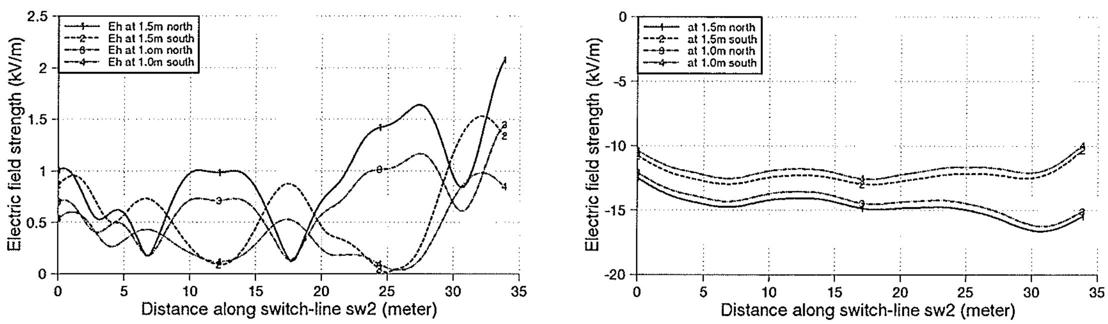

Fig.5.14 Comparison of field components of Eh (left) and Ez (right) at different heights

Some general conclusions can be drawn which are in agreement with theoretical analysis:

(1). The vertical field components are much higher than horizontal field components, and dominate the field strengths (Figs. 5.7 and 5.8).

(2). The electric field values are higher on the northern side of sw2 due to the existence of the neighboring live structures of the same polarity (Figs. 5.12 and 5.13).

(3). Higher electric fields are observed at the east end of sw2 because the energized neighboring structures close to the east end of sw2 cover a larger area than the only horizontal bus conductor (EF in Fig. 5.3) does at the west end (Fig. 5.13).

(4). The overall characteristics of the field components at 1.5m is similar to those at 1.0m level except that the magnitudes are larger.

The calculated results are essentially electrostatic values. No corona effects are taken into account.

5.5 Comparison with Measured Values

Comparison of measurement and calculation results can be made at corresponding locations, or more specifically, at the ground level locations and at locations at 1.0m and 1.5m above ground along the switch–line sw2.

Figure 5.15 shows the measured and calculated values at 10 ground level locations near the switch–line sw2. The measured data Emax and Eav in Fig. 5.15 are values from overall wind speeds (see Table 4.2). A small difference exists between the measured average and calculated vertical values on the west side. A much larger difference occurs near the east side. As analyzed in section 4.1.1, the larger difference can be attributed to a combined influence of space charges and wind direction. Since the charge simulation model only generates the electrostatic values of the electric field, therefore these values are undoubtedly less than measured data which are enhanced by space charges and wind.

The production of the positive space charges by the bus structures on the west side is much weaker than that by the large areas consisting of coronating conductors near the east ends of sw1 and sw2 (see Fig.3.2 or 5.3). Therefore the enhancement of electric field by positive space charges is more significant at locations near the east end. Also the prevailing north and northwest wind blow off space charges at the west end but bring in space charges at the east end. This further decreases the enhancement effect of space charge and wind at the west end, but increases at the east end.

Similar differences between the average measured vertical field component and calculated vertical component at 1.0m and 1.5m above ground are also illustrated in Figs. 5.16 – 5.19.

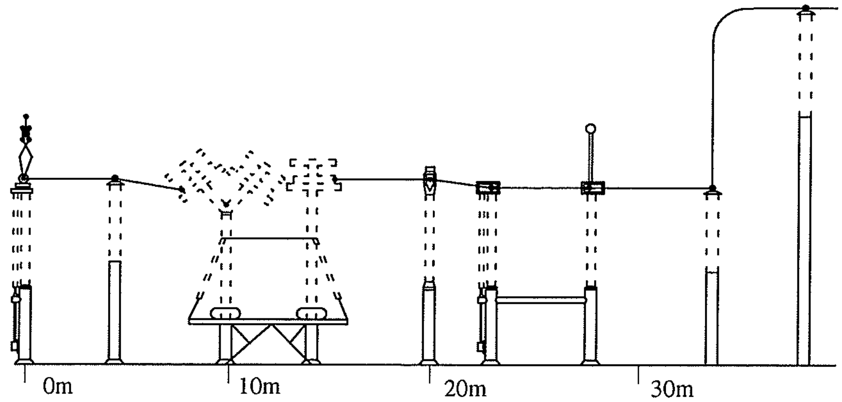

(a)

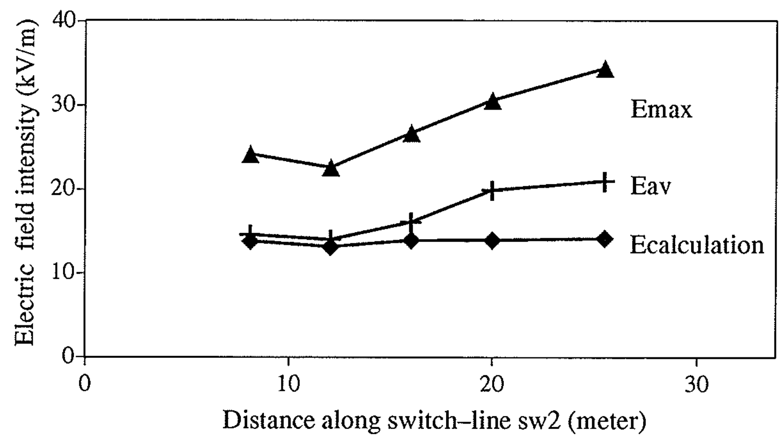

(b)

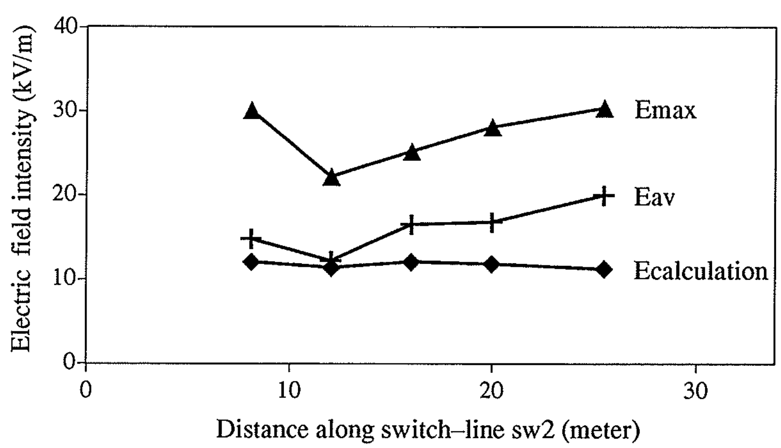

(c)

Fig.5.15 Comparison of measured and calculated data at ground level along switch–line sw2 (500 kV)

(a) Elevation layout of switch–line sw2
(b) Comparison on north side (overall wind speeds)
(c) Comparison on south side (overall wind speeds)

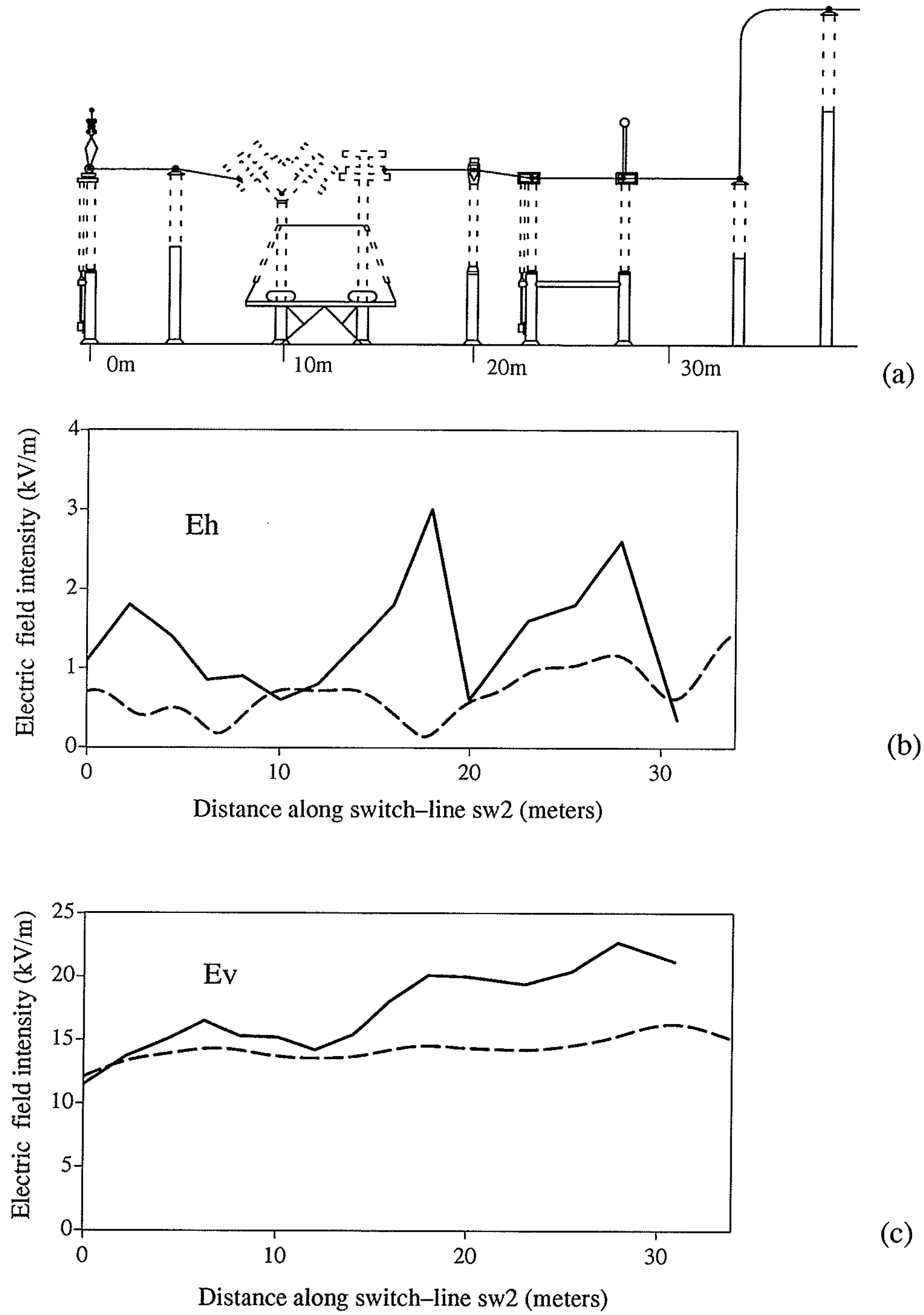

Fig.5.16 Comparison of measured and calculated data at 1m above ground on the north side of sw2 (500kV)

(a) Elevation layout of switch–line sw2
(b) Comparison of horizontal components Eh
(c) Comparison of vertical components Ev

—— Measured values (low wind)
– – – – Calculated values

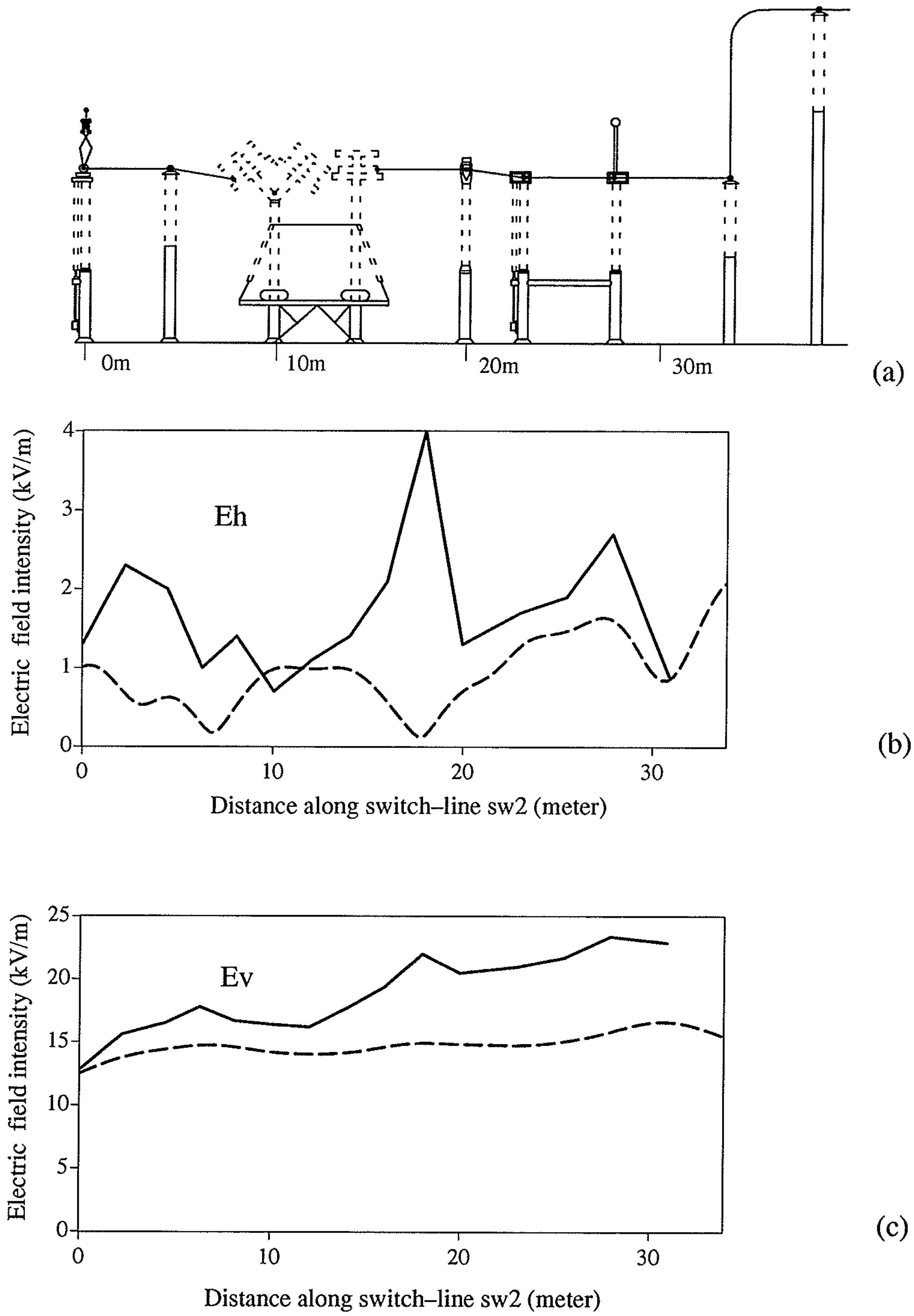

Fig.5.17 Comparison of measured and calculated data at 1.5m above ground on the north side of sw2 (500kV)

(a) Elevation layout of switch–line sw2
(b) Comparison of horizontal components Eh
(c) Comparison of vertical components Ev
——— Measured values (low wind)
– – – – Calculated values

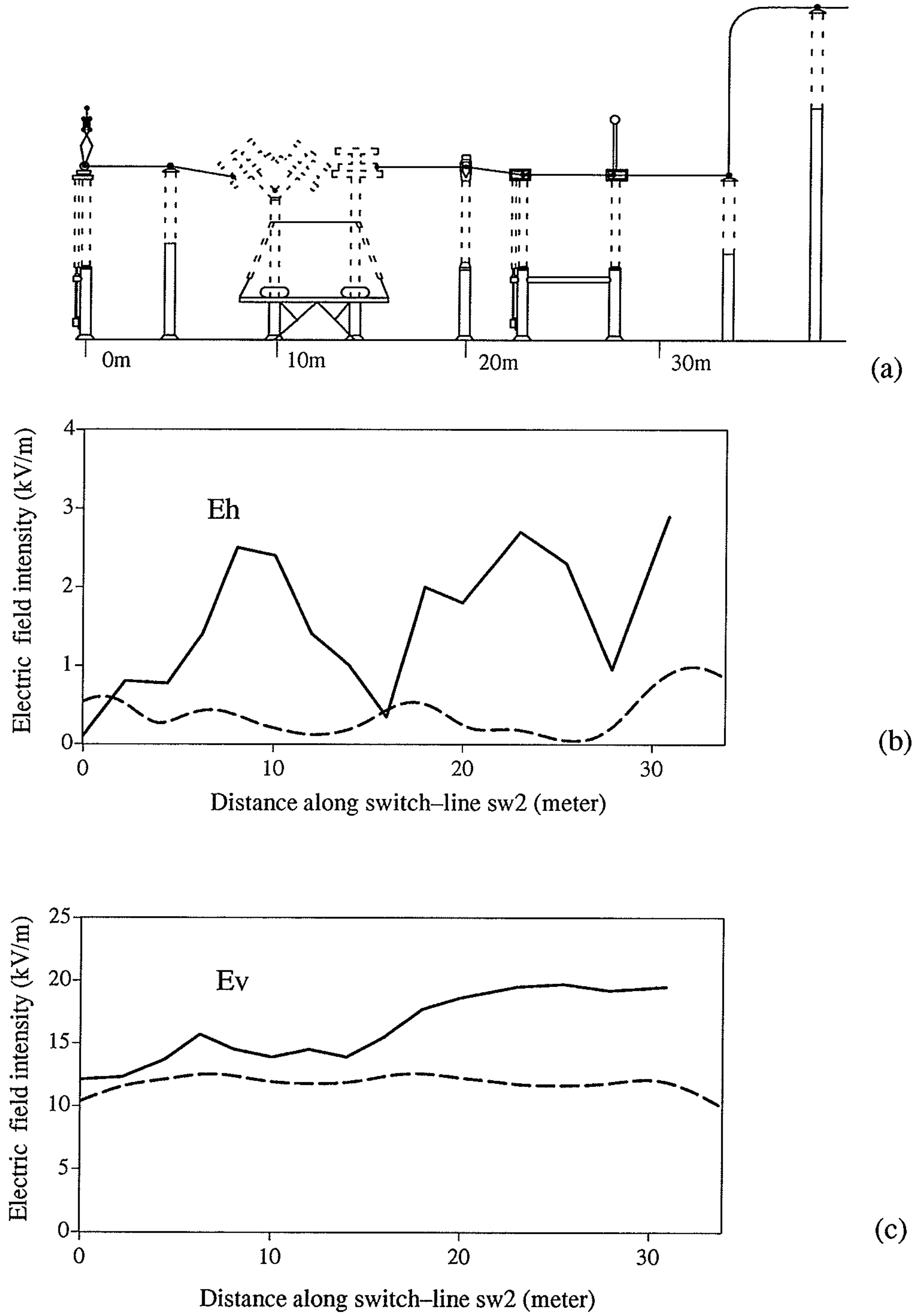

Fig.5.18 Comparison of measured and calculated data at 1m above ground on the south side of sw2 (500kV)

(a) Elevation layout of switch–line sw2

(b) Comparison of horizontal components Eh

(c) Comparison of vertical components Ev

——— Measured values (low wind)

– – – – Calculated values

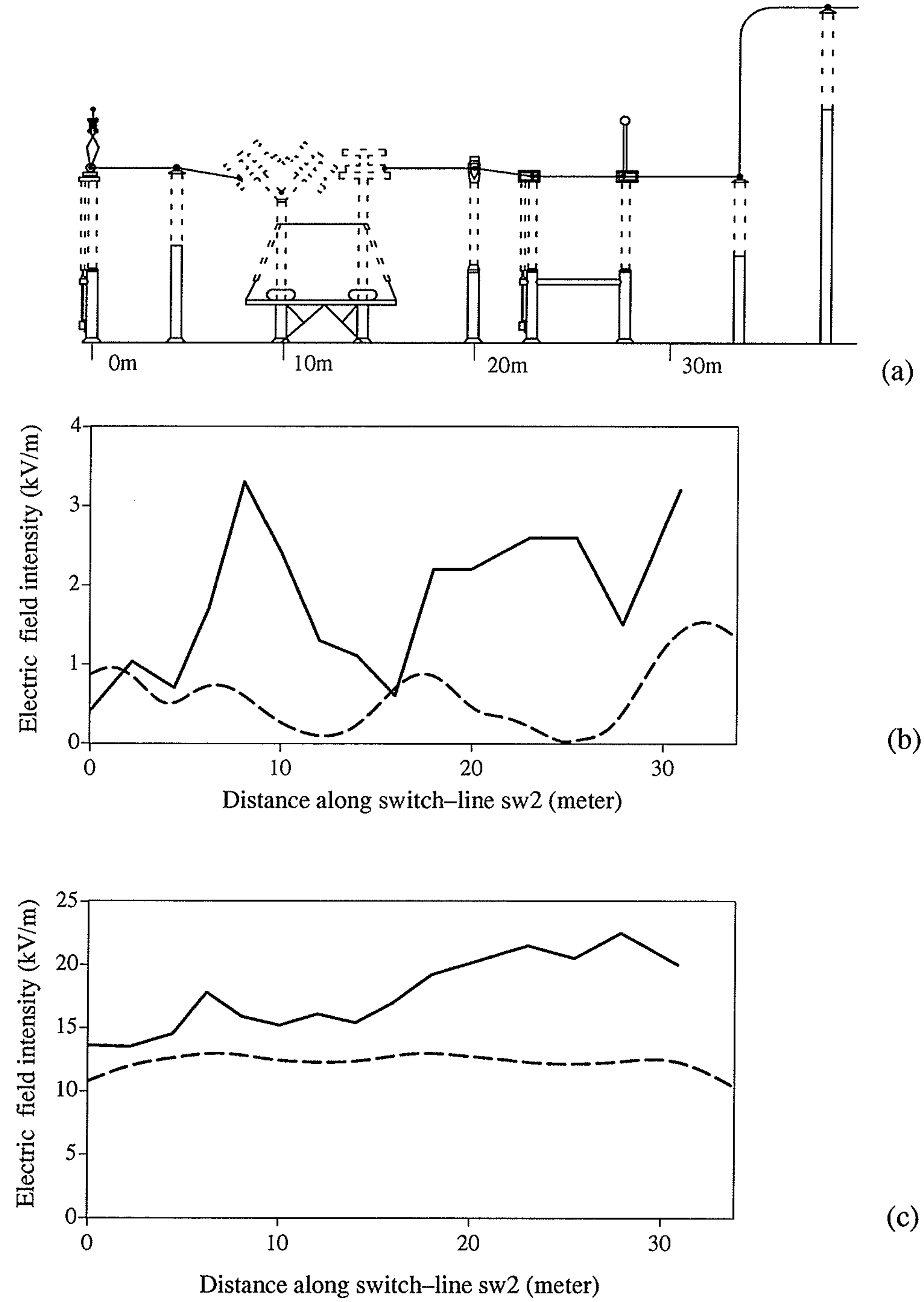

Fig.5.19 Comparison of measured and calculated data at 1.5m above ground on the south side of sw2 (500kV)

(a) Elevation layout of switch–line sw2
(b) Comparison of horizontal components Ehorizontal
(c) Comparison of vertical components Evertical

——— Measured values (mild wind)
– – – – Calculated values

For the horizontal component Eh, discrepancies are large and not predictable. This is because the existing grounded structures make the horizontal Eh distribution more complicated and irregular and also because the small value of Eh is more vulnerable to the external influence.

One interesting observation is that compared with external influences, i.e. effect of space charge and wind, the electrostatic switchyard configuration seems to play a less dominant role in determining the electric field values. This conclusion is evident upon examination of the measured and calculated lateral variation of the vertical component of the electric field Ev in Figs. 5.16 – 5.19. The east side measured values are much larger than those recorded on the west side. However the calculated profile of Ev does not show much difference. The calculated values are obtained from electrostatic model which has already included the effects of the presence of the neighboring energized bus structures in the area. In spite of this, larger electric field values are not predicted at that location. Therefore the conclusion is that the increased fields as evidenced by the measurements must be attributed due to the effects of wind and space charges.

In a dc switchyard there are numerous corona sources and the situation is made more complicated by the effect of wind. Electric field data generated by the electrostatic simulation models can not be expected to be in good agreement with measured data in spite of the small error level and good behavior of electric field components along the switch–line as illustrated in Section 5.4.

CHAPTER 6

Conclusions and Suggestions for Future Work

6.1 Conclusions

1. Data acquired continuously over a period of several months yields important information when analyzed using a database approach. Assessment of the field levels in a dc switchyard is best carried out by examination of average and maximum values computed from data corresponding to all wind speeds.

2. The measured field quantities are influenced by system voltages, neighboring bus conductors and the effects of wind and space charge. It is not unusual to observe both positive and negative readings at a location and at some locations their magnitudes are comparable.

3. The measured maximum and average values of field quantities are comparable to corresponding values under the dc line. The maximum value of electric field in a 500 kV dc switchyard is much higher than the measured maximum values in 500 kV and 735 kV ac substations.

4. Higher corona activities occurred near high speed line switches where maximum values of ion current density exceeded by an order of magnitude those recorded beneath the incoming lines.

5. In a dc switchyard there are numerous corona sources. Therefore calculated values of electric field using electrostatic simulation models do not agree well with measured results.

6.2 Suggestions for Future Research on Field Investigation in a DC Switchyard

1. Ideally measurements should be conducted simultaneously at all selected locations so that within certain period of time some related parameters can be regarded as constant, for example, the system voltages and corona activity (depending on atmospheric paprametrs). This will significantly improve the efficiency of the recordings and therefore provide more valid data for analysis. It is also more meaningful to compare the results obtained from different locations at the same time so that more accurate conclusions can be drawn.

2. Due to the inherent defects of the electrostatic modelling of electric fields in a dc switchyard, poor agreement between results obtained from calculation and measurement can not be improved by increasing more simulation charges or by using other electrostatic models. Simulation models which have the capability of taking the space charge and its drifting in wind into account are recommended.

References

1. W.B, Kouwenhoven, et al, "Medical evaluation of men working in an electric fields", IEEE Trans. on Power Apparatus and Systems, Vol. PAS–86, No.4, April 1967, pp. 506–511.

2. R. P. Comsa and J. G. Rene, "Air model for the study of electrostatic induction by transmission lines" IEEE Transactions on Power Apparatus and Systems, vol. PAS–87, April 1968, pp. 1002–1010.

3. J.D. Tranen and G.L. Wilson, "Electrostatically induced voltages and currents on conducting objects under EHV transmission lines" IEEE Transactions on Power Apparatus and Systems, vol. PAS–90, March/April 1971, pp. 768–775.

4. V.P. Korobkova, Y.A. Morozov, M.D. Stolarov and Y.A. Yakub, "Influence of the electric field in 500 and 750 kV switchyards on maintenance staff and means for its protection" CIGRE Paper 23–06, 1972.

5. P.W. Barber, J.S.T. Looms, D.F. Oakeshott, J. Prest, G.C. Stringfellow, R.P.E. Watson, D.R. Stevens, "Transmission lines in the environment of England and Wales", CIGRE Paper 22–01, 1974.

6. G. Balderston Jr., J.M. Schamberger, G.W. Juette and L.E. Zaffanella, "UHV AC transmission line design based on project UHV test results", CIGRE Paper 31–12, 1972.

7. H. C. Barnes and B. Thoren, "The AEP–ASEA UHV project: results to 1973 and planning of a system test station and line", CIGRE Paper 31–10, 1974.

8. T.D. Bracken, "Field Measurement and Calculations of Electrostatic Effects of Overhead Transmission Lines", IEEE Trans. on Power Apparatus and Systems, Vol. PAS–95, no. 2, March/April 1976, pp. 494–504.

9. P.S. Maruvada, N. Hylten–Cavallius, N. Giao Trinh and M. De Vizio, "Electrostatic field effects from high voltage power lines and in substations", CIGRE Paper 36–04, 1976.

10. P.S. Maruvada, R.D. Dallaire, O.C. Norris–Elye and C.V.Thio, "Environmental effects of the Nelson river HVdc transmission lines – RI, AN, electric field, induced voltage, and ion current distribution tests", IEEE trans. on Power Apparatus and Systems, Vol. PAS–101, No.4, 1982, pp951–959.

11. C. W. Mott, et al., "Design of substations for systems operating at 765 and 1050 kV", CIGRE Paper 23–12, 1976.

12. J. Johnson, K. Connelly and D.C. Smith, "Influence of electric field effects on 500–kV system design", CIGRE Paper 31–05, 1976.

13. EPRI, TRANSMISSION LINE REFERENCE BOOK, 345 kV and Above, Chapter 8, New York: Fred Weidner and Son, 1975.

14. C. Mihaileanu. et al., "Electrical field measurement in the vicinity of HV equipment and assessment of its bio–physiological perturbing effects", Report 368, CIGRE, Paris, 1976.

15. M. Jaczewski and A. Pilatowicz, "Transient touch current near EHV lines", CIGRE Paper 36–02, 1972, Paris.

16. J. Deuse, P. Pirotte, "Calculation and measurement of electric field strength near H.V. structures", CIGRE paper 36–03, Paris, 1976

17. CIGRE Working Group 36–01, "Measurements of electric field in the vicinity of HV installations, results and lessons", CIGRE Paper 36–07, 1978.

18. T. Vinh, C.W. Yi and C.H. Shih, "Measurements and analysis of electric fields in HV and EHV stations", IEEE Trans. on Power Apparatus and Systems, Vol. PAS–101, No.10, 1982, pp4122–4130.

19. R.J. Caola, D.W. Deno and V.S.W. Dymek, “Measurement of Electric and Magnetic Fields in and around Homes near a 500 kV Transmission Lines”, IEEE Trans. Power App. Syst., Vol. PAS–102, October, 1983, pp3338–3347.

20. B.J. Maddock, J.C. Male, and W.T. Norris, “50 Hz electric and magnetic fields near power transmission circuits and some associated exposure and health studies”, International Conference on Electric and Magnetic Fields in Medicine and Biology, IEE Conference Publication No. 257, 1985, pp112–116.

21. Z. Yan, J.X. Li, Z.Y. Dong and Y. Zhu, “Prediction and Improvement of the Electric Field Distribution in High Voltage AC Substations”, Electric Power System Research, no.11, 1986, pp. 153–169.

22. W. T. Kaune, R. G. Stevens, N. J. Callahan, R. K. Severson, and D. B. Thomas, “Residential Magnetic and Electric Fields”, Bioelectromagnetics, Vol. 8, pp. 315–335, 1987.

23. M. Paulusz, “Effects of Electric Field near 750 kV Transmission Line and Protection against their Harmful Consequences”, Proc. of International Conference on Electric and Magnetic Fields in Medicine and Biology, IEE 257, 1985, pp. 112–116.

24. S.V. Biryukov, et al, “Calculation and Measurement of Fields on EHV and UHV substations and near transmission lines”, CIGRE Paper 36–06, Paris, 1986.

25. R. DeVore, M. Yee and J. Bhatti, “Prediction of Ground Level Electric Field Strength outside an HVDC Converter Station”, Electric Power System Research, v14, n1, 1988, pp. 35–40.

26. P.S. Maruvada, R.A. Malewski and P.S. Wong, “Measurement of the Electromagnetic Environment of HVDC Converter Stations”, IEEE Trans. Power Delivery, Vol. 4, No. 2, April 1989, pp. 1129–1136.

27. J.E. Bridges, "Environmental consideration concerning the biological effects of power frequency (50 or 60 Hz) electric fields", IEEE Trans. on Power Apparatus and Systems, Vol. PAS–97, pp19–32, 1978.

28. F.S. Barnes, "Mechanisms of interaction of magnetic fields with biological systems", IEEE Trans. on Magnetics, No. 24, pp2101–2104, July, 1988.

29. M. Coleman et al, "Leukemia and electromagnetic fields: a case control study", International Conference on Electric and Magnetic Fields in Medicine and Biology, pp122–125, IEEE, 1985.

30. I. Nair, M.G. Morgan and H.K. Florig, "Biological effects of power frequency electric and magnetic fields – Background paper", United States Congress, Office of Technology Assessment, May, 1989.

31. Bridlewood Residents Hydro Line Committee, "Electromagnetic fields health effects information", Internet resources at freenet.carleton.ca accessible via Gopher or Telnet.

32. D.W. Deno, "Calculating electrostatic effects of overhead transmission lines", IEEE Trans. on PAS, Vol. PAS–93, pp1458–1466, 1974.

33. S. Sebo and R. Caldecott, "Scale model studies of ac substations electric fields", IEEE Trans. on PAS, Vol. PAS–98, pp926–939, 1979.

34. "DC Electric Field Analyzer (M–300A)", Hydro Quebec manual, July 1988.

35. "Ion Current Analyzer (M–3000A)", Hydro Quebec manual, July, 1988.

36. A.R. Johnston, H. Kirkham, "A Miniature Space–Potential DC Electric Field Meter", IEEE Trans. Power Delivery, Vol. 4, No. 2, April, 1989, pp. 1253 – 1261.

37. The Institute of Electrical and Electronics Engineers, "IEEE Standard Procedures for Measurement of Power Frequency Electric and Magnetic Fields from ac Power Lines", ANSI/IEEE Std. 644–1987, March, 1987.

38. Manitoba HVDC Research Centre, *Nelson River HVDC Transmission Line External Electrical Effects Phase III Final Report*, May 1992.

39. Van Nostrand's Scientific Encyclopedia, 6th Edition, VNR Company, 1983.

40. Encyclopedia of Science and Technology, Vol. 14, 5th Edition, McGraw–Hill, 1982.

41. N.H. Malik, "A review of the charge simulation method and its applications", IEEE Trans. on Electrical Insulation, Vol.24, No.1, 1989, pp3–20.

42. F. Shao and S. Li, "Calculation of three–dimensional electric field in a substation by means of equivalent charge method", 4th ISH paper 12.02, Athens, Greece, 1983.

43. T.Kouno, T.Takuma, ELECTRIC NUMERICAL CALCULATION METHOD OF ELECTRIC FIELD, Corona Publishing Co. Ltd., 1980.(in Japanese)

44. J.Shen et al, NUMERICAL ANALYSIS OF ENGINEERING ELECTROMAG–NETIC FIELD, Xi'an Jiaotong University Publishing Co., 1991.(in Chinese).

45. H.Singer, H.Steinbigler, P.Weiss, "A Charge Simulation Method for the Calculation of High Voltage Fields", IEEE Trans. on power Apparatus and Systems, Vol. PAS–93, pp1660–1668, 1974.

46. C.M.Portela, N.H.C.Santiago and L.O.Ortiz, "Substation Electric Field – Error Estimation of Charge Simulation Method", 7th ISH, 12.06, Dresden Germany, 1991.

47. T.Kouno, "Computer Calculation of Electrical Fields", IEEE Trans. on EI, Vol–21, No.6, 1986, pp869–872.

48. M. Akazaki, K. Mishijima and S. Sato, "Calculation of three–dimensional axisymmetric fields by charge simulation method", Electrical Engineering in Japan, Vol.98, No.4, 1978, pp1–7.